The forgotten chemistry of group(IV) metals: a survey on the synthesis, structure, and properties of discrete Zr(IV), Hf(IV), and Ti(IV) oxo clusters

Yujie Zhang, Francisco de Azambuja* and Tatjana N. Parac-Vogt*

Department of Chemistry, KU Leuven, Celestijnenlaan 200F, 3001 Leuven, Belgium

*tatjana.vogt@kuleuven.be; *francisco.deazambuja@kuleuven.be

Abstract

Group (IV) metal oxo clusters are a diverse class of compounds with rapidly growing applications in catalysis, materials chemistry, electronics and optics. They possess unique structural stability, reactivity and electronic properties; however, their potential remains underexplored due to the gaps in fundamental understanding about their structure, intrinsic features, and nuances in their synthesis that overall would allow for greater tunability of their properties. In this context, here we review the chemistry of discrete zirconium, hafnium, and titanium metal oxo clusters reported in the literature in order to provide a critical overview of the structural features, properties and reactivity disclosed to date. While a comprehensive summary of Zr and Hf clusters is presented, only the most recent Ti oxo clusters are discussed in addition to some key compounds that have been revised elsewhere. Envisioning the growing relevance group (IV) metal oxo clusters for the synthesis of nanostructure materials and in catalysis, we also summarize key principles of their surface chemistry, and the photoactivity of Ti oxo clusters, given the paramount importance of these properties for the development of future applications.

Keywords. Metal oxo clusters, Zirconium, Hafnium, Titanium, ligand exchange, photoactivity, nanomaterials, catalysis

1. Introduction

Metal oxo clusters (MOCs) are a large and diverse class of molecules typically formed by groups III-VI metals in their highest oxidation state linked by oxygen atoms, resulting in discrete polyhedral nanosized clusters which are stabilized by capping ligands. At the atomic/molecular-level, MOCs are between isolated complexes and extended solids, and can be therefore regarded as models for studying the surface chemistry of related materials. They have been used to probe the reaction pathways for the formation of thin solid films and materials,[1, 2] and to study molecular features of metal oxide based catalysts.[3-6] In this context, fundamental knowledge about the isolation, structure characterization, and solution chemistry of MOCs is of paramount importance for rationally advancing areas of metal oxide based materials or metal oxide catalysts, among others.

Although similar in nature, MOCs and polyoxometalates (POMs) are frequently distinguished in the literature since POMs are intrinsically anionic compounds, while MOCs consist of cationic inorganic cores stabilized by organic (eg. carboxylate) or inorganic (eg. sulfate and peroxide) capping ligands, rendering final compounds typically neutral. POMs are very well-known and extensively studied cluster compounds,[7-13] and they have been broadly applied in catalysis,[14, 15] including biologically relevant reactions,[16-21] CO_2 conversion,[22] and photo-/electrocatalytic reactions.[23-26] Further, POMs have been used as building blocks for materials with a wide range of applications,[10, 27-29] such as memory devices,[30] energy production[31] and storage,[32] and as contrast agents for medical imaging.[33-35] Such versatility observed for POMs highlights the high potential of cluster compounds based on metals and oxygen, prompting the exploration of other classes of clusters as well.

In comparison with POMs, MOCs are far less explored as discrete species. Nevertheless, MOCs have been widely used as building blocks for hybrid materials,[36, 37] including the intensively studied metal-organic frameworks (MOFs).[38-41] Notably, MOC-based hybrid materials find applications across many areas of science such as catalysis, thin-films, magnetism, or gas adsorption/storage,[41-46] making the design and tuning of MOCs' properties an important challenge to further develop the technological potential of these materials. For example, the type of MOC used as a secondary building unit for a given MOF directly impacts the structural features such as surface area and pore apertures.[41] Similarly,

the number, arrangement and the density of functional groups on the surface of MOCs affect the crosslinking density of the final extended material, which in turn influences its mechanical and thermal properties.[42] Therefore, MOCs arguably are among the most promising class of compounds for the development novel materials, and a broader understanding of their fundamental chemistry is essential to advance this and related fields like the heterogeneous catalysis.

In order to support and inspire some new directions in the development of metal oxo based materials, we compile here key fundamental aspects of MOCs formed by group IV transition metals (Zr, Hf and Ti). A larger number of studies have been disclosed with group IV based MOCs in comparison to other elements like lanthanides and late transition metals, most likely due to their good overall stability and easily isolated structures.[47-50] Thus, the unique properties of group IV based MOCs can be used to illustrate key principles that shall support the development of MOCs based on metals that have been little explored so far.

To this end, we review the current state of the art in Zr oxo, Hf oxo, Ti oxo clusters. Titanium, Zirconium, and Hafnium present several similarities between them. They all have +4 oxidation state (d^0 configuration) as the most common one, which imparts a strong Lewis acidity to these cations. Such Lewis acidity makes their intrinsic reactivity challenging to control, given that minor amounts of water can react with the metallic species in solution, forming stable metal-oxygen bonds. Consequently, their organometallic complexes usually require handling under strict inert atmosphere to avoid decomposition, which shadows their utility to activate organic substrates towards useful transformations. In this sense, many compounds, including the metal oxo clusters discussed in this review, have been devised over the decades in order to understand, control and leverage this reactivity in a fruitful manner. Notably, such demand grew rapidly in the last few years due to their relative high abundancy compared to late transition metals and rare-earth elements.[51]

On the other hand, Titanium, Zirconium, and Hafnium have important intrinsic differences, such as for example their atomic size, that likely influence their reactivity. Titanium is the smallest in the series, with an atomic radius of 140 pm, while both Zr and Hf's have atomic radius of 155 pm, even though Hf is one row below Zr in the periodic table.[52] In line with their atomic size, Ti(IV) ions in the clusters favor (with few exceptions) an octahedral 6-

coordinated ligand sphere. In contrast, Zr(IV) and Hf(IV) centers usually vary between 7- or 8-coordination sphere. Another difference is the M-O bond strength between these elements, which increases in the order of Ti < Zr < Hf.[53] This difference in bond strength might play a role in the cluster synthesis and solution dynamics. For example, Ti oxo clusters have a richer dynamics in solution due to the relative facile ligand exchange, which can even involve complete rearrangement of the metal oxo core structure. This flexibility, which makes challenging to rationalize their synthesis routes, might result from the weaker Ti-O bond compared to Zr-O and Hf-O bonds. Accordingly, Zr and Hf oxo clusters are more prone to preserve their inorganic core, and ligand exchange rarely causes the clusters to collapse. Besides ligand exchange, metal-oxygen bond strength seems to also influence cluster synthesis. For example, Hf compounds usually require heating in aqueous solutions to favor the formation of oxo clusters, imparting easier control over the products formed. Between Ti and Hf, Zr seems to present a good balance between reactivity and cluster stability allowing for great exploration of oxo cluster formation, as clearly observed by the larger number of examples reported for Zr clusters in comparison with Hf.

In the following sections, we discuss the chemistry of group IV MOCs first by introducing their structures, and pointing out the similarities and differences among them. Moreover, we present the reaction conditions in which they are formed in order to give an overview of key factors driving the formation of a specific cluster structure, such as the stoichiometric ratio between metal precursors and ligands.

At first, we introduce the Zr oxo clusters (ZrOC). These compounds have essentially been prepared by two distinct approaches, which differ by the aqueous or organic nature of the reaction medium. For aqueous solutions, sulfate and peroxide are common capping ligands, and their concentration clearly affects the reaction outcome. On the other hand, organic solutions were found to conveniently provide some control over the remarkable tendency of these tetravalent ions to hydrolyze even in very acidic aqueous solutions.[54] This resulted in the formation of several discrete ZrOCs,[55] featuring nuclearities from 3 to 26 Zr atoms. Moreover, the relatively well-established and structural stability of tetra-, hexa- and dodecanuclear clusters enabled a more detail study of the ligand sphere dynamics, including examples of clusters with mixed-carboxylate ligands.[56] We will highlight how the composition and structure of these ZrOCs depends on the metal alkoxide, the carboxylic acid, and the stoichiometric ratio between them.[56, 57]

Following the detail discussion about ZrOCs, Hf oxo clusters (HfOCs) that have been described to date are discussed in the second part. HfOCs are generally formed at higher temperature than ZrOCs in aqueous conditions, while the few HfOC synthesized in organic medium have been obtained under essentially the same conditions used for ZrOC. The great similarity between the cluster shapes, metal coordination numbers and chemical properties, results in HfOCs being often isomorphous to the ZrOCs. The similar reaction conditions used for the synthesis of these clusters likely entails from the similar atomic sizes and chemical properties of Hf^{4+} and Zr^{4+} ions.[1, 58] Moreover, we will discuss also HfOCs such as the nonamer and the undecamer, which have been only observed when hafnium was used as the source of metal, and have no known Zr counterpart described yet.[58]

In the last section, given that structure and applications of Ti oxo clusters (TiOCs) has been reviewed in detail recently,[40, 59, 60] we present only selected representative TiOCs to emphasize their distinct properties such as photocatalytic and redox abilities, and also their prominent role as building units of well-defined nanostructured composites. Moreover, since the coordination mode and chemical reactivity of Ti^{4+} is different from those of Hf^{4+} and Zr^{4+}, the similarities and differences between Ti-oxo and Zr/Hf-oxo clusters are briefly discussed.

2. Structure and properties of Zirconium oxo clusters (ZrOC)

2.1 Formation of Zr oxo cluster in aqueous medium and their chemical relationship

The tetrameric structure $\mathbf{[Zr_4(OH)_8(OH_2)_{16}]^{8+}}$ is the primary hydrolysis product when $ZrOCl_2 \cdot 8H_2O$ salt is dissolved in water. A crystal with the composition of $\mathbf{[Zr_4(OH)_8(OH_2)_{16}]Cl_8} \bullet 12H_2O$ was first isolated and analyzed using single-crystal X-ray diffraction by Clearfied *et al*, which disclosed a tetragonal crystal structure in which the four zirconium atoms were located at corners of a square.[61] Later, a tetrameric zirconium cluster was also isolated in a supramolecular complex with cucurbituril.[62] Patterson and Fourier projections, from which the distribution of the interatomic vectors in the structure can be obtained, illustrates that the metal ions are connected through double hydroxo bridges, and that four water molecules are bound to each zirconium to complete a distorted square

antiprismatic configuration (Figure 1a).[61] The viscosity measurements of the zirconyl chloride solutions showed that the formation of larger polymeric structures was generally not favored.[61] Increasing pH and refluxing the zirconyl chloride solution can lead to additional polymerization of tetramers. Such polymerization results in two-dimensional sheet-like structures that turn into amorphous gels or precipitates with monoclinic or tetragonal phases, but the formation of species other than tetramers has not been postulated.[63]

Early observations about the formation of other structures depending on the pH were consistent with later measurements by small-angle X-ray scattering (SAXS),[64] which have shown that **$[Zr_4(OH)_8(H_2O)_{16}]^{8+}$** is in equilibrium with an octameric species depending on the acidity of the $ZrOCl_2$ solution. After considering the effect of chloride ions on the scattering intensity, the calculated scattering curves of tetrameric **$[Zr_4(OH)_8(OH_2)_{16}Cl_6]^{2+}$** and octameric **$[Zr_8(OH)_{20}(H_2O)_{24}Cl_{12}]$** (**$Zr_8$** cluster) species were scaled to the experimental curve. According to SAXS measurements, in a highly acidic solution ($[H^+]$ > 0.6M) the tetramer is the main species present in solution. Upon lowering the acid concentration, the octamer starts to form by stacking of two tetramers on top of each other with four single OH^- bridges, and it becomes the most dominant species when $[H^+]$ ≤0.05M. Further indication of octamer formation stemmed from the radius of gyration (the root-mean-square distance of all scattering elements from the center of the gravity), which has been determined to be 3.7 Å for the tetramer, while the value for the octamer was around 5.0 Å, suggesting that larger polynuclear species were formed.[64] However, despite being identified in solution, the octamer has not been isolated yet.

Reacting the primary tetramer **$[Zr_4(OH)_8(H_2O)_{16}]^{8+}$** with different ligands, namely the Kläui Tripodal ($[CpCo\{P(O)(OEt)_2\}_3]^-$, L_{OEt}) and peroxide ligands, led to the isolation of new structures (Figures 1b and 2a, respectively). Dilution of a HNO_3 solution containing $Zr(NO_3)_4$ and NaL_{OEt} provided Kläui Tripodal capped tetranuclear **$[(L_{OEt})_4Zr_4(\mu_3\text{-}O)_2(\mu\text{-}OH)_4(H_2O)_2]$**$(NO_3)_4$ (**Zr_4-1** cluster, Figure 1b). In this structure, the three aqua ligands bound to each zirconium in the **$[Zr_4(OH)_8(H_2O)_{16}]^{8+}$** are replaced by one Kläui Tripodal ligand, and four of the original hydroxo bridges are replaced by two μ_3-O ligands, thereby reducing the coordination number of two zirconium atoms from eight to seven. **Zr_4-1** cluster decomposed to mononuclear species when the pH <1. Moreover, this cluster hydrolyzed (4-$NO_2C_6H_4O)_2P(O)OH$ (BNPP) in 2.5 h, forming **$[(L_{OEt})_4Zr_4(\mu_3\text{-}PO_3)_4]$** (**$Zr_4$-2** cluster), which has intercalated Zr and P atoms at the corners of a cube (volume ~41 $Å^3$) with O atoms at the middle of the edges (Figure 1c).[65] Attempt to independently synthesize **Zr_4-2** cluster by adding Na_3PO_4 to the original solution led to isolation of a distinct trinuclear cluster with the

formula of **[(L_{OEt})$_3$Zr$_3$(μ$_3$-O)(μ-OH)$_3$(μ$_3$-PO$_4$)]**(NO_3), in which zirconium atoms are seven-coordinated by one μ$_3$-LOEt, two μ$_2$-OH, one μ$_3$-O_2- and one μ$_3$-PO_4^{3-}.[65]

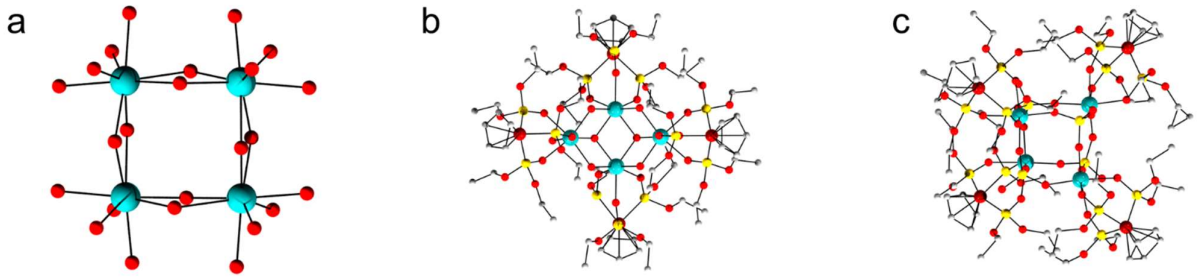

Figure 1. (a) Ball and stick representation of **[$Zr_4(OH)_8(H_2O)_{16}$]$^{8+}$**. (b) Ball and stick representation of **[(L_{OEt})$_4$$Zr_4$(μ$_3$-O)$_2$(μ-OH)$_4$]$^{4-}$** (**$Zr_4$-1** cluster). (c) Ball and stick representation of **[(L_{OEt})$_4$$Zr_4$(μ$_3$-$PO_3$)$_4$]** (**$Zr_4$-2** cluster). Color code: Zr (teal), O (red), P (gold), C (light gray). L_{OEt} = [CpCo{P(O)$(OEt)_2$}$_3$]$^-$. Hydrogens omitted for clarity.

Addition of peroxide ligands to a solution of **[$Zr_4(OH)_8(OH_2)_{16}$]$^{8+}$** induced its transformation to tetrahedral **[$Zr_4(OH)_4$(μ-O_2)$_2$(μ$_4$-O)(H_2O)$_{12}$](ClO_4)$_6$•4H_2O** (**Zr_4-3**).[66] This tetrameric cluster is formed from a 10:1 peroxide/Zr solution that slowly evaporates over 20 days, through the disassembly and reassembly of the **[$Zr_4(OH)_8(OH_2)_{16}$]$^{8+}$**. According to the single-crystal X-ray diffraction study, **Zr_4-3** has C_2 symmetry in which the zirconium coordinates eight oxygen atoms with a distorted square antiprism geometry (Figure 2a). The edges of Zr-tetrahedron are connected by four hydroxyl and two peroxide ligands. ESI-MS analysis in methanol and water gave evidence for the existence of other species like Zr_3, Zr_5, and Zr_6, which interestingly, had different charge depending on the solvent. These species exhibit negative charge in methanol and the positive charge in water, which is consistent with the strong Lewis-Brønsted acid behavior of Zr^{4+}.

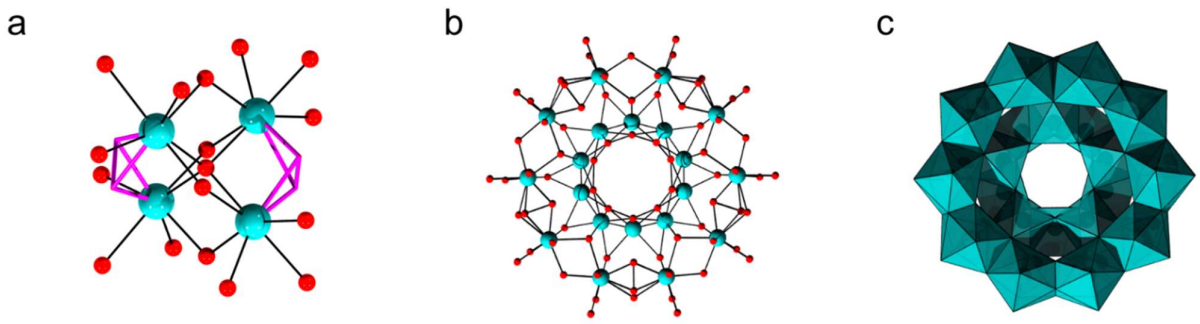

Figure 2. (a) Ball and stick representation of **$[Zr_4(OH)_4(\mu\text{-}O_2)_2(\mu_4\text{-}O)(H_2O)_{12}](ClO_4)_6 \cdot 4H_2O$** (**$Zr_4$-3** cluster)**.** (b) Ball and stick and (c) polyhedron representation of **$[Zr_{25}O_{10}(OH)_{50}(O_2)_5(H_2O)_{40}](ClO_4)_{10} \cdot xH_2O$** (**$Zr_{25}$** cluster). Color code: Zr (teal), O (red), peroxide (pink wires), {ZrO_8} (teal). Hydrogen and chloride atoms omitted for clarity.

$[Zr_{25}O_{10}(OH)_{50}(O_2)_5(H_2O)_{40}](ClO_4)_{10} \cdot xH_2O$ (**Zr_{25}** cluster) was isolated from a similar system used for the synthesis of **Zr_4-3.**[66] A mixture of 1:1 peroxide acid and zirconium carbonate in aqueous solution was slowly evaporated over 4 days, yielding crystals of **Zr_{25}** cluster. The reaction pathway involves disassembly and reassembly reaction of **$[Zr_4(OH)_8(OH_2)_{16}]^{8+}$**, which is partially reversible depending on the solution pH. Single-crystal X-ray diffraction shows that the pentagonal topology of this cluster contains an inner five-membered ring connected to the outer ring via μ_3-oxo and hydroxyl groups (Figure 2b). The inner Zr atoms are connected via two bridging hydroxyl groups, and the external ring consisting of five tetrameric units are linked together by disordered peroxo and hydroxyl groups. All the zirconium atoms have the same square antiprism coordination geometry. **Zr_{25}** cluster assembles in an orthorhombic space group C_{mcm} oriented along a bidimensional plane with an interlayer distance of 6Å between adjacent planes. Curiously, the **Zr_{25}** cluster is completely soluble in common organic solvent such as MeOH and DMF, and comparison between simulated and experimental SAXS data for these solutions strongly suggests the **Zr_{25}** structure remains intact upon dissolution. On the other hand, ESI-MS spectrum of **Zr_{25}** methanolic solution is dominated by Zr_8 clusters, which were only observed in negative mode, probably resulting from ionization-promoted fragmentation. ESI-MS analysis of aqueous **Zr_{25}** in positive mode predominantly detected Zr_3 and Zr_5 species.[66]

2.1.1 Effect of sulfate on the formation of ZrOC

In general, the addition of sulfate anions to Zr solutions leads to the formation of larger Zr oxo clusters, which can be also isolated from solution after crystallization. Based on the methods reported so far, it is clear that the amount of sulfate influences the degree of condensation. In general, lower concentration of sulfate affords larger clusters, while the higher amounts of sulfate tend to inhibit the condensation of discrete ZrOC (similar behavior is also observed for the formation of HfOC, see discussion on Hf section below), though the increase of the temperature may promote the formation of clusters with higher nuclearity.[67, 68] The specific role of sulfate is still under debate. It has been suggested that the sulfate anions can disrupt the Zr tetramers which form when Zr^{4+} first dissolve in water, affording mono-/dimeric species that would more easily condense into larger clusters.[1] Moreover, the greater extension of Zr-sulfate oligomers condensation resulting in larger clusters would be facilitated by the charge balancing effect of anionic sulfate groups. This effect would lead to a lower positive surface charge of the particles that would decrease the electrostatic repulsion between them.[69] On the other hand, increasing amounts of sulfate would gradually replace the Zr-(OH_2)-Zr bridges, disfavoring the formation of large clusters in favor of oligomeric Zr-SO_4 structures.[1]

A pinwheel shaped molecule, **$[Zr_{17}O_8(OH)_{24}(OH_2)_{12}(HCOO)_{12}(SO_4)_8]$**•6HCl·30$H_2O$ (**Zr_{17}** cluster), is produced in the form of colorless octahedral crystals at room temperature by evaporation of an aqueous solution consisting of $ZrOCl_2$•8H_2O, H_2SO_4 and HCOOH, in which [H_2SO_4] < 0.15 M.[70] This cluster can also be prepared through hydrothermal treatment of the same solution at 40 to 100ºC by sealing the reaction mixture with a rubber stopper.[70] Single-crystal X-ray diffraction shows that heptadecameric **Zr_{17}** cluster adopts S4 symmetry, with the size of 'square shape' measuring 17Å (Figure 3a), and having the core composed of four {Zr_5} building blocks. Each zirconium is coordinated by eight oxygen atoms, and the terminal oxygen atoms are doubly protonated based on the bond valence sum calculation. The sulfate groups chelate to the exterior of the Zr oxo core through a bidentate coordination mode, and the cluster affinity for water molecules is suggested to contribute for the enhanced ionic conductivity of **Zr_{17}** in comparison to smaller **Zr_6** clusters of similar composition that were obtained under similar reaction conditions (Figure 4).[70]

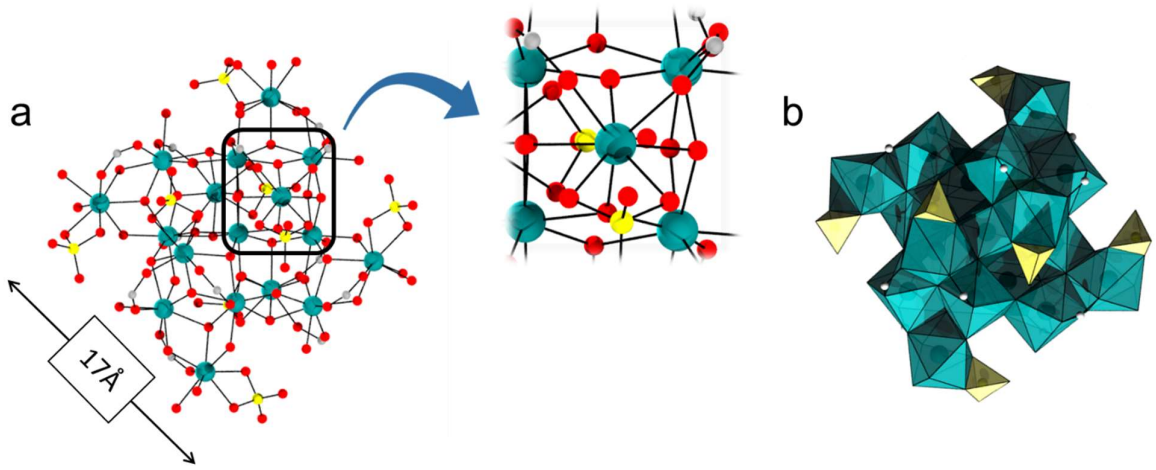

Figure 3. (a) Ball and stick representation of the structure **[$Zr_{17}O_8(OH)_{24}(OH_2)_{12}(HCOO)_{12}(SO_4)_8$]**•6HCl·30$H_2O$ (**Zr_{17}** cluster) with a zoom of the {Zr_5} building block. (b) The polyhedral arrangements of the **Zr_{17}** cluster. Color code: Zr (teal), O (red), {ZrO_8} (teal), {SO_4} (yellow). Hydrogen atoms omitted for clarity.

Interestingly, a new compound, **[$Zr_6O_4(OH)_4(OH_2)_8(HCOO)_4(SO_4)_4$]**, was obtained from the same solution when the concentration of H_2SO_4 was higher than 0.15 M (Figure 4). This hexanuclear cluster has an octahedral $[Zr_6O_4(OH)_4]^{12+}$ core, similar to other Zr_6 clusters commonly formed in organic medium (Figure 9). A study of reaction conditions revealed that the nature of final products was influenced both by the concentration of H_2SO_4 and temperature. At high temperatures (90-100 ºC), only larger clusters with higher condensation degrees on the order of 17mer were formed. At lower temperatures, the larger cluster was favored when the concentration of sulfate was lower than 0.10 M, regardless of the concentration of formic acid. When the concentration of sulfate increases to 0.15 M, the hexamer was formed, suggesting that sulfate passivates the cluster surface, inhibiting further aggregation.[70]

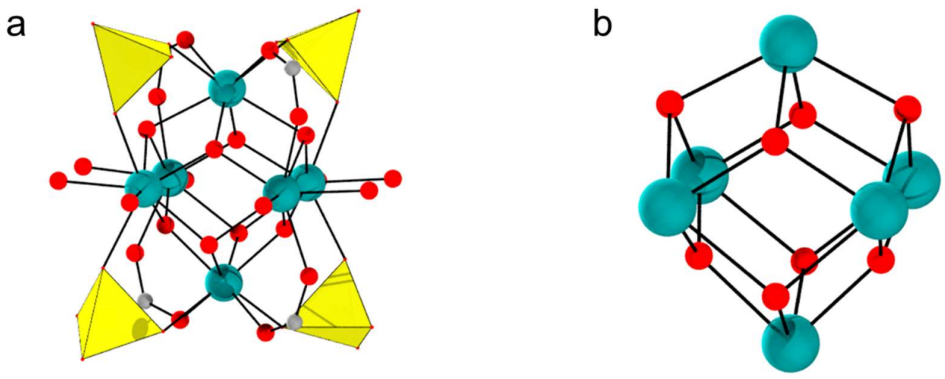

Figure 4. (a) Ball and stick representation of **$[Zr_6O_4(OH)_4(OH_2)_8(HCOO)_4(SO_4)_4]$**. (b) The structure of $[Zr_6O_4(OH)_4]^{12+}$ core of cluster in (a). Color code: Zr (teal), oxygen (red), {SO_4} yellow. Hydrogen atoms omitted for clarity.

In the absence of formic acid, **$[Zr_{18}O_4(OH)_{38.8}(SO_4)_{12.6}]\bullet 33H_2O$**, a **$Zr_{18}$** cluster crystallizes out of acidic solutions diluted with $HClO_4$ or HCl, when the Zr:SO_4 molar ratio is around 1:0.6.[1, 71] On the outer sphere of this discrete compound there is a ring of ten Zr atoms connected by oxide or hydroxide bridges. In the center, an octahedral Zr hexamer shares opposite edges with two Zr pentamers. Based on the single-crystal X-ray structure, the hexagonal crystals connect to the remaining Zr via μ_2-hydroxo, μ_3-hydroxo/oxo, and μ_4-oxo (Figure 5b). The crystal structure also reveals that 16 Zr atoms are coordinated by eight oxygen atoms with square anti-prismatic or dodecahedral geometry while the remaining two are coordinated by seven oxygen atoms (dark blue in Figure 5b) adopting capped trigonal prismatic geometry. The sulfate anions located at the perimeter have little influence on the Zr framework and adjacent 18mer clusters are linked into chains via bridging bidentate sulfate anions. [1, 71]

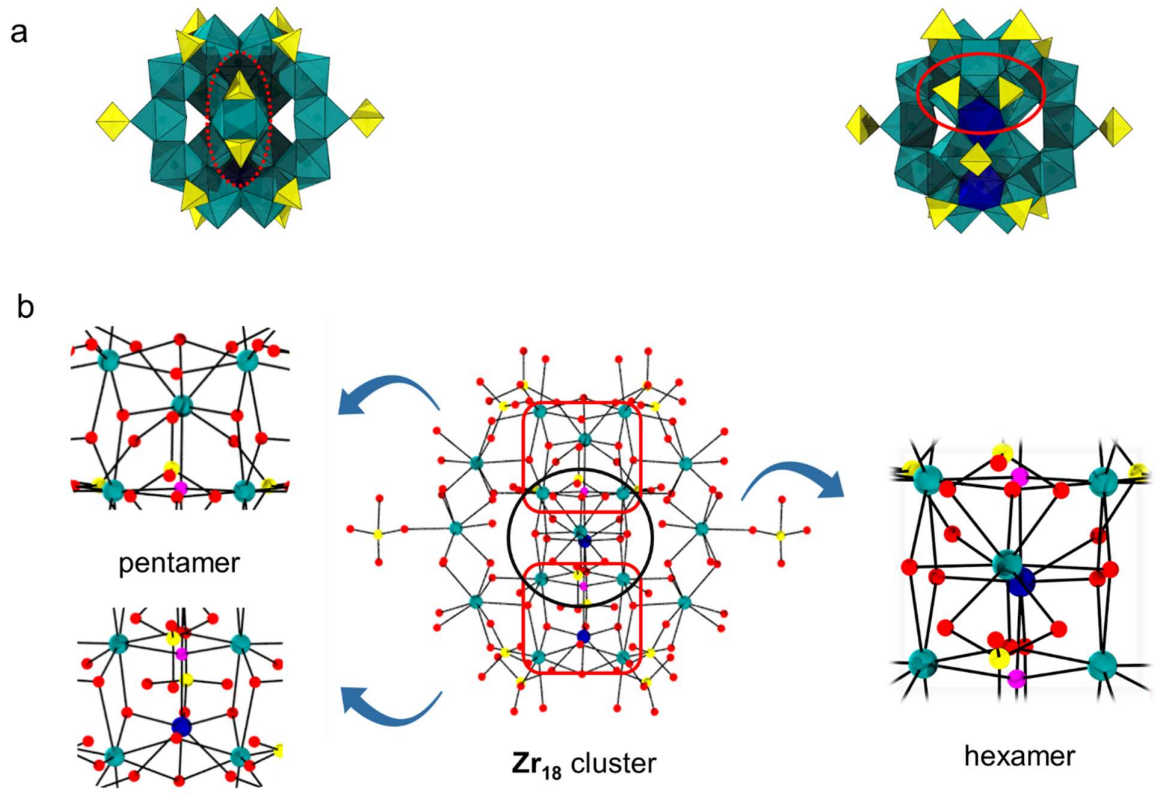

Figure 5. (a) Front and back views of polyhedron representation of **$[Zr_{18}O_4(OH)_{38.8}(SO_4)_{12.6}]$•$33H_2O$** (**$Zr_{18}$** cluster). Chelating sulfate ligands are highlighted by red dashed circle and tridentate sulfate ligands by red solid circle. (b) Ball and stick representation of **Zr_{18}** cluster featuring insets with hexamer (black circle) and pentamer (red squares) building block structures. Color code: Zr (teal), oxygen (red), μ_4-oxo (pink), {ZrO_8} teal, {ZrO_7} dark blue, {SO_4} yellow. Hydrogen atoms omitted for clarity.

The **Zr_{18}** cluster mentioned above was the largest species crystallized from aqueous sulfate-containing solutions until toroidal **$Zr_{70}(SO_4)_{58}(O/OH)_{146}.x(H_2O)$** (**$Zr_{70}$**) cluster was isolated from solutions with an excess of sulfate (Zr:SO_4 molar ratio 1:~2.1) in the presence of several metal nitrates as co-crystallization agents.[68] The solutions were hydrothermally reacted (185 ℃) for 24 h before resting at ambient conditions to afford the final compound. Common structural features observed between **Zr_{18}** and the **Zr_{70}** clusters, and the similar final Zr:SO_4 molar ratio observed for both products suggest that the higher temperature induces further oxolation of oligomeric species leading to the formation of larger species. **Zr_{70}** cluster structure shows a pseudo-10-fold rotational symmetry with repeating **Zr_6** sub-units bridged by an additional Zr center in the outer rim. Zr units are connected by two tridentate sulfates parallel to each other in the inner rim, while in the outer rim 4 to 5 Zr-Zr pairs are linked by

bridging bidentate sulfate, leaving these Zr atoms hepta-coordinated. Monodentate sulfates have been observed on the side of the torus for all structures obtained. Interestingly, the co-crystallizing species influenced the observed packing mode, and a permanent porosity was observed when a tetragonal phase was obtained (BET surface area of 241 m^2g^{-1}). **Zr_{70}** cluster exhibits very poor solubility in water and in ethanol.

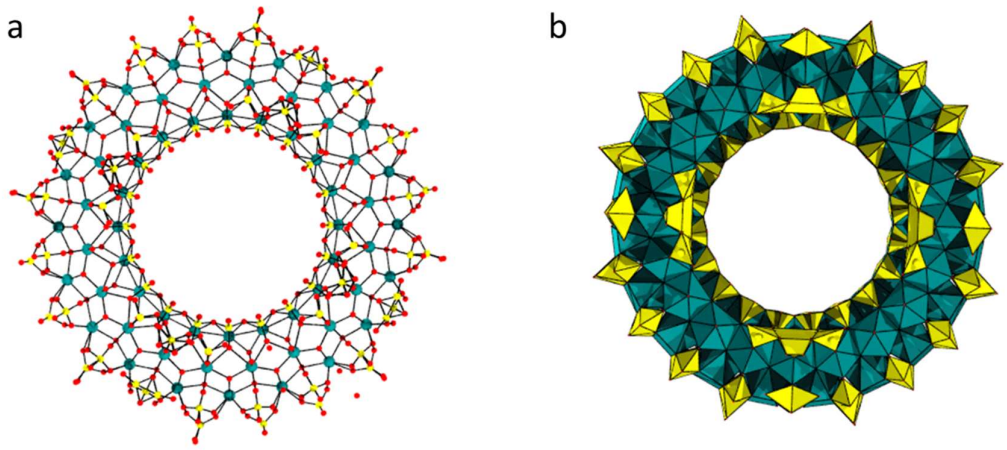

Figure 6. (a) Ball and stick and (b) polyhedron representation of **$Zr_{70}(SO_4)_{58}(O/OH)_{146}.x(H_2O)$** (**$Zr_{70}$** cluster). Color code: Zr (teal), O (red), S (yellow). Hydrogen atoms omitted for clarity.

2.1.2 Summary of ZrOC formation in aqueous systems

Based on the formation of ZrOC in aqueous solution discussed in this section, we developed a roadmap for the synthesis of these clusters, which could be used to direct the formation of novel structures (Scheme 1). In general, the Zr-tetramer **$[Zr_4(OH)_8(OH_2)_{16}]^{8+}$** is ubiquitous in acidic solutions. However, the introduction of different ligands leads to the formation of diverse compounds. For example, comparing the formation reactions of **Zr_{17}** and **Zr_{18}**, the sulfate concentration used for **Zr_{17}** synthesis is lower than for **Zr_{18},** even though the sulfate will generally suppress the condensation to a larger cluster. This might be due to the addition of carboxylates to the system that afforded **Zr_{17}**, which could help to inhibit the formation of larger clusters in the presence of lower amounts of sulfate. Furthermore, the concentration of the ligands also plays a role in the final product structure. For example, a 1:1 ratio of peroxide acid/zirconium source results in **Zr_{25}** cluster, while a ratio of 10:1 of peroxide acid/zirconium source leads to **Zr_4-1**. Meanwhile, sulfate has been also shown to inhibit the

condensation of the clusters, as an increase of sulfate concentration leads to the decrease of the nuclearity from 17/18 to 6. Finally, the synthesis of **Zr_{70}** cluster shows that further tuning might be achieved by varying the temperature, with higher nuclearities obtained at higher temperatures without significant change in the nature of the ligand and/or its concentration.

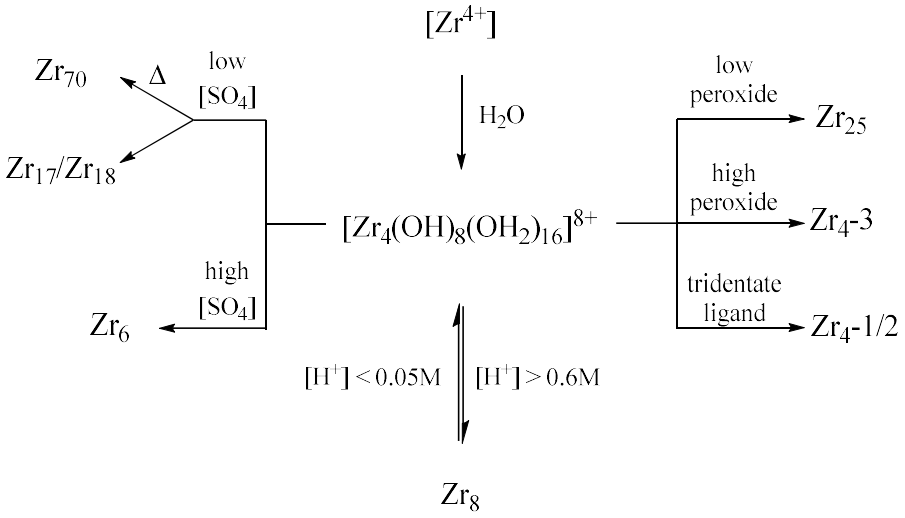

Scheme 1. Chemical relationship between the ZrOCs discussed in this section, and the key factors influencing the structure of the cluster obtained.

2.2 Formation of Zr oxo clusters in organic medium: interplay between alkoxy and carboxylate ligands

Formation of ZrOC is not restricted to aqueous solutions, as several examples of ZrOC prepared in organic solvents have been reported. However, instead of sulfate or peroxide ligands, alkoxy and carboxylate moieties have been predominantly used to stabilize the ZrOC formed. One of the main assets of the reactions in organic medium is their dependence on the condensation between organic species (e.g., the organic part of the precursor and the solvent), which could allow some control of the reactivity in future works. In aqueous solution, hydrolysis and condensation reactions responsible for the formation of M-O-M bonds, and subsequently MOCs, are directly mediated by the aqueous solvent. For the reactions in the organic medium, clusters are presumably formed by a three-step mechanism, in which the second step involves formation of water. This is presumably a key step, since the water

necessary to trigger metal hydrolysis and condensation is formed upon reaction of the carboxylate ligands and the alcoholic solvent to give an ester by-product (Scheme 2).[72, 73]

$$(R^1O)_nM + mHOOC\text{-}R^2 \rightleftharpoons (R^1O)_{n-m}M[OOC\text{-}R^2]_m + m\ R^1OH \quad (1)$$

$$R^1OH + HOOC\text{-}R^2 \rightleftharpoons R^1OOC\text{-}R^2 + H_2O \quad (2)$$

$$(R^1O)_{n-m}M[OOC\text{-}R^2]_m + H_2O \rightleftharpoons M_wO_x(OR^1)_y[OOC\text{-}R^2]_m \quad (3)$$

Scheme 2. A three-step mechanism for the formation of carboxylate-based clusters, R = alkyl group, R^1,R^2 = alkyl, alkenyl or aryl.

In organic medium, Zr alkoxides (e.g., $Zr(OPr)_4$, $Zr(OBu)_4$) are commonly used as a Zr source, and clusters containing 3 to 26 zirconium centers have been reported using mostly carboxylic acids as ligands, though other ligands have been also used. Carboxylated tetra-, hexa- and dodecanuclear Zr oxo clusters (**Zr_4**, **Zr_6**, **Zr_{12}** clusters, respectively) have been more commonly reported, while other structures remain largely unexplored as a whole. Given its apparent greater stability and easier formation, the more numerous **Zr_6** and **Zr_{12}** clusters based on octahedral Zr oxo cores provided opportunities to study the ligand-exchange dynamics of these species and probe the formation of mixed-carboxylate species. Though these findings have yet to be experimentally extended to other clusters, they provide a useful platform for further developing the metal oxo cluster chemistry. In this section, we initially introduce known structures, which were organized by nuclearity, and then present an overview about the ligand exchange in **Zr_6** and **Zr_{12}** clusters.

Zr_3 Clusters: **$[Zr_3(\mu_3\text{-}O)(DMPD)_4(DMPDH)_2]$** (**$Zr_3$-1**) ($DMPDH_2$= 2,4-dimethylpentane-2,4-diol) is synthesized by reacting of $Zr(O^nPr)_4$ with 2,4-dimethylpentane-2,4-diol in toluene at room temperature. This Zr_3 cluster features a central μ_3-O within the plane formed by three Zr atoms, which were each additionally capped by one chelating DMPD moieties on one side of the plane (two of the DMPD were monoprotonated), and by another chelating-bridging DMPD group on the other side.[74] Similarly, **$[(Cp_2Zr)_3(\mu_2\text{-}OH)_3(\mu_3\text{-}O)]$**($BPh_4$) has been obtained by hydrolyzing [Cp_2ZrCH_3(tetrahydrofuran)](BPh_4) with a 5-fold excess of H_2O in dichloromethane/tetrahydrofuran at -78 °C. This cluster is approximately C_{3v} symmetric and features the same O-centered Zr_3 plane of **Zr_3-1**, with two Cp ligands bound to each Zr (Figure

7a), and surrounded by three H-bonded tetrahydrofuran molecules.[75] Variants of this Cp-containing cluster having a carboxylate ligand bridging the Zr centers instead of only oxygen atoms have also been reported (Figure 7b).[76] Later using the carboxylates proved to be valuable for the assembly of supramolecular cages, either by a carboxylate exchange step[77] or by having another metal coordination site in the carboxylate moiety and then combining it with other metals.[78]

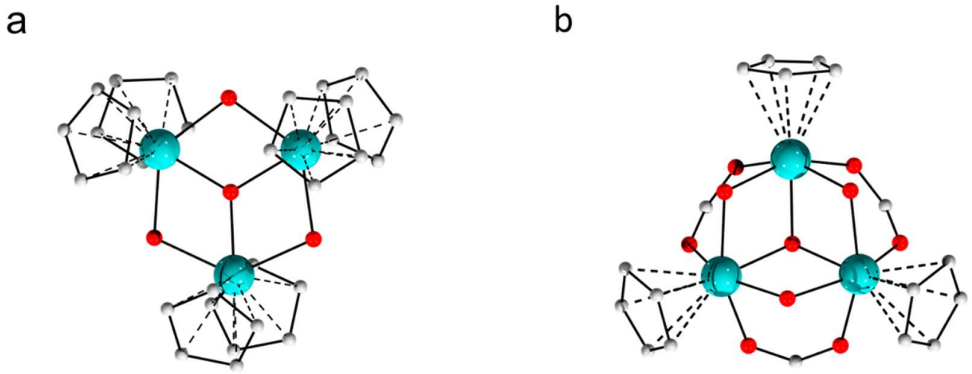

Figure 7. Ball and stick representation of (a) **$[(Cp_2Zr)_3(\mu_2\text{-}OH)_3(\mu_3\text{-}O)]^+$** and (b) **$[(CpZr)_3(\mu_2\text{-}OH)_3(\mu_3\text{-}O)(OOCH)_3]^+$**. Color code: Zr (teal), O (red), C (light gray). Hydrogen atoms omitted for clarity. Cp = cyclopentadienyl.

Interestingly, a trinuclear Zr oxo cluster featuring a similar planar O-centered Zr_3 core has formed in the binding cleft of bacterial transferrin protein when $[Zr(NTA)_2]^{2-}$ (NTA = N,N-bis(carboxymethyl)glycine) was reacted with the apo-protein in a HEPES buffer solution (HEPES = 2-(4-(2-hydroxyethyl)-1-piperazinyl)ethanesulfonic acid) at pH 7.4 containing phosphate as synergistic anion. Crystal structure showed all the zirconium to be seven-coordinated with the coordination sphere being completed by two oxygen atoms of tyrosine residues of the protein, water and phosphate.[79]

Zr_4 clusters: **$[Zr_4O_2(OMc)_{12}]$** (OMc = methacrylate) is the reaction product of $Zr(O^nPr)_4$ solution in *n*-propanol and a 15-fold excess of methacrylic acid.[57] This cluster has non-symmetric butterfly shape with a distorted arrangement of the Zr centers, which contrasts the planar arrangement of Zr atoms observed for the solid state structure **$[Zr_4(O^nPr)_{16}]$** of $Zr(O^nPr)_4$ (Figure 8a).[80] Three Zr atoms of the **$[Zr_4O_2(OMc)_{12}]$** cluster are coordinated by

eight oxygen atoms while the remaining one is seven coordinated. Two carboxylate ligands chelate two Zr [Zr(2) and Zr(3)] atoms and nine carboxylate ligands bridge Zr-Zr edges, except for the edge between Zr_1 and Zr_4. The remaining carboxylate not only chelates to Zr(4) atom, but also coordinates to Zr(2) via the oxygen [O(41)] (Figure 8c). An isomer of **$[Zr_4O_2(OMc)_{12}]$** with a planar rhombic Zr_4 core is obtained with only a seven fold excess of methacrylic acid, prompting methacrylate ligand containing [O(41)] to convert to a bridging mode, which makes the structure symmetric. Both isomers provide the same NMR spectra in solution, suggesting they interconvert in solution.[81] Notably, when acetylacetone was added to a solution of **$[Zr_4O_2(OMc)_{12}]$**, the core of the cluster was completely degraded to monomeric species.[82] Finally, formation of tetranuclear ZrOCs has also been observed as the hydrolysis products of dinuclear Zr complexes.[83, 84]

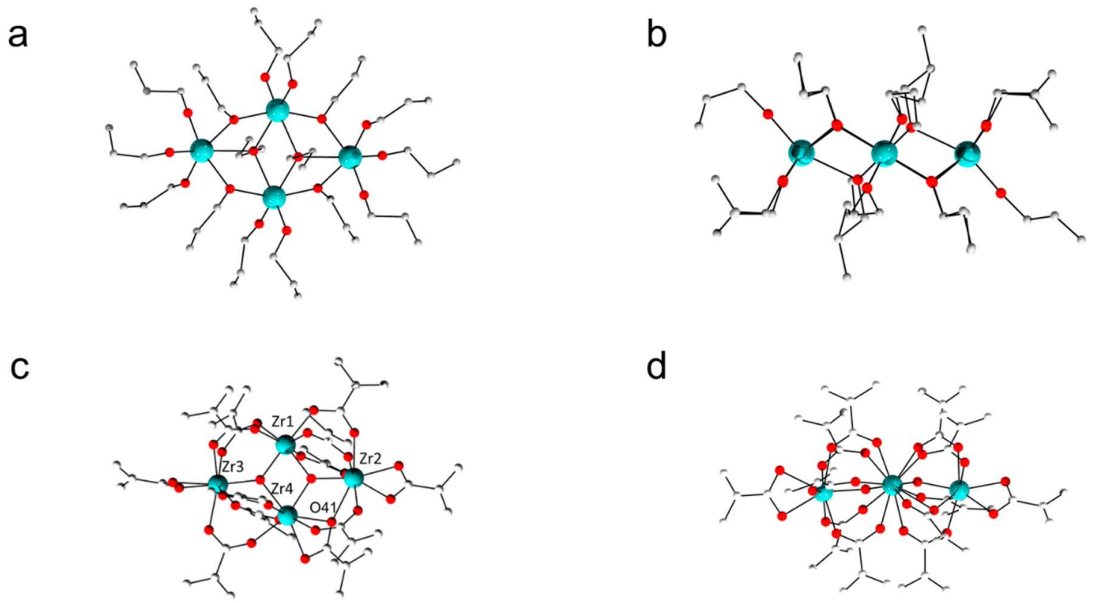

Figure 8. (a) Top and (b) side view of tetramer **$[Zr_4(O^nPr)_{16}]$**. (c) Top and (d) side view of **$[Zr_4O_2(OMc)_{12}]$** cluster. Color code: Zr (teal), O (red), C (light gray). Hydrogen atoms omitted for clarity. OMc = methacrylate.

Zr_5 cluster. Although isobutyric acid has been shown to provide a **Zr_6** cluster, the reaction of $Zr(O^nPr)_4$ with 4 equivalent of 2-bromoisobutyric acid resulted in the formation of the only **Zr_5** cluster reported so far.[55] Curiously, **$[Zr_5O_4((CH_3)_2BrCCO_2)_{10}(O^nPr)_2(^nPrOH)_4]$** cluster

structure can be regarded as an {Zr_6} octahedron with a missing Zr center, which suggests that the additional steric hindrance posed by the replacement of H by Br hampered the accommodation of a sixth metal in the structure, given that a **Zr_6** cluster having isobutanoate ligands has been reported (Table 1). Such additional hindrance might also be responsible for the unusual monodentate coordination of some carboxylates to **Zr_5**, since they usually coordinate **Zr_6** clusters in a chelating or bridging mode. Visual inspection of the structure suggested the bromine groups are exposed on the cluster surface, rendering them amenable to further transformations. Such reactivity has been showcased by **Zr_5** use as macro initiator in an atom transfer radical polymerization that afforded inorganic-organic core-shell nanoparticles.

Zr_6 clusters: Essentially three groups of **Zr_6**-carboxylate clusters have been reported in the literature, those featuring an octahedral Zr_6O_8 core being the most prevalent. Additionally, open structures bridging two trimeric units have also been observed, and recently a stacked variant of this bridged structure has been disclosed. However, the use of other ligands such as phosphates or ligand containing additional coordinating groups have generated unique structures, showing that several factors may influence the final cluster structure. Our discussion below emphasizes the most comonly studied octahedral structures, and then highlights the other two groups of **Zr_6** clusters.

The oxo zirconium methacrylate clusters **$[Zr_6(OH)_4O_4(OMc)_{12}]$** (OMc = methacrylate) crystallizes when $Zr(O^nPr)_4$ is reacted with a 4-fold excess of methacrylic acid (OMc) in n-propanol for one day.[57, 72] Analysis by X-ray diffraction shows that all Zr atoms have an octahedral arrangement. The compound has a C_{3v} symmetry with C_3 axis passing through the center of opposite faces of the octahedron (Figure 9a). The triangular faces of the Zr_6 core are capped by alternate μ_3-O and μ_3-OH ligands. From the twelve methacrylate ligands, three chelate the zirconium atoms [Zr(1), Zr(2), Zr(3)] of one μ_3-O capped face and nine carboxylate groups bridge all the edges of the Zr_6 core apart from the ones in the chelated face (Figure 9b). Each zirconium is square-anti prismatically coordinated by eight oxygen atoms. NMR and HPLC analysis indicated fast formation of the ester in solution, which is presumably catalyzed by the Zr alkoxide, consistent with the mechanism proposed in Scheme 2.[72]

When the ratio of methacrylic acid to $Zr(O^nPr)_4$ is increased to 9:1, the cluster **$[Zr_6(OH)_4O_4(OMc)_{12}(^nPrOH)]$**•3McOH is formed, in which one bridging methacrylic acid ligand becomes monodentate, and the vacant site on the Zr is occupied by a propanol molecule (Figure 9c).[85] The methacrylic acid molecules not coordinated to Zr are hydrogen-bonded to cluster's periphery, and help stabilizing the structure. When $Zr(O^nBu)_4$ is reacted with seven equivalents of iso-butyric acid, **$[Zr_6O_4(OH)_4$(*iso*-butanoate)$_{12}(H_2O)]$** forms with a water molecule capping the coordination site 'opened' by conversion of one of the bridging carboxylates into a monodentate ligand.[56] Likewise, other related clusters were obtained using similar conditions. For example, **$[Zr_6(OH)_4O_4(BzO)_{12}(BzOH)]$**•4BzOH (BzO = benzoate) was obtained by reacting $Zr(O^nPr)_4$ with a 20-fold excess of benzoic acid (BzOH),[85] and **$[Zr_6O_4(OH)_4(OOC–Norb)_{12}]$** (OOC–Norb = *endo*-5-Norbornene-2-carboxylate) resulted from the mixture $Zr(OBu)_4$ with a 7-fold excess of *endo*-5-norbornene-2-carboxylic acid,[86] among others (see Table 1 and 5 for a detailed list of similar **Zr_6** clusters).

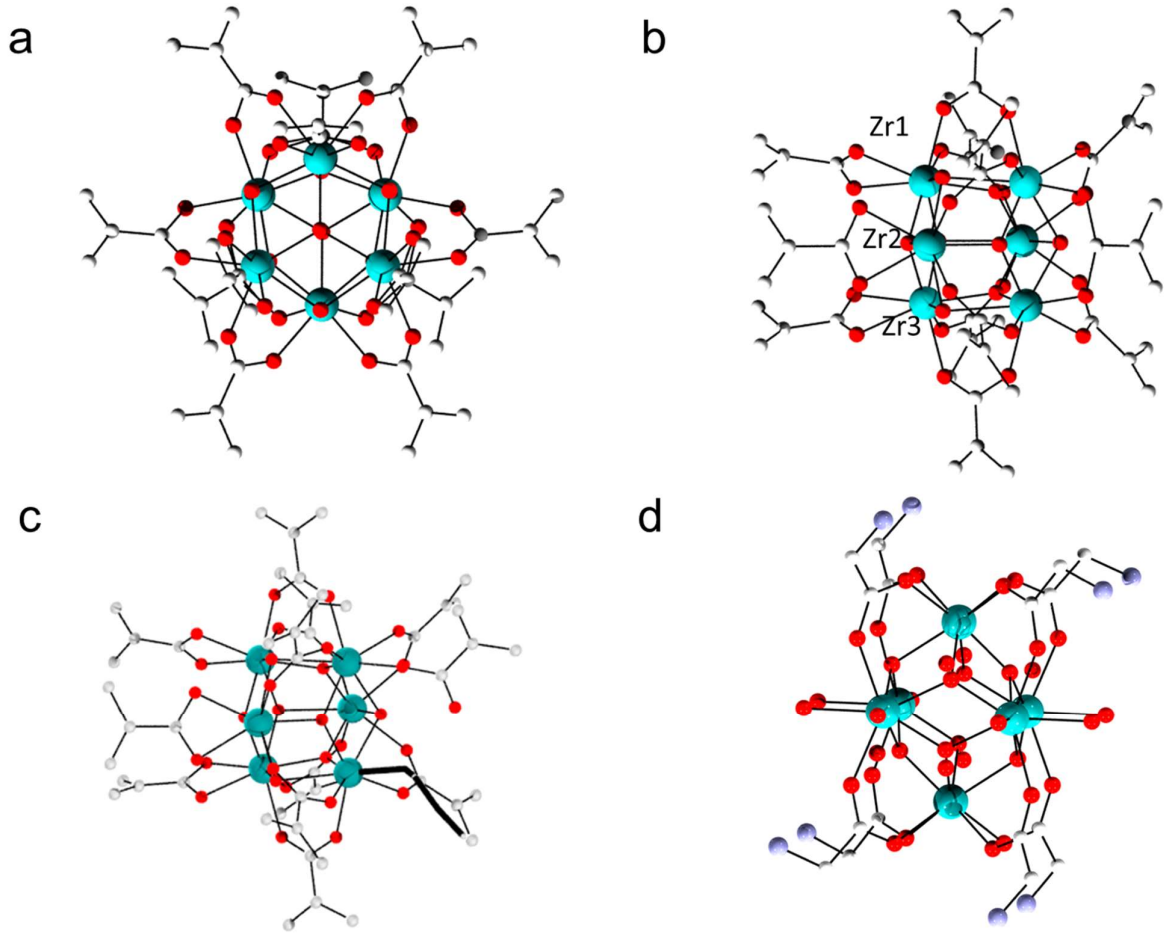

Figure 9. (a) Top and (b) side view of the structure of the hexamer **[$Zr_6(OH)_4O_4(OMc)_{12}$]**. (c) Structure of **[$Zr_6(OH)_4O_4(OMc)_{12}(PrOH)$]**. Propanol ligand is represented by black wire. (d) Structure of **[$Zr_6(OH)_8(H_2O)_8(HGly)_4(Gly)_4]^{12+}$**. Color code: Zr (teal), O (red), C (light gray), N (blue gray). Hydrogen atoms and molecules non-coordinated to Zr omitted for clarity. HGly: ($^{-}O_2CCH_2NH_3^{+}$), Gly: ($^{-}O_2CCH_2NH_2$).

The same reactivity reported in organic solutions was also observed in aqueous medium, as evidenced by the synthesis of a Zr_6 glycine-based cluster, in which glycine coordinated to the hexazirconium octahedral cluster through its carboxylic group (Figure 9d).[87] By mixing hydrated zirconyl chloride, glycine, and sulfuric acid in a molar ratio of 1:14.07:2.76 in water, the product **[$Zr_6(OH)_8(H_2O)_8(HGly)_4(Gly)_4$]**$(SO_4)_6$•$14H_2O$ was obtained. The colorless column-like crystals turned opaque white due to the loss of solvent after separation from the mother liquor. This structure has an approximate diameter of 13.4 Å, and contains a hexanuclear zirconium core $[Zr_6(OH)_8]^{16+}$ with a pseudo D_{4h} symmetry. Eight faces are capped by μ_3-OH^{-} groups and zirconium atoms in the equatorial plane connect to the apical zirconium by eight glycine carboxylate groups in a *syn-syn* mode (Figure 9d). Glycine was present in two different protonation states ($^{-}$OOC-CH_2-NH_3^{+} and $^{-}$OOC-CH_2-NH_2), which together with six sulfates keeps the overall neutral charge balance of the cluster. In addition, 14 water molecules have been found to bind to the cluster via H-bonding interactions, further contributing to stabilization of the cluster. Additional reports of an isostructural Zr_6-glycine cluster having chloride anions instead of sulfates,[88] and the Zr_6 cluster $[Zr_6(\mu_3\text{-}O)_4(\mu_3\text{-}OH)_4(OOCMe)_{12}]$,[89] which were both prepared from aqueous solutions, further attested that the reactivity of carboxylates with Zr cations is similar in water and organic mediums. In these works, the beneficial effect of the temperature on the cluster formation, and the influence of carboxylate concentration on the formation of Zr_6 cluster have also been demonstrated by means of Dynamic Light Scattering and extended X-ray absorption fine structure spectroscopy (EXAFS). Essentially, higher temperature and higher carboxylic acid concentration favor the conversion of the Zr tetramer **[$Zr_4(OH)_8(H_2O)_{16}]^{8+}$** into the thermodynamically stable $[Zr_6(OH)_8]^{16+}$ cluster structure, via presumable involvement of monomeric or dimeric Zr species.

Table 1. Tetrameric and octahedral hexameric ZrOC clusters obtained from carboxylic acids and Zr alkoxides at room temperature.

Cluster	Zr	RCOOH	Solvent	Time (days)	RCOOH/ Zr[1]
$[Zr_4O_2(OMc)_{12}]$ [57]	$Zr(O^nPr)_4$	Methacrylic acid	^{n}PrOH	7	15:1
$[Zr_4O_2(OMc)_{12}]$[81]	$Zr(OBu)_4$	Methacrylic acid	^{n}BuOH	1	7:1
Zr_6 clusters					
$[Zr_6(OH)_4O_4(OMc)_{12}]$ [57]	$Zr(O^nPr)_4$	Methacrylic acid	^{n}PrOH	1	4:1
$[Zr_6O_4(OH)_4(^iPrCO_2)_{12}(H_2O)]$ [56]	$Zr(OBu)_4$	Isobutyric acid	^{i}BuOH	28	7:1
$[Zr_6(OH)_4O_4(OMc)_{12}(PrOH)]$ •3McOH [85]	$Zr(OPr)_4$	Methacrylic acid	^{n}PrOH	11	9:1
$[Zr_6(OH)_4O_4(BzO)_{12}(BzOH)]$ •4BzOH [85]	$Zr(OPr)_4$	Benzoic acid	^{n}PrOH	14	20:1
$[Zr_6O_4(OH)_4(OOC–Norb)_{12}]$ [86]	$Zr(OBu)_4$	*endo*-5-Norbornene-2-carboxylic acid	*n*-heptane	7	7:1
$[Zr_6O_4(OH)_4(OOC^tBu)_{12}]$[90]	$Zr(O^iPr)_4$	Pivalic acid	*n*-Hexane: ^{i}PrOH (1:1)	1	2:1
$[Zr_6O_4(OH)_4(OOCC(CH_3)_2Et)_{12}]$[90]	$Zr(OC(CH_3)_2Et)_4$	2,2-Dimethylbutanoic acid	*n*-Hexane: $Et(CH_3)_2COH$ (1:1)	1	2:1
$[Zr_6(OH)_8(H_2O)_8(HGly)_4(Gly)_4]$ $(SO_4)_6$ •$14H_2O$ [87]	$ZrOCl_2$	Glycine	H_2O[2]	7	14:1

[1] Molar ratio. [2] Sulfuric acid was added into the solution to provide acid environment and as counterions for charge balance. OMc = methacrylate, BzO = benzoate, OOC–Norb = *endo*-5-Norbornene-2-carboxylate

A large excess of carboxylic acids seems not to be strictly necessary to prepare these clusters since **$[Zr_6O_4(OH)_4(OOC^tBu)_{12}]$** and **$[Zr_6O_4(OH)_4(OOCC(CH_3)_2Et)_{12}]$** were obtained by treating $Zr(O^iPr)_4$ with only two-fold excess of HOOCR' (R' = ^{t}Bu, $C(CH_3)_2Et$) at room temperature under Ar atmosphere. However, in this case all the carboxylate ligands adopt bidentate bridging mode. IR and X-ray analysis suggest proton migration between oxygen bridges, while stability of the clusters in the solution was demonstrated by ^{13}C NMR analysis.[90]

On the other hand, further reduction in the amount of carboxylic acid used might result in only partial ligand exchange of the precursor. For example, when $Zr(O^nBu)_4$ reacted with 1.6 equivalents of methacrylic acid, the mixed ligands cluster **$[Zr_6O_2(OBu)_{10}(OMc)_{10}]$** was formed. Probably related to the short supply of carboxylate ligands, this cluster shows a lower degree of condensation, and instead of an octahedral core, the structure consisted of two Zr_3 units dimerized through two bridging butoxy ligands (Figure 10a). This structure is centrosymmetric with Zr(1) adopting pentagonal bipyramidal, and Zr(2) and Zr(3) adopting capped trigonal prism coordination geometry. Further tuning of the Zr precursor reactivity was probed by triggering a partial butoxy-methoxy ligand exchange with 1 equivalent of (3-methacryloxypropyl)trimethoxysilane. In the presence of the latter, the mixture of $Zr(O^nBu)_4$ and 7 equivalents of methacrylic acid also resulted in a dimeric [Zr_3-Zr_3] core, namely **$[Zr_6O_2(OMe)_4(OBu)_2(OMc)_{14}]$**, but with the previous terminal butoxy groups replaced by methacrylate ligands and four of the six butoxy groups replaced by methoxy ligands (Figure 10b).[91]

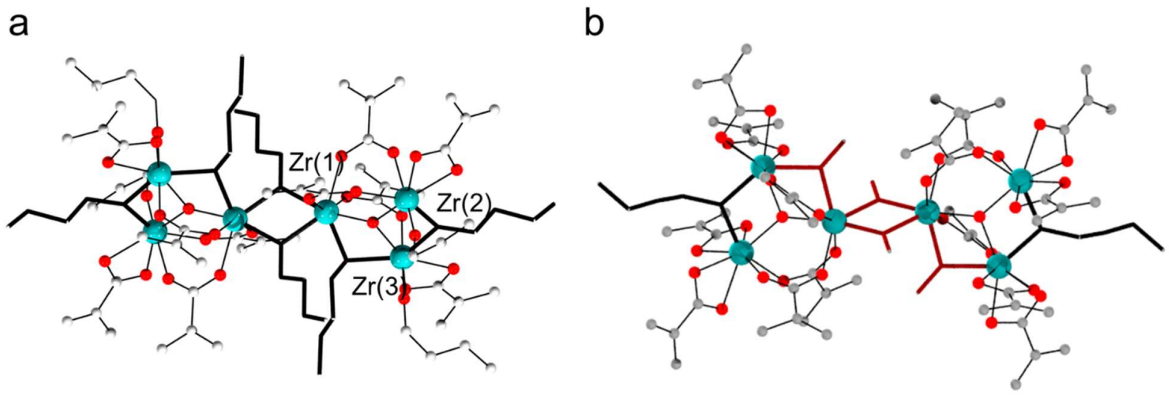

Figure 10. (a) Ball and stick representation of **[$Zr_6O_2(OBu)_{10}(OMc)_{10}$]**. (b) Ball and stick representation of **[$Zr_6O_2(OMe)_4(OBu)_2(OMc)_{14}$]**. Bridging butoxy and methoxy groups represented by black and red wires, respectively. Color code: Zr (teal), O (red), C (light gray). Hydrogen atoms omitted for clarity.

The presence of a second coordinating group in the carboxylate ligand afforded a rather 'open' Zr_6 cluster structure. Specifically, the reaction of $Zr(OPr)_4$ in propanol with 10 equivalents of 1-hydroxy-2-naphthoic acid ($C_{10}H_6(OH)CO_2H$) formed the cluster **[$Zr_6O_2(OPr)_{16}(O_2C(O)C_{10}H_6)_2(PrOH)_2$]**. This structure has two μ_3-O atoms, ten terminal and six bridging propanoate ligands, two propanol molecules, and two anionic tetradentate $[C_{10}H_6(O)CO_2]^{2-}$ moieties (Figure 11). This centrosymmetric cluster has Zr(1) hepta coordinated with a pentagonal-bipyramidal geometry, and Zr(2) and Zr(3) six coordinated with octahedron geometry. The carboxylate group of dianionic $[C_{10}H_6(O)CO_2]^{2-}$ ligand forms a chelate with Zr(1), while Zr(2) is stabilized by the aryloxide group and one of the oxygen atoms of carboxylate, forming a 6-membered metallacycle.[92] Considering that the formation of an octahedral Zr_6 core unit was observed when the ligand's naphtalene ring was replaced by a benzene ring (see details on Zr_{10} clusters below), not only an additional coordinating OH group but also the ligand's steric hindrance might be responsible for the open nature of the resulting structure.

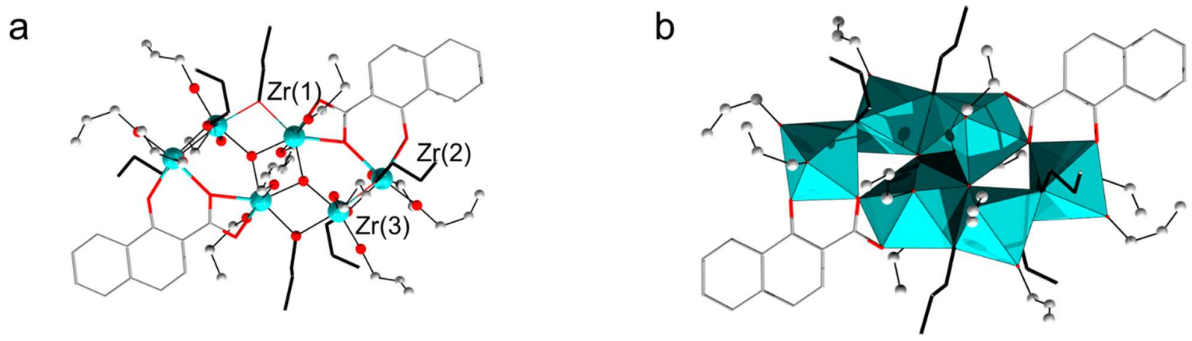

Figure 11. (a) Ball and stick and (b) polyhedron representation of **[$Zr_6O_2(OPr)_{16}(O_2C(O)C_{10}H_6)_2(PrOH)_2$]**. Bridging propanoate ligands are represented by black wires. 1-hydroxy-2-naphthoate ligands are represented by two colored-wires. Color code: Zr (teal), O (red), C (light gray). Hydrogen atoms omitted for clarity.

The effect of additional coordinating group in the ligand on the final cluster structure was also observed in the Zr_6 oxo cluster obtained in the presence of a tridentate oxime/cathecol ligand. Mixing $ZrCl_4$ and 2,3-dihydroxybenzaldehyde oxime (H_3dihybo) in the presence of Bu_4NOH in methanol afforded the cluster **[$Zr_6(\mu_3\text{-}O)_2(\mu\text{-}O)_3(\mu\text{-}Hdihybo)_6(OH_2)_6$]**·$2Bu_4NCl\cdot 2CH_3OH$ (**Zr_6-1**, Figure 12).[93] This structure features a trigonal-prismatic arrangement of the six Zr atoms, in which all the Zr atoms are seven coordinated with a pentagonal-bipyramid geometry, and can be seen as an stacked variant of the Zr_3 clusters reported previously (Figure 7). In fact, both the hexanuclear metal core and its Zr_3 subunits have been observed by ESI-MS in methanol. Within a Zr_3 unit, Zr are connected by an μ_3-O and three bridging chelating Hdihybo ligands (Figure 12c). The two Zr_3 are connected by three O atoms, and DFT calculations showed that the Zr_3 rings exhibit metalloaromaticity. Finally, a thorough NMR study evidenced cluster integrity in methanol and in aqueous solutions, showing that the structure is also hydrolytically stable.

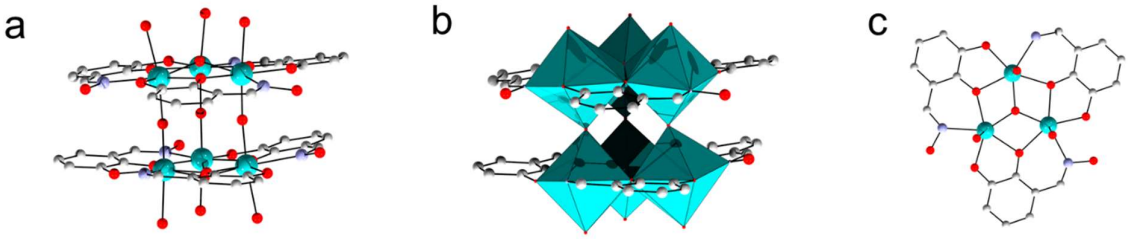

Figure 12. (a) Ball and stick and (b) polyhedral representation of **[$Zr_6(\mu_3\text{-}O)_2(\mu\text{-}O)_3(\mu\text{-}Hdihybo)_6(OH_2)_6$]** (**$Zr_6$-1**). (c) Ball and stick representation of **[$Zr_3(\mu_3\text{-}O)$ (μ-Hdihybo)$_3(OH_2)_3$]**. Color code: Zr (teal), O (red), C (gray), N (blue gray). Hydrogen atoms omitted for clarity.

A similar stacked architecture was observed also when using tridentate phosphonate ligands instead of carboxylates. The phosphonate-substituted ZrOC **[$Zr_6(\mu_3\text{-}O)_2(\mu_2\text{-}OBu)_{12}(O_3PPh)_4$]** was isolated upon incubation of $Zr(OBu)_4$ with bis(trimethylsilyl)phenylphosphonate in n-butanol (molar ratio = 2:1) at room temperature for 16 weeks. The long reaction was attributed to the slow esterification of phosphonic acid group. Similar to the **Zr_6-1** core described above, this structure features two Zr_3 units ($Zr_3(\mu_3\text{-}O)(\mu_2\text{-}OBu)_3(OBu)_3$) linked together, though by four phenyl phosphonate groups instead of simple oxygen atoms. Another key difference is that the Zr_3 units are not planar as in the **Zr_6-1** cluster, with the bridging oxygens above and below the Zr plane. Such structural accommodation most likely derives from the geometry of

the tridentate phosphonate ligands. Interestingly, in this structure Zr atoms are octahedrally coordinated with three butoxy groups existing as bridging ligands, while the remaining three act as terminal ligands (Figure 13a). The phosphonates adopt tridentate modes, binding two zirconium atoms in one Zr_3 unit and one zirconium atom in the other Zr_3 unit.[94]

Zr_7 cluster: A Zr_7 cluster was also obtained under slightly modified conditions to those reported for the Zr_6-phosphonate cluster discussed above. Addition of water and methacrylic acid to a mixture of $Zr(O^iPr)_4$ and bis(trimethyl)silyl(3-bromopropyl)phosphonate in isopropanol resulted in the formation of **$[Zr_7O_2(\mu_2\text{-}O^iPr)_6(O^iPr)_6(O_3PCH_2CH_2CH_2Br)_6]$**. Methacrylic acid was added envisioning a mixed ligand environment, but curiously only phosphonate ligands have been incorporated into the final structure. This cluster consists of the same two $[Zr_3(\mu_3\text{-}O)(\mu_2\text{-}OBu)_3(OBu)_3]$ units which in this case are connected through a central zirconium atom. All the zirconium atoms are octahedrally coordinated, while each phosphate coordinates two zirconium atoms within one Zr_3 unit and the central zirconium atom (Figure 13b).[94]

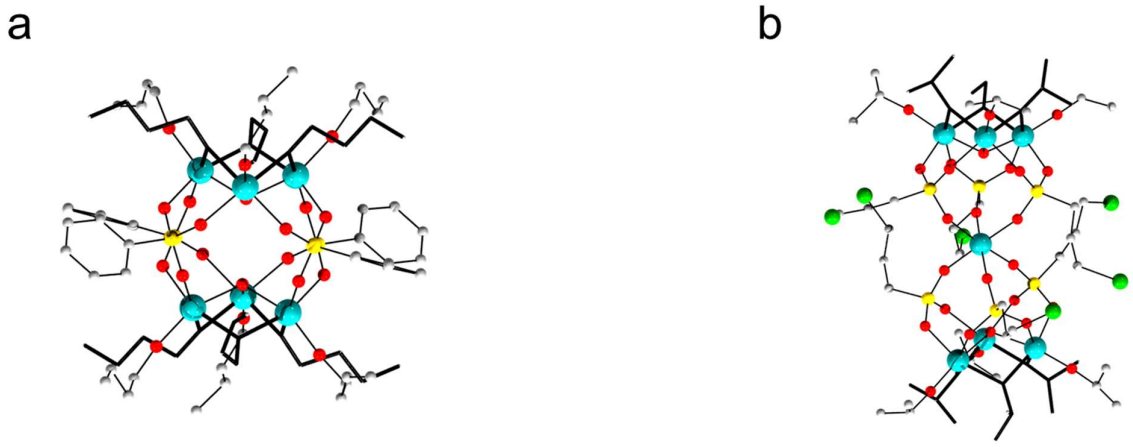

Figure 13. (a) Ball and stick representation of **$[Zr_6(\mu_3\text{-}O)_2(\mu_2\text{-}OBu)_{12}(O_3PPh)_4]$**. (b) Ball and stick representation of **$[Zr_7O_2(\mu_2\text{-}OiPr)_6(O^iPr)_6(O_3PCH_2CH_2CH_2Br)_6]$**. Bridging alkoxide groups are represented by black wires. Color code: Zr (teal), P(gold), O (red), C(gray), Br (green). Hydrogen atoms omitted for clarity.

Zr_8 clusters: Octanuclear Zr clusters have not been observed as discrete species yet, but their formation has been observed in the synthesis of a Zr-porphyrin metal-organic frameworks (MOFs).[95] The solvothermal reaction of zirconium chloride and M'-TCPP (M'= Fe, Co, Cu, no metal, TCCP = tetrakis(4-carboxyphenyl)porphyrin) in N,N-dimethylformamide generated a MOF with the formula **$[M_8O_6(M'–TCPP)_3]$**, which features a Zr_8O_6 cluster as a secondary building unit (Figure 14). In this cluster, the eight Zr atoms have a distorted octahedral coordination environment, and are found at the vertices of an idealized Zr_8 cube, having the six μ_4-O located at the cube's faces. Interestingly, each edge of the cube is capped by a carboxylate group of a TCCP ligand, resulting in a twelve connected **$[Zr_8O_6(CO_2)_{12}]^{8+}$** unit. Interestingly, this structure is O_h symmetric, similar to the more common Zr_6O_8 cores observed within MOF structures, though the carboxylate arrangement in both is very distinct.

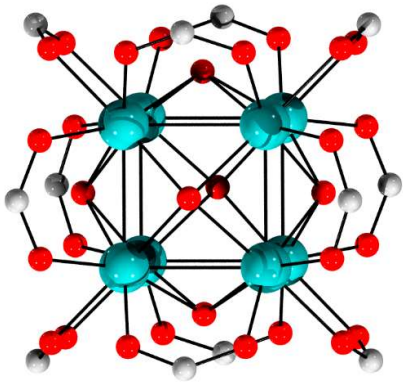

Figure 14. Ball and stick representation of **$[Zr_8O_6(CO_2)_{12}]^{8+}$** cluster observed inside of a Zr-porphyrin MOFs. Color code: Zr (teal), O (red), C(gray). Hydrogen atoms omitted for clarity.

Zr_9 clusters: Similarly to the Zr_8 cluster discussed above, a nonanuclear Johnson-type Zr_9 oxo cluster has only been observed as a MOF secondary building unit.[96] The **$[(CpZr)_3(\kappa_2,O',O''C–C_5H_4N)_3(\mu_3\text{-}O)(\mu_2\text{-}OH)_3]^+$** (**$Zr_3$-2**) precursor underwent a disassembly-reassembly process upon the introduction of Pb^{2+} cations (originating from PbI_2 or $Pb(NO_3)_2$) that led to the formation of the 2D heterometallic MOFs JMOF-1 and JMOF-2. JMOF-1 has a six-connected nonanuclear ZrOC clusters (**$[Zr_9(\mu_3–O)_8(\mu_3–OH)_6(COO)_6]$**, Figure 15b) as the secondary building unit, while JMOF-2 features a twelve-connected one (**$[Zr_9(\mu_3–O)_8(\mu_3\text{-}$**

OH)$_6$(COO)$_{12}$], Figure 15c) (COO = carboxylate ligand). In this cluster, the nonameric **[Zr$_9$(μ$_3$–O)$_8$(μ$_3$–OH)$_6$]** core has octacoordinated zirconium atoms, and can be regarded as a triaugmented triangular prism (J_{51} Johnson solid), with faces capped by μ$_3$-O or μ$_3$-OH groups (Figure 15d).

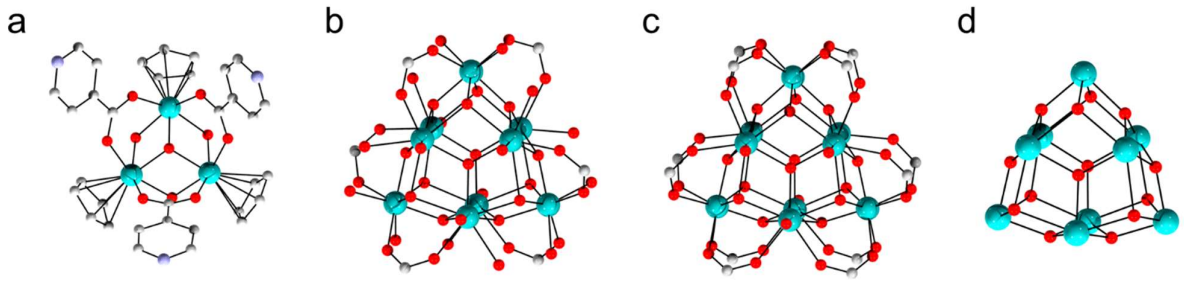

Figure 15. Ball and stick representation of (a) **[(CpZr)$_3$(κ$_2$,O′,O″C−C$_5$H$_4$N)$_3$(μ$_3$-O)(μ$_2$-OH)$_3$]$^+$** (**Zr$_3$-2** precursor), (b) **[Zr$_9$(μ$_3$–O)$_8$(μ$_3$–OH)$_6$(COO)$_6$]**, (c) **[Zr$_9$(μ$_3$–O)$_8$(μ$_3$-OH)$_6$(COO)$_{12}$]**, and (d) **[Zr$_9$(μ$_3$–O)$_8$(μ$_3$–OH)$_6$]**. COO = carboxylate ligand. Color code: Zr (teal), O (red), C (gray), N (blue gray). Hydrogen atoms omitted for clarity.

Unlike the Johnson-type nonanuclear ZrOC above, the Zr$_9$ cluster **[Zr$_9$O$_6$(OBu)$_{18}$(OOCC≡CEt)$_6$]** has been isolated as a discrete species.[97] It has been formed by adding small amount water into a equimolar mixture of Zr(OBu)$_4$ and 2-pentynoic acid in butanol. This cluster is similar to **[Zr$_{10}$O$_8$(OBu)$_{16}$(OOC–C$_6$H$_4$–CH$_2$Cl)$_8$]** discussed below (Figure 17), except that one zirconium and its carboxylate chelating ligands are removed, and μ$_4$-O/μ$_3$-O bridges are replaced by μ$_3$-O/μ$_2$-OBu moieties to keep charge neutrality.

Zr$_{10}$ clusters: A condensed structure **[Zr$_{10}$O$_6$(OH)$_4$(OOC–C$_6$H$_4$OH)$_8$(OOC–C$_6$H$_4$O)$_8$]**·6PrOH has been formed when Zr(OPr)$_4$ was reacted with 10 equivalent of salicylic acid in propanol.[92] This C_2 symmetric structure consist of a central **Zr$_6$** octahedron with four of the edges in the axial plane, capped by the carboxylate groups of the salicylate ligands. On each side of the core, two zirconium atoms are linked together through two bridging bidentate salicylate ligands. These two Zr centers are connected to the octahedral Zr$_6$ core through eight bridging-chelating salicylate ligands with tetradentate binding mode (Figure 16). The two additional Zr(2) and Zr(3) atoms on each side of the core are seven coordinated, while

Zr(1) atom and its symmetry equivalent are 9 coordinated. The remaining zirconium atoms of the Zr_6 octahedron are eight-coordinated, as in other **Zr_6** clusters discussed above.

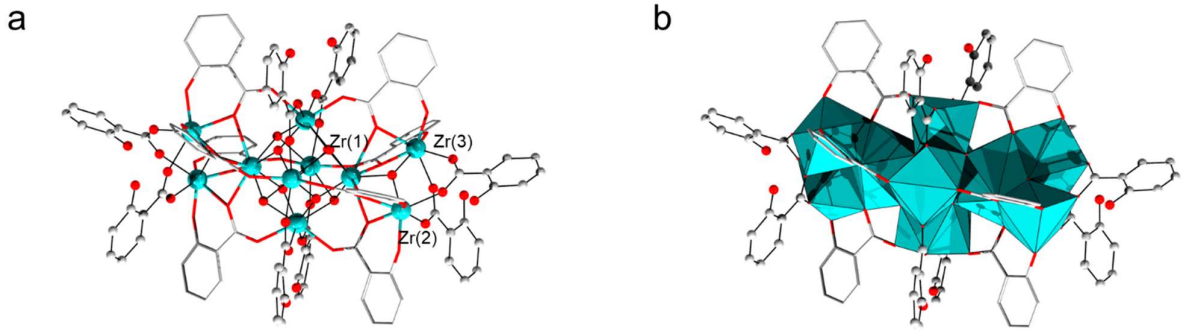

Figure 16. (a) Ball and stick, and (b) Polyhedron representations of **$[Zr_{10}O_6(OH)_4(OOC–C_6H_4OH)_8(OOC–C_6H_4O)_8]$**. The bridging-chelating salicylate ligands are represented by two-colored wires. Color code: Zr (teal), O (red), C (gray). Hydrogen atoms omitted for clarity.

$[Zr_{10}O_8(OBu)_{16}(OOC–C_6H_4–CH_2Cl)_8]$, a second Zr_{10} type cluster, which is related to the discrete Zr_9 mentioned above, is formed by reaction of $Zr(OBu)_4$ with 4-(chloromethyl)benzoic acid in butanol.[97] This structure is analogous to the **$[Zr_6O_4(OH_4)(OOCR)_{12}]$** cluster, but four carboxylate ligands are replaced by eight butoxy groups, which act as bridging ligands between the four additional zirconium atoms and the Zr_6O_8 core (Figure 17). These additional four Zr atoms are located over alternate faces of the Zr_6O_8 octahedron. They coordinate the μ_3-OH group on these faces, which becomes deprotonated. Moreover, each additional Zr also binds two other Zr atoms of the Zr_6 core by two bridging butoxy ligands. Four of the carboxylate groups 'shift' their coordination mode to reach the additional Zr atoms, thus reducing the coordination number of four zirconium atoms from eight to seven. The zirconium chelated by two carboxylate ligands and the one on the opposite site of the Zr_6O_8 core are coordinated by eight oxygen atoms while the remaining zirconium atoms of the Zr_6O_8 core are seven-coordinated. The octahedral coordination of additional zirconium atoms are completed by two terminal and two bridging butoxy ligands, one μ_4-O and one oxygen of the carbonyl group.

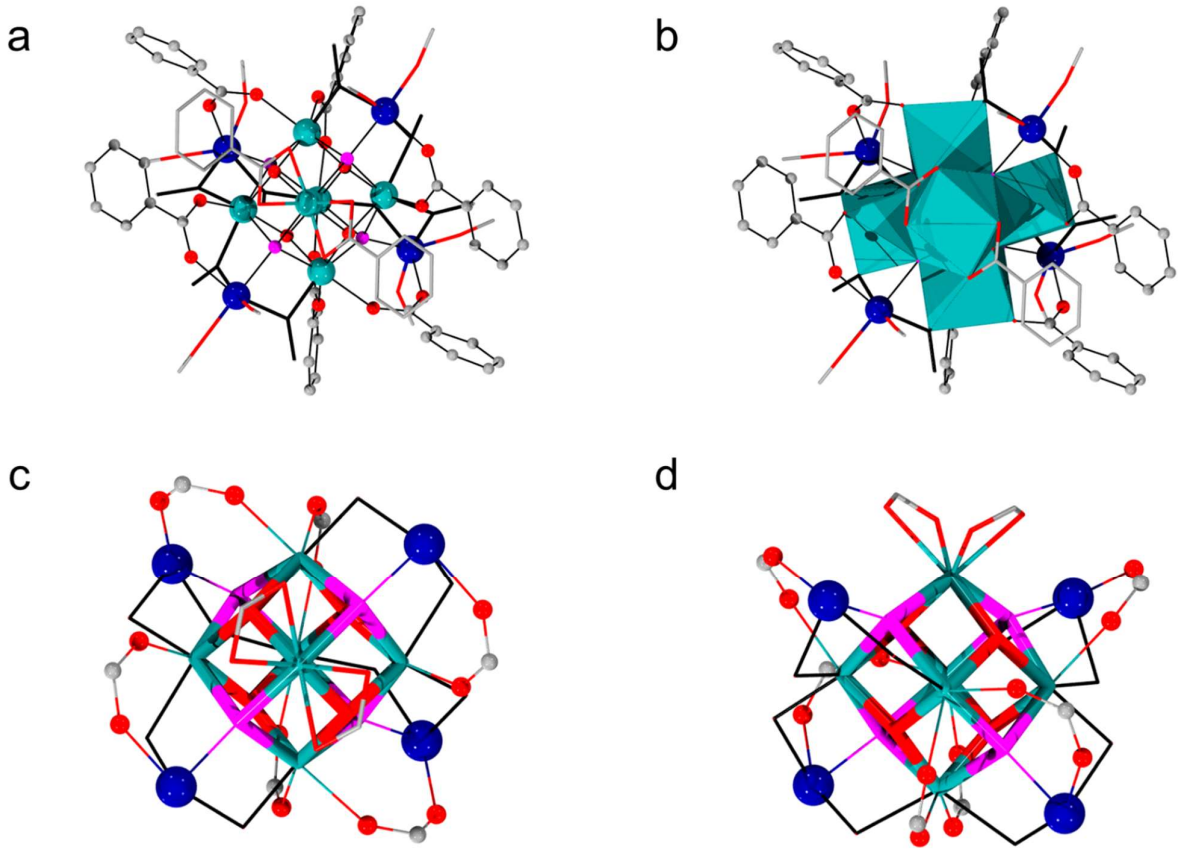

Figure 17. (a) Top view of **[$Zr_{10}O_8(OBu)_{16}(OOC)_8$]**. (b) Polyhedron representations of Zr_6O_8 core in **[$Zr_{10}O_8(OBu)_{16}(OOC)_8$]**. Bridging butoxy groups are represented by black wires. Terminal butoxy and chelating carboxylate groups are represented by two-color wires. For (a) and (b), carbon chain of butoxy groups omitted for clarity. (c) Top view and (d) side view of **[$Zr_{10}O_8(OBu)_{16}(OOC)_8$]** with the core represented by thick wires. For (c) and (d), the terminal butoxy groups, the carbon chain of bridging butoxy groups and carboxylate groups omitted for clarity. Color code: Zr of the octahedron (teal), additional Zr (dark blue), O (red), μ_4-O (pink), C (gray). Hydrogen atoms, and carbon chain of butoxy ligands omitted for clarity.

Zr_{12} clusters: Formal **Zr_6** dimers of the type **[$Zr_6O_4(OH)_4(OOCR)_{12}]_2$** (**$Zr_{12}$**) are the only **$Zr_{12}$** clusters reported so far. They have been synthesized with a broad range of carboxylate ligands under reaction conditions similar to those that afforded **Zr_6** clusters. Although the existence **Zr_6** monomer and **Zr_{12}** dimer has been extensively supported by crystallographic evidence, the reasons that lead to their formation are still not fully understood. Some evidence points to the importance of the acidity of the employed carboxylic acid, since this can

influence the rate of ester formation, as well as the bond strength of the coordinated carboxylate ligand.[98] Interestingly, interconversion between **Zr_6** monomer and **Zr_{12}** dimer has not been observed, and mixtures of **Zr_6** and **Zr_{12}** are typically not detected in the same reaction. In fact, generally only one type of product is obtained for a given reaction condition.[98]

Zr_{12} clusters described so far have all been synthesized using essentially one experimental protocol, which involved mixing the Zr source with an excess of a carboxylic acid under inert atmosphere at room temperature, and letting the reaction mixture stand until crystals are obtained. For example, mixing $Zr(O^nPr)_4$ in n-propanol with 6.5 fold acrylic acid results in the formation of a **Zr_6** dimeric structure, **$[Zr_6(OH)_4O_4(OAcr)_{12}]_2$** (OAcr = acrylate), in which four of the carboxylate ligands bridge the two **Zr_6** cluster units together (Figure 18).[85] The basic features of the **$[Zr_6(OH)_4O_4(OAcr)_{12}]$** are preserved in the **Zr_{12}** cluster, except that the two originally bridging carboxylates situated opposite to the chelate face convert to an 'intermolecular mode' bridging between both **Zr_6** units (Figure 18). Such conversion has little effect on the rest of the structure. Apart from this cluster, others of formula **$[Zr_6O_4(OH)_4(OOCR)_{12}]_2$**•nRCOOH, (R = Me, Et, allyl, n = 6; R = isobutenyl, 2-mercaptoethyl, n = 4) have been produced by treating $Zr(OBu)_4$ with an excess of acetic acid (10 fold), propionic acid (2-10 fold), vinyl acetic acid (7 fold) and 3,3'-dimethylacrylic acid (4 fold), 3-marcaptopropionic acid (MPAH, 7 fold) respectively (Table 2).[98, 99] In these clusters, six carboxylate acid groups interact with the cluster through hydrogen bonds, with the exception of dimethylacrylate and 3-mercaptopropionate which form only four hydrogen-bonds, most likely due to steric hindrance. Finally, an example featuring oxo/hydroxo bridges instead of carboxylate ones, has been observed when 3,3-dimethylbutyric acid has been used as the carboxylate source.[100]

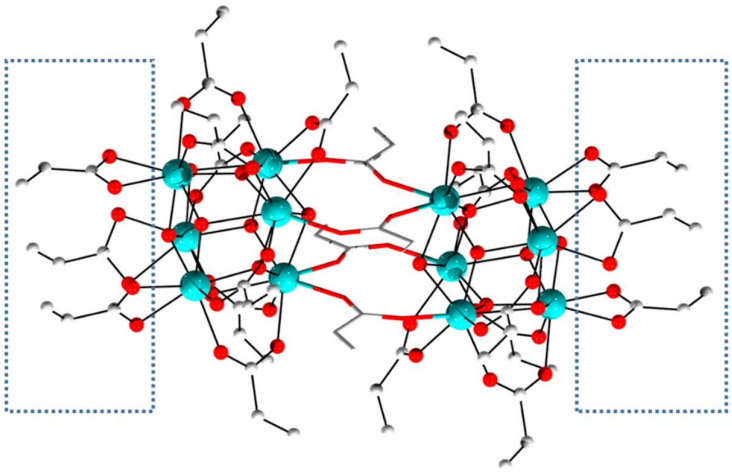

Figure 18. Structure of the **$[Zr_6(OH)_4O_4(OAcr)_{12}]_2$**. Dashed blue boxes mark the chelating ligands. The four carboxylate ligands bridging the two Zr_6 sub-units are represented by two-color wires. Color code: Zr (teal), O (red), C (gray). Hydrogen atoms omitted for clarity.

Table 2. Dodecanuclear ZrOC obtained from carboxylic acids and $Zr(OBu)_4$ at room temperature.

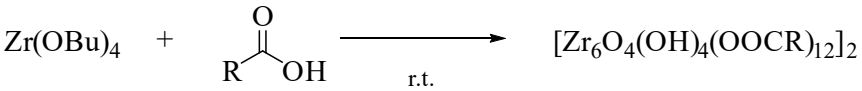

Cluster	RCOOH	Solvent	Time	RCOOH:Zr[(1)]
$[Zr_6O_4(OH)_4(OOCCH{=}CH_2)_{12}]_2$ [85]	Acrylic acid	^{i}PrOH	3 days	6.5:1
$[Zr_6O_4(OH)_4(OOCMe)_{12}]_2$ [98]	Acetic acid	^{n}BuOH	3 h	10:1
$[Zr_6O_4(OH)_4(OOCEt)_{12}]_2$ [98]	Propionic acid	^{n}BuOH	7-8 h	2-10:1
$[Zr_6O_4(OH)_4(OOCCH_2CH{=}CH_2)_{12}]_2$ [98]	Vinylacetic acid	^{n}BuOH	2 days	7:1
$[Zr_6O_4(OH)_4(OOCCH{=}CMe_2)_{12}]_2$ [98]	3,3'-Dimethylacrylic acid	^{n}BuOH	20 days	4:1
$[Zr_{12}(\mu_3\text{-}O)_8(\mu_3\text{-}OH)_8(MPA)_{24}]$ [99]	3-Mercapto propionic acid	^{n}BuOH	3 days	7:1
$[Zr_6(\mu_3\text{-}O)_4(\mu_3\text{-}OH)_4(OOCCH_2{}^{t}Bu)_9]_2$ [100]	3,3-dimethyl butyric acid	*n*-Hexane: ^{i}PrOH (1:1)	1 day	2:1

(1) Molar ratio.

Zr_{13} cluster. A single example of a tridecazirconium oxide of formula of **$[Zr_{13}O_8(OCH_3)_{36}]$** was obtained by mixing a dilute NaOH methanolic solution and a zirconium alkoxide (Figure 19).[101] The structure of this cluster is similar to the Keggin structure observed for polyoxometalates, in which a central plane containing seven Zr atoms is capped by three additional Zr centers above and below this plane. The central zirconium atom is eight-coordinated, while others are seven-coordinated, and feature bridging and terminal methoxide groups completing their coordination sphere. This compound was reported to be highly sensitive to ambient air and moisture.

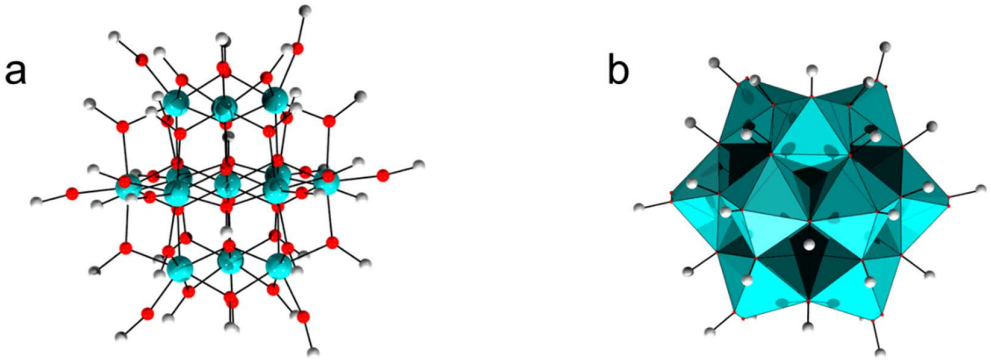

Figure 19. (a) Ball and stick, and (b) Polyhedron representations of **$[Zr_{13}O_8(OCH_3)_{36}]$**. Color code: Zr (teal), O (red), C (gray). Hydrogen atoms omitted for clarity.

Zr_{18} cluster. An octadecanuclear Zr cluster has been also prepared through a reaction in organic medium, but the structure is completely different to the **Zr_{18}** cluster prepared in sulfate-containing aqueous solution. By reacting $ZrCl_4$ and benzoic acid in dried acetonitrile in the presence of thiourea as an essential additive, the **Zr_{18}** cluster **$[Zr_{18}O_{21}(OH)_2(OOCPh)_{28}]$** was obtained (Figure 20).[102] This cluster has a C_2 symmetric structure in which the Zr atoms are organized around a pentagonal $\{Zr_5Zr(\mu\text{-}O)_5\}$ unit, adopting 6-, 7- or 8- coordination modes. Remarkably, this cluster is thermally stable (up to 200 ℃), and photoactive in the visible region with an estimated optical band gap of 2.75 eV, which has been attributed to the oxygen vacancies in the cluster rather than the benzoate ligands. Proof-of-concept for H_2 production in the presence of platinum nanoparticles has also been disclosed.

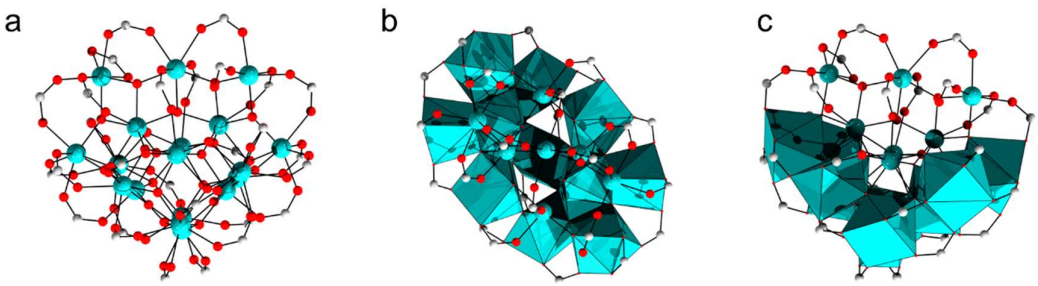

Figure 20. (a) Ball and stick of **[$Zr_{18}O_{21}(OH)_2(OOC)_{28}$]**. (b)(c) Top view and side view of **[$Zr_{18}O_{21}(OH)_2(OOC)_{28}$]** respectively with the pentagonal {$Zr_5Zr(\mu\text{-}O)_5$} building units being represented by teal polyhedron. Color code: Zr (teal), O (red), C (gray). Hydrogen atoms omitted for clarity.

Zr_{26} cluster. [$Zr_{26}O_{18}(OH)_{30}(HCOO)_{38}$]·5(HCOOH)·*k*$H_2O$ (**Zr_{26}**) has been obtained from a $ZrOCl_2 \cdot 8H_2O$ solution in DMF in the presence of a high concentration of formic acid after four days at 140 ℃.[103] Successful scale up allowed for ~1 g synthesis of the **Zr_{26}** cluster, which is interesting considering the potential of this cluster to show permanent porosity. This cluster is the extension of an octahedral {Zr_6} cluster, with a central {Zr_6} unit connected to the other four {Zr_6} moieties through corner sharing mode (Figure 21). Bridges of μ-OH and μ-COOH ligands linked the four external {Zr_6} units, forming a ring structure. All zirconium atoms are eight-coordinated with the coordination sphere completed by 26 bridging, 8 terminal and 4 chelating carboxylate ligands. Defects caused by the substitution of bridging or terminal carboxylate groups by aqua ligands were evident by single crystal X-ray diffraction studies (SCXRD).

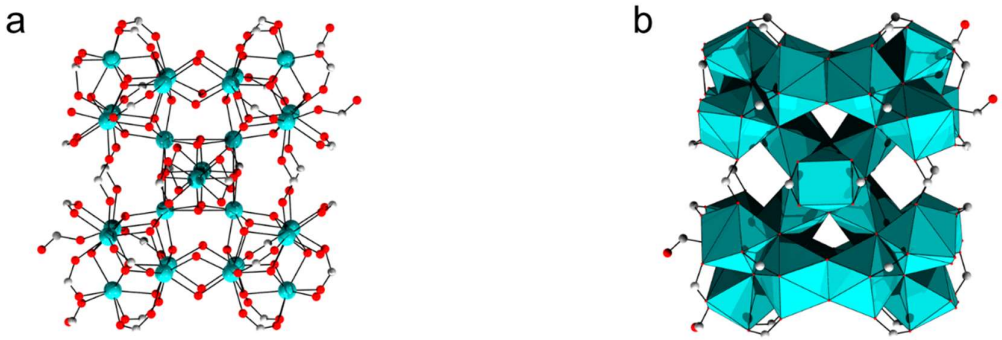

Figure 21. (a) Ball and stick, and (b) Polyhedron representations of **[$Zr_{26}O_{18}(OH)_{30}(HCOO)_{38}$]**. Color code: Zr (teal), O (red), C (gray). Hydrogen atoms omitted for clarity.

2.2.1 *Zr_6/Zr_{12} with mixed carboxylate ligands: direct synthesis and ligand exchange in solution*

ZrOCs with mixed carboxylate ligands are an important class of compounds due to the possibility of tuning the cluster properties by adding ligands with additional functional groups, different hydrophobicity and/or size, among others. However, this apparently simple problem is in fact quite complex given that site selectivity, rate and extent of carboxylate exchange/incorporation and structural integrity of the inorganic core during ligand-exchange steps are quite challenging to prove experimentally, especially in solution. Consequently, these compounds are still marginally understood, though great insights have been obtained in some studies using ZrOC. In this section we present an overview of these studies, which targeted mainly the more prevalent **Zr_6** and **Zr_{12}** clusters, likely due to their stability, availability, and experimental versatility.

ZrOC with mixed carboxylate ligands can be obtained by direct synthesis or by post-synthetic ligand exchange. In the direct synthesis, clusters are formed under similar reaction conditions but using a mixture of carboxylic acids. These reactions afford single products that can be easily isolated using the same techniques developed for non-mixed ligand clusters. However, the few examples known preclude a clear rationalization of the structures obtained, particularly in terms of which ligand is incorporated preferentially, and what controls the site where these ligands are incorporated in the structure.

Besides direct synthesis, mixed-carboxylate clusters have been obtained by full or partial carboxylate exchange after the synthesis, which can be done by adding another carboxylic acid in solution or even another cluster.[104] However, a key challenge in this process is to keep cluster's inorganic core integrity, which has been shown for a few examples reported so far. This alternative is rather appealing in terms of experimental control that can be achieved over the process, and consequently the post-synthetic ligand exchange has been attracting increasing attention. Such approach is particularly interesting given that it might enable: *i)* introducing ligands that are difficult to directly introduce during cluster synthesis; *ii)* controlling the ratio of different functional carboxylate ligands, thereby tuning the properties of the final product;[105] and/or *iii)* controlling the assemble of hybrid structures like MOFs,

since di- or tricarboxylate units used to connect the clusters can be introduced for the preparation of MOFs through a ligand exchange process.[106]

Direct synthesis: Mixed carboxylate **Zr_6** clusters can be obtained directly from two different carboxylic acids. When $Zr(OBu)_4$ in n-butanol was mixed with 3.5 molar equivalents of both methacrylic acid and isobutyric acid, the crystalline mixed-carboxylate species **[$Zr_6O_4(OH)_4(OMc)_8$(iso-butanoate)$_4$(BuOH)]** was formed (Scheme 3).[56] In this structure, a bridging carboxylate opposite of the chelating face converts to a monodentate form, and the vacant site is occupied by a n-butanol ligand. This butanol molecule can be removed through solvent elimination, indicating that this conversion is reversible. The cross-peaks between different types of carboxylate ligands in ROESY and NOESY NMR spectra illustrates that the locations of carboxylic acids with similar acidity are not specific, which means that these two kinds of carboxylate ligands are distributed uniformly in the cluster.

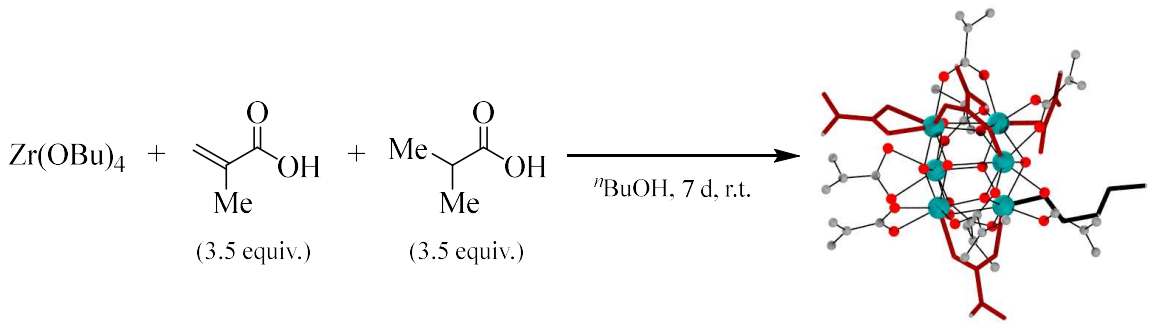

Scheme 3. Structure of the **[$Zr_6O_4(OH)_4(OMc)_8$(iso-butanoate)$_4$(BuOH)]** obtained from equimolar mixtures of isobutyric and methacrylic acids with $Zr(OBu_4)$. Iso-butanoate ligands are represented by dark red wires, n-butanol is represented by black wire, and ball and stick model represent methacrylate ligands. Color code: Zr (teal), O (red), carbon (gray). Hydrogen atoms omitted for clarity.

Mixed-ligand **Zr_{12}** clusters can also be obtained by directly mixing a Zr alkoxide with two different carboxylic acids (Table 3). **[$Zr_6O_4(OH)_4(OOCEt)_3(OMc)_9]_2$** •McOH•5EtCOOH (**$Zr_{12}$-1**) (OMc = methacrylate) was obtained by reaction of $Zr(OBu)_4$ with a 2:5 or 1:6 mixture of propionic and methacrylic acid.[98] Similarly, **[$Zr_6O_4(OH)_4(OOCMe)_8(OMc)_4]_2$**•6MeCOOH (**$Zr_{12}$-2**) was prepared by reacting $Zr(OBu)_4$ with five equivalents of methacrylic acid/acetic acid mixture in 1.4 : 3.6 molar ratio.[98] An example in which acetic acid has been generated *in situ*, presumably from the $Zr(acac)_4$ precursor (acac = acetylacetonate), and resulted in the

mixed-carboxylate cluster **[$Zr_{12}(\mu_3\text{-}O)_{16}(OOCEt)_{12}(OOCMe)_8(\mu_2\text{-}OOCEt)_4$]** has also been reported.[107]

$^1H/^{13}C$ Heteronuclear Multiple Bond Correlation (HMBC) NMR investigations revealed that the **Zr_{12}** clusters have either C_{2h} or C_i symmetry. For **Zr_{12}-1**, three propionate ligands of each Zr_6 subunit are located at the face which is opposite to the intermolecular bridging face of Zr_6 octahedron, where four propionates bridge the two Zr_6 subunits (Figure 22). For **Zr_{12}-2**, prepared with a lower ratio of methacrylate ligand, the acetate ligands bind the sites opposed to the chelating face, while the methacrylate ligands prefer the chelating sites. Moreover, following the formation of **Zr_{12}-1** by $^1H/^{13}C$ HMBC NMR spectra revealed that only butyl proprionate ester was formed, despite the presence of two carboxylic acids. In light of this discovery, the rate of ester formation was suggested to play a role in determining whether a **Zr_6** or a **Zr_{12}** cluster is formed, as ester formation provides the water necessary for cluster formation (Scheme 2).[72] Such selective formation of one ester over the other, could also be related to the preference of carboxylate ligands to remain in opposite or chelating faces, thus indicating that the cluster design could be achieved by controlling the pK_a and/or by the steric hindrance of the carboxylic acid substrates.

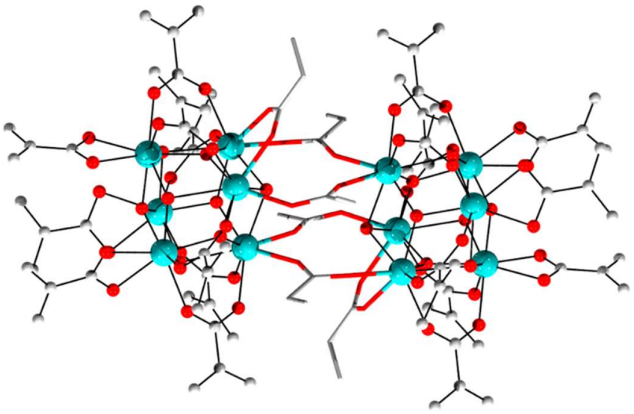

Figure 22. Structure of **[$Zr_6O_4(OH)_4(OOCCH_2Me)_3(OMc)_9]_2$** (**$Zr_{12}$-1** cluster), the six propionate ligands are represented by wires, and the methacrylate ligands are represented by balls and sticks. Color code: Zr (teal), O (red), C (gray). Hydrogen atoms omitted for clarity.

Table 3. Dodecanuclear Zr-oxo clusters featuring a mixed-carboxylate coordination sphere obtained by reacting a mixture of carboxylic acids with $Zr(OBu)_4$ in n-butanol.[1]

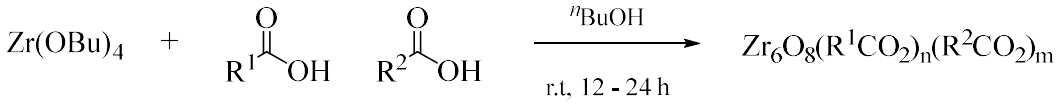

Cluster	RCOOH	RCOOH/Zr[2]
$[Zr_6O_4(OH)_4(O_2CEt)_3(OMc)_9]_2$ (**Zr_{12}-1**)[98]	Propionic (**1**) and Methacrylic acid (**2**)	(**1**:**2** = 2:5):1
$[Zr_6O_4(OH)_4(O_2CMe)_8(OMc)_9]_2$ (**Zr_{12}-2**)[98]	Methacrylic acid (**2**) and Acetic acid (**3**)	(**2**:**3** = 1.4:3.6):1
$[Zr_{12}(\mu_3\text{-}O)_{16}(\mu_2\text{-}OOCEt)_4(OOCEt)_{12}(OOCMe)_8]$ [107]	Propionic acid[3]	26:1

[1] Mixture of the carboxylic acids added dropwise to an 80% solution of $Zr(OBu)_4$ in ^{n}BuOH. [2] Molar ratio. [3] $Zr(acac)_4$ used as Zr source; acetate ligands formed *in situ* presumably from the acac ligand.

Ligand exchange in solution: Mixed carboxylate **Zr_6** clusters have also been formed by ligand exchange in solution with other carboxylic acids. When **$[Zr_6(OH)_4O_4(OMc)_{12}]$** was reacted with a large excess of propionic or isobutyric acids, all the methacrylate ligands were replaced, generating the **$[Zr_6O_4(OH)_4(OOCCEt)_{12}]$** [98] or the **$[Zr_6O_4(OH)_4$(iso-butanoate)$_{12}]$** [56] clusters, respectively. However, using only 3 – 6 molar equivalents of propionic and isobutyric acids, only partial exchange was clearly observed by NMR.[56] The initial structure of the Zr_6 core was retained based on the conserved pattern of the NMR signals before and after the exchange. Comparison with single carboxylate model compounds suggested that the ligand exchange is a substitution-driven rather than a disassemble/re-assemble process. Similar observations were reported for the **$[Zr_4O_2(OMc)_{12}]$** cluster. [108]

The possibility of post-synthetic ligand exchanged in **Zr_{12}** clusters was evident from the reaction of **Zr_{12}-1** cluster with an excess of propionic acid, in which all the methacrylate ligands were exchanged and the structure of the final product **$[Zr_6O_4(OH)_4(OOCEt)_{12}]_2$**•6EtCOOH (**$Zr_{12}$-3**) was similar to the one prepared through the direct method (Table 2). To confirm whether the bridging sites are susceptible to carboxylate exchange, **Zr_{12}-3** was reacted with an excess of acetic acid. The ^{1}H NMR showed that the ratio of acetate to propionate was 3:1, which indicated that the carboxylate ligands bridging

the two **Zr_6** subunits (the 'intermolecular sites') were not accessible for ligand exchange in solution.[98] These experiments illustrates that apart from the ligands bridging the two **Zr_6** subunits (the 'intermolecular sites' occupied by propionate ligands in Figure 22), ligands bound to the other remaining sites can be easily substituted by other carboxylate ligands without affecting the inorganic core structure.

Noteworthy, ligand exchange of **Zr_{12}** clusters **$Zr_6O_4(OH)_4(OOCEt)_{12}$** and **$[Zr_6O_4(OH)_4(OOCCH_2CH{=}CH_2)_{12}]_2$** with a non-carboxylate ligand, namely acetylacetone, has also been probed.[109] Reaction of these clusters with 50 molar equivalents of acetylacetone led to exchange of one chelating carboxylate ligand on each Zr_6 unit, resulting in the formation of **$[Zr_6O_4(OH)_4(OOCR)_{11}(acac)]_2$** (acac = acetylacetonate). These results indicate that for ligands other than carboxylates, site-selective exchange might be possible, based on the lability of the carboxylate group coordination mode. Moreover, this single substitution despite the large excess of acetylacetone used, sharply contrasts with the complete disassembly of the inorganic core observed for **$[Zr_4O_2(OMc)_{12}]$** (see Zr_4 clusters).[82] This suggests a greater stability of the Zr_6 unit in comparison with the tetramer of **$[Zr_4O_2(OMc)_{12}]$**, and directly implicates the stability of the inorganic core structure for the outcome of the reaction.

The mechanism of these ligand exchange reactions is only partially understood. Based on the reported cases, a plausible five-step mechanism for the post-synthetic ligand exchange has been proposed by Schubert (Scheme 4): 1) the original bidentate carboxylate convert to monodentate; 2) the vacant site is occupied by the entering acid group; 3) proton transfer between the entering and leaving carboxylates; 4) the departure of the original carboxylate group; 5) the entering monodentate carboxylate group changes to the bidentate mode of binding.[104]

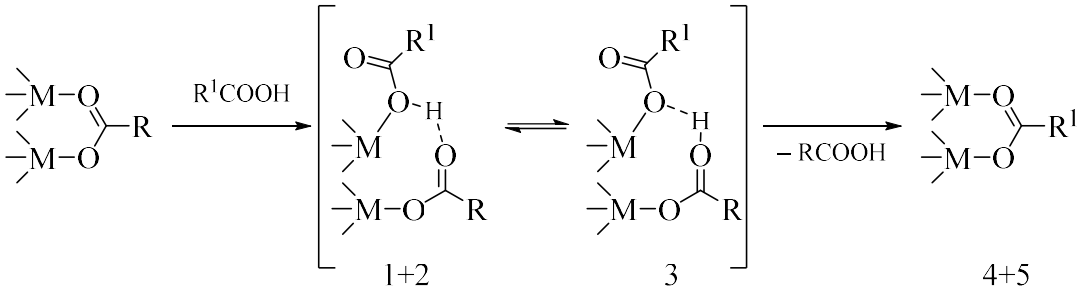

Scheme 4. Mechanism for the carboxylate exchange proposed by Schubert.[104]

The proposed mechanism is supported by the recurring examples of cluster core stability upon ligand exchange, detailed spectroscopic evidence, and molecular dynamics studies of the dynamics of carboxylate ligands on the cluster surface.[108, 110] These studies evidenced the dynamic nature of the carboxylate ligands, which constantly switch between chelating and bridging coordination mode through a metastable intermediate in which the moving carboxylate is H-bonded to the facial μ_3-OH group, thereby momentarily leaving a Zr center with a vacant site that can be approached by an external ligand.[110] Such scenario also implies that the ligand exchange is an equilibrium that can be driven by the concentration of the carboxylates in solution, which has been elegantly demonstrated for the **$[Zr_4O_2(OMc)_{12}]$** cluster.[108] Finally, additional evidence of the dynamic nature of these clusters has been observed through an interesting carboxylate scrambling reaction. In this reaction, equimolar amounts of **$[Zr_4O_2(OMc)_{12}]$** and **$[Zr_4O_2(OPiv)_{12}]$** (OPiv = OOC^{t}Bu) were mixed in solution affording the mixed-carboxylate cluster **$[Zr_4O_2(OMc)_6(OPiv)_6]$** as the single product, which presents an interesting prospect for using such approach in preparation of mixed clusters. Importantly, cluster stability after scrambling has been thoroughly confirmed by infrared (IR) analysis supported by Density Functional Theory (DFT) calculations of the Zr-O bridges vibrations in the region below 600 cm^{-1}.[108]

2.2.2 Summary of ZrOC formation in organic systems

Based on the syntheses discussed above, the ratio of carboxylate acid with respect to Zr source seems to play an important role in the formation of ZrOC in organic medium. The variation of the ratio can lead to different clusters as the increase of the ratio may favor the cluster with lower nuclearity, as exemplified by the formation of **$[Zr_4O_2(OMc)_{12}]$** and **$[Zr_6(OH)_4O_4(OMc)_{12}]$**. In addition, comparison of the reaction conditions used in the formation of **$[Zr_6(OH)_4O_4(OMc)_{12}]$** and **$[Zr_6(OH)_4O_4(OMc)_{12}(PrOH)]$**•3McOH also suggests higher carboxylic acid/Zr ratios can prompt a carboxylate ligand bridging two Zr into monodentate binding mode, opening a vacant site on one Zr that is then filled by XOH (X= H, Pr, Bu). Moreover, the steric hindrance may also affect the formation of the cluster, since the formation of **$[Zr_6(OH)_4O_4(BzO)_{12}(BzOH)]$**•4BzOH required a higher excess of benzoic acid compared to smaller acids, while the formation of **$[Zr_6O_4(OH)_4(OOCCH_2CH{=}CH_2)_{12}]_2$** required longer reaction time in comparison to **$[Zr_6O_4(OH)_4(OOCMe)_{12}]_2$**. Moreover, ZrOCs with mixed carboxylate ligands can be obtained by either one-pot synthesis or post-synthetic ligand

exchange, allowing to introduce different functional groups and tune the structure and properties of the final product. Finally, ligands with additional coordinating groups or non-carboxylate ones have afforded a variety of structures having different sizes and shapes, showing that many more clusters might be obtained by continuous evolution of ligand structures.

3. Structure and properties of Hafnium oxo clusters (HfOC)

In comparison with Zr and Ti oxo clusters, far less HfOC compounds have been reported. Moreover, many of the examples available in the literature have been mainly studied under the general assumption that Hf and Zr cluster chemistries are similar in nature due to the similar atomic radii and comparable chemical properties of Zr^{4+} and Hf^{4+}. For example, both metals give isostructural clusters such as Zr_4/Hf_4,[61, 62] Zr_6/Hf_6,[57, 111] Zr_{12}/Hf_{12},[98] Zr_{17}/Hf_{17} [70] and Zr_{18}/Hf_{18}.[71, 112] Despite the similarities between Zr and Hf oxo clusters, there are also some important differences between them. Below, we highlight the structure and properties of the main HfOC reported to date, pointing out their similarities and differences with respect to their Zr counterparts. The discussion is organized according to nuclearity only, since less HfOC examples than ZrOC have been reported, and several aspects discussed for ZrOC also apply to HfOC. A list of the HfOC structures available in the literature is given in Table 5.

Hf_4 clusters: In the absence of sulfates or other complexing ligands, **$[Hf_4(OH)_8(H_2O)_{16}]^{8+}$** (**$Hf_4$**), which has similar structure and properties as zirconium tetramer **$[Zr_4(OH)_8(OH_2)_{16}]^{8+}$**, is formed in aqueous solutions (Figure 23a).[113] Crystals of **Hf_4** were obtained by heating $HfOCl_2$•$8H_2O$ salt in 1M HCl solution, followed by addition of cucurbituril ($C_{36}H_{36}N_{24}O_{12}$), which results in the isolation of adduct **$[Hf_4(OH)_8(H_2O)_{16}]Cl_8$**•($C_{36}H_{36}N_{24}O_{12}$)•$16H_2O$ (**Hf_4-1**) (Figure 23b).[62] The cation **$[Hf_4(OH)_8(H_2O)_{16}]^{8+}$** can also be isolated as its *p*-toluenesulfonate salt, **$[Hf_4(OH)_8(H_2O)_{16}]$**[(p-toluenesulfonate)$_8$]•$4H_2O$, by simply adding diluted 1 M p-toluenesulfonic acid solution to a 0.13 M aqueous solution of hafnium triflate,[114] or by evaporation of a perchloric acid solution.[115] The MOC cations in these crystals are very similar, except for minor differences in angles of bridging hydroxo or aqua ligands.

In contrast to the cluster rearrangement to a tetrahedral geometry observed for **$[Zr_4(OH)_8(OH_2)_{16}]^{8+}$,** addition of peroxide ligands to a solution of **$[Hf_4(OH)_8(H_2O)_{16}]$**$(ClO_4)_8$ led only to a formal replacement of one or two OH ligands, depending on the amount of peroxide added. Two peroxide containing compounds **$[Hf_4(\mu\text{-}OH)_6(\mu\text{-}O_2)(H_2O)_{16}]$**•$(ClO_4)_8$•$15H_2O$ (Figure 23c) and **$[Hf_4(\mu\text{-}OH)_4(\mu\text{-}O_2)_2(H_2O)_{16}]$**•$(ClO_4)_8$•$5H_2O$ (Figure 23d) crystalized when peroxide/Hf molar ratios were respectively 20:1 and 1:1, within which one and two bridging OH pairs were replaced by peroxide ligands, causing a small distortion of the tetramer.[115]

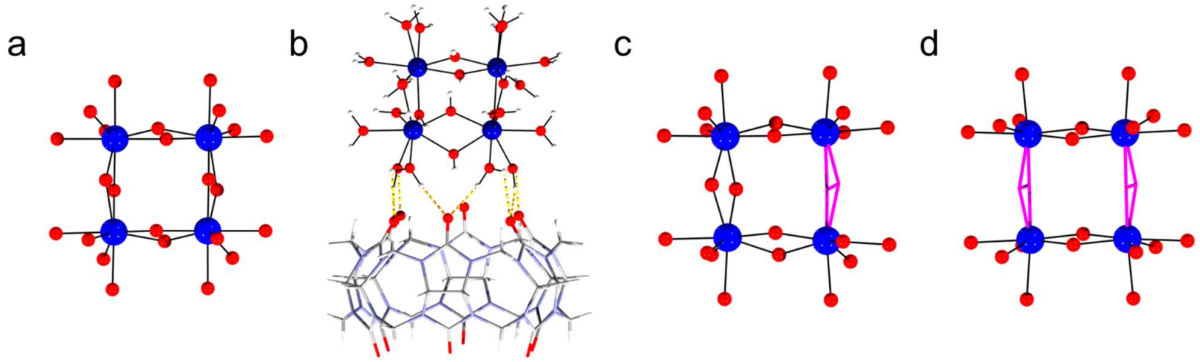

Figure 23**.** (a) Ball and stick representation of **$[Hf_4(OH)_8(H_2O)_{16}]^{8+}$**. (b) Structure of **$[Hf_4(OH)_8(H_2O)_{16}]Cl_8$•$(C_{36}H_{36}N_{24}O_{12})$** (**$Hf_4$-1**), cucurbituril group is represented by wires, **$[Hf_4(OH)_8(H_2O)_{16}]^{8+}$** (**$Hf_4$**) is represented by ball and stick. (c) Ball and stick representation of **$[Hf_4(\mu\text{-}OH)_6(\mu\text{-}O_2)(H_2O)_{16}]$** and (d) **$[Hf_4(\mu\text{-}OH)_4(\mu\text{-}O_2)_2(H_2O)_{16}]$** with peroxide ligands represented by pink wires. Color code Hf (blue), O (red), C (gray), N (gray blue). Hydrogen and chloride atoms omitted for clarity.

Tetrameric HfOCs featuring organic (thio)carboxylates have also been reported. For example, **$[Hf_4O_2(OMc)_{12}]$** cluster, which is isostructural to **$[Zr_4O_2(OMc)_{12}]$**, was obtained when $Hf(OBu)_4$ was mixed with a 4-fold excess of methacrylic acid in BuOH and let to crystallize for 1-2 weeks at 4 °C. ^1H NMR analysis indicated a fast exchange of the methacrylate ligands. Interestingly, formation of this highly substituted cluster needed a lower amount of methacrylic compared to **$[Zr_4O_2(OMc)_{12}]$** (4 vs. 15 molar equivalents, respectively), which has been attributed to the difference in reactivity of the precursors. [111] Furthermore, the tetranuclear planar HfOC **$[Hf_4(\mu_2\text{-}SAc)_6(\mu_2\text{-}BuO)_4(BuO)_2(\mu_3\text{-}O)_2]$** [SAc = $CH_3C(O)S$] has been obtained by reaction of hafnium butoxide with thioacetic acid. This structure is centrosymmetric with all hafnium atoms being seven-coordinated. They are connected to each other by four bridging butoxy group and two thioacetate groups with the triangular Hf_3 units capped by μ_3-

O ligands (Figure 24). The coordination sphere of hafnium atom is completed by terminal butoxy and chelating thioacetate ligands.[116]

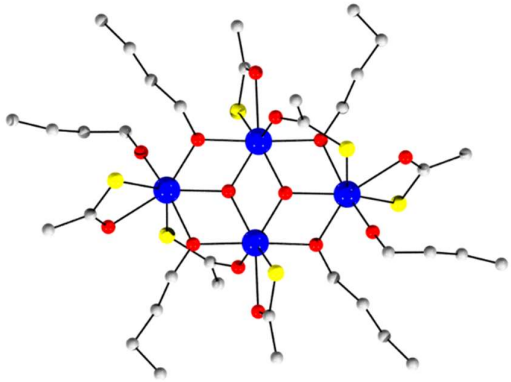

Figure 24. Ball and stick representation of **[$Hf_4(\mu_2\text{-}SAc)_6(\mu_2\text{-}BuO)_4(BuO)_2(\mu_3\text{-}O)_2$]**. The bridging butoxy groups are represented by black wires. Color code Hf (blue), O (red), C (gray). Hydrogen atoms omitted for clarity.

Hf_6 clusters: Apart from the carboxylated octahedral **[$Hf_6O_4(OH)_4(OMc)_{12}(BuOH)$]** cluster, [111] which is isostructural to the **[$Zr_6(OH)_4O_4(OMc)_{12}(PrOH)$]** (Figure 25a), two different structures of hexanuclear Hf clusters have been identified, with and without the participation of sulfate ligands into the Hf framework. Without sulfate ligands, **[$Me_3NH]_6[Hf_6(\mu\text{-}O_2)_6(\mu\text{-}OH)_6(OH)_{12}]$**•$38H_2O$ (**Hf_6-1**) was isolated from basic solutions containing peroxides, in contrast to other Hf_6 clusters obtained from acidic medium (Figure 25b).[117] X-ray crystallographic analysis indicates that **Hf_6-1** belongs to a triclinic crystal system and contains a hexanuclear Hf ring with a radius of 5.5Å. The eight-coordinated Hf(IV) ions are connected by μ-peroxo and μ-hydroxo ligands, and the terminal hydroxy ligands are critical for further condensation both in solid state and in solution. The existence of peroxide ligands was confirmed by Raman spectroscopy, and the ratio of Hf to peroxide was determined by potassium permanganate titration. The amount of water was determined quantitively by thermogravimetric analysis (TGA). The ESI-MS analysis of **Hf_6-1** in water indicated the labile character of hydroxo ligands in solution, and the robustness of the hexameric ring. Small-angle X-ray scattering (SAXS) study detected the formation of elongated particles when cluster was dissolved in water, suggesting formation of oligomers through terminal hydroxo ligands.[117]

On the other hand, introduction of sulfate results in the formation of **$(NH_4)_5[Hf_6(O_4OH)(SO_4)_{10}(H_2O)_7]$** (**$Hf_6$-2**) cluster, which features a planar centered pentagon structure.[58] The **Hf_6-2** was formed when the mixture of $HfOCl_2 \cdot 8H_2O$ (0.3 M), $(NH_4)_2SO_4$ (1.5 M) and H_2SO_4 (1.25 M) has reacted at 95 °C for 3 days (Figure 25c). X-ray diffraction analysis showed that **Hf_6-2** consists of a pentagonal bipyramid with one Hf in the center, and five other Hf atoms surrounding it. Each of the hafnium atoms has one in-plane H_2O ligand pointing away from the center. Every Hf is coordinated by seven oxygen atoms, with the central Hf having pentagonal bipyramid geometry and the remaining Hf ions are coordinated in monocapped trigonal prism geometry. Sulfate groups which are located above and below the mirror plane bind the central Hf, while remaining sulfates bridge two adjacent hafnium atoms along the central plane.[118]

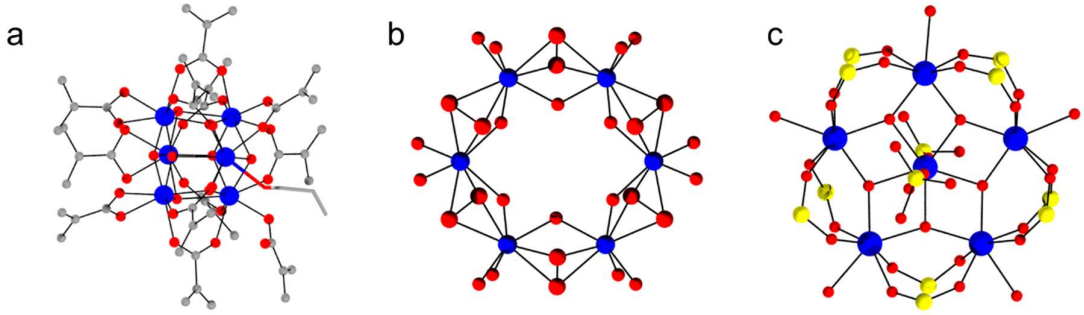

Figure 25. (a) Structure of the Hf_6 clusters: (a) **$Hf_6O_4(OH)_4(OMc)_{12}(BuOH)$**, (b) **$[Me_3NH]_6[Hf_6(\mu\text{-}O_2)_6(\mu\text{-}OH)_6(OH)_{12}]$** (**$Hf_6$-1**), and (c) **$(NH_4)_5[Hf_6(O_4OH)(SO_4)_{10}(H_2O)_7]$** (**$Hf_6$-2**). Color code: Hf (blue), O (red), S (yellow). Hydrogen atoms omitted for clarity.

Hf_9 cluster: The cage-like nonamer with D_{3h}-like symmetry **$(NH_4)_{14}[Hf_9O_8(OH)_6(SO_4)_{14}] \cdot nH_2O$** (**$Hf_9$**) is one of the two structures that were only reported for hafnium (see Hf_{11} below for the other one), as opposed to other clusters that have also been described for zirconium. **Hf_9** is formed by heating a mixture of $HfOCl_2 \cdot 8H_2O$ (0.2 M), $(NH_4)_2SO_4$ (2 M) and H_2SO_4 (0.5 M) at 80ºC for 10 days. Crystallographic data revealed that this cluster crystallizes in the monoclinic space group $P2_1/c$. Each hafnium coordinates eight oxygen atoms, with μ_3-O and μ_3-OH ligands connecting three Hf atoms. Curiously, there are no H_2O ligands present in the structure (Figure 26). Twelve sulfate groups arranged above and below the equatorial plane bridge two adjacent Hf atoms, while the remaining two sulfates link three Hf atoms on the top and bottom face of the cluster.[58, 119] In contrast to most of the clusters presented so far, **Hf_9** is strongly negatively charged, most likely due to the presence of many sulfate ligands that stabilize the core HfOC structure.

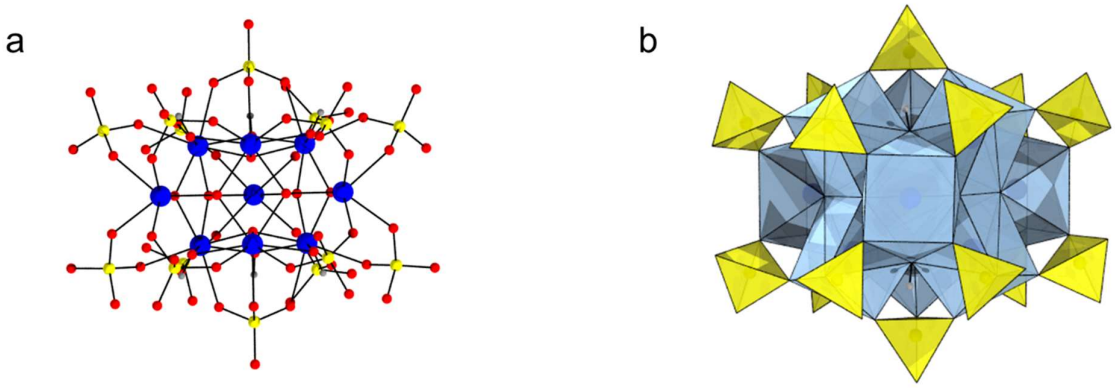

Figure 26. (a) Ball and stick and (b) polyhedron representation of nonameric cluster **$[Hf_9O_8(OH)_6(SO_4)_{14}]^{14-}$** (**$Hf_9$**). Color code: Hf (blue), O(red), S (yellow), {SO_4} (yellow polyhedron), {HfO_8} (pale blue polyhedron). Hydrogen atoms omitted for clarity.

Hf_{11} cluster: The other structure that has been only reported for HfOC but not for ZrOC, is the undecamer **$(NH_4)_{11}[Hf_{11}O_7(OH)_{11}(SO_4)_{15}(H_2O)_6]$•$nH_2O$** (**$Hf_{11}$**). Heating a mixture of $HfOCl_2$•$8H_2O$ (0.3M), $(NH_4)_2SO_4$ (4M) and H_2SO_4 (0.25M) at 60-95 °C for 3 days results in the formation of **$(NH_4)_{11}[Hf_{11}O_7(OH)_{11}(SO_4)_{15}(H_2O)_6]$•$nH_2O$**. The core of **$Hf_{11}$** consists of octahedral hexamer surrounded on one side by five hafnium atoms, similar to what is observed in 18-mers of the same type. Alike **Hf_9**, **Hf_{11}** is strongly anionic (charge = −11), and it contains five bidentate, eight bridging, and two μ_3-sulfate ligands (Figure 27).[58]

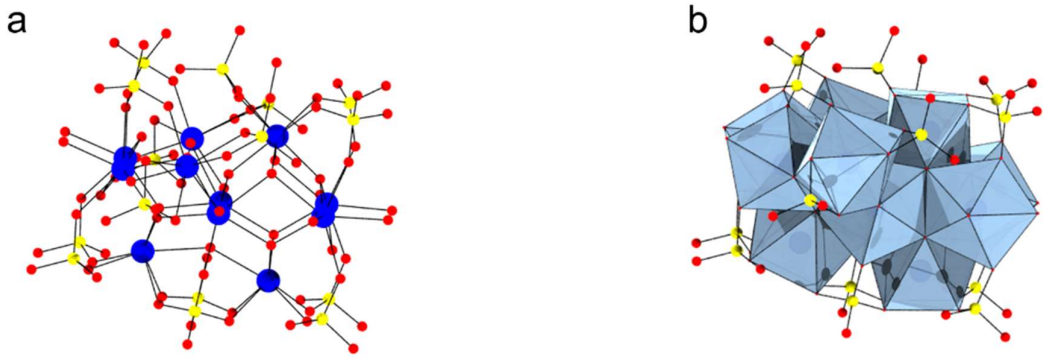

Figure 27. (a) Ball and stick and (b) Polyhedron representation of **$[Hf_{11}O_7(OH)_{11}(SO_4)_{15}(H_2O)_6]^{11-}$** (**$Hf_{11}$**). Color code: Hf (blue), O (red), {HfO_8} (pale blue polyhedron), {SO_4} (yellow polyhedron). Hydrogen atoms omitted for clarity.

Hf_{12} clusters: **Hf_{12}** clusters analogous to **Zr_{12}** carboxylate clusters such as **$[Hf_{12}(\mu_3\text{-}O)_8(\mu_3\text{-}OH)_8(MPA)_{24}]$**•5(MPAH)[99] (MPA = 3-mearcaptopropionate) and **$[Hf_6O_4(OH)_4(OOCMe)_{12}]_2$**•6MeCOOH•6$CH_2Cl_2$[98] have been disclosed along with their Zr counterparts. Their structure and properties are largely similar to Zr-based clusters. See Table 5 for a detailed list of the reported structures.

Hf_{17} clusters: A pinwheel structure **$[Hf_{17}O_8(OH)_{24}(OH_2)_{12}(HCOO)_{12}(SO_4)_8]$**•6HCl•30$H_2O$, that is isostructural to the **Zr_{17}** cluster, has been synthesized under similar conditions reported for its zirconium counterpart, except that $HfCl_4$ was used as the precursor instead of the $ZrOCl_2$.[70] In addition to this analogous structure, an alternative Hf_{17} cluster has been isolated from a solution prepared by addition of diluted sulfuric acid (1 M) to an aqueous solution of hafnium triflate (0.13 M) at room temperature. Slow evaporation of this solution at room temperature resulted in the formation of **$[Hf_{17}O_8(OH)_{28}(SO_4)_{11}(H_2O)_{23}]$**[$SO_4$]•32.25$H_2O$ (**Hf_{17}-1**) monoclinic crystals (Figure 28b).[114] This structure is similar to the one observed for the **Zr_{18}** and **Hf_{18}** clusters (Figure 28a), except for a few differences deriving from the "removal" of one Hf atom. In contrast to the **Zr_{18}**/**Hf_{18}** cluster structure that has a Zr/Hf-pentamer above the central octahedral hexameric unit, **Hf_{17}** features a tetramer ring in analogous position (black squares in Figure 28). Consequently, **Hf_{17}** has no μ_3-SO_4^{2-} group, which would hold the fifth Hf atom in place. Likewise, only one μ_4-O^{2-} is present in the structure, instead of the two that are found in the structure of **Zr_{18}**/**Hf_{18}** clusters. Finally, there are no sulfate groups that link different **Hf_{17}** clusters as observed in the crystal structure of **Zr_{18}**/**Hf_{18}** clusters.

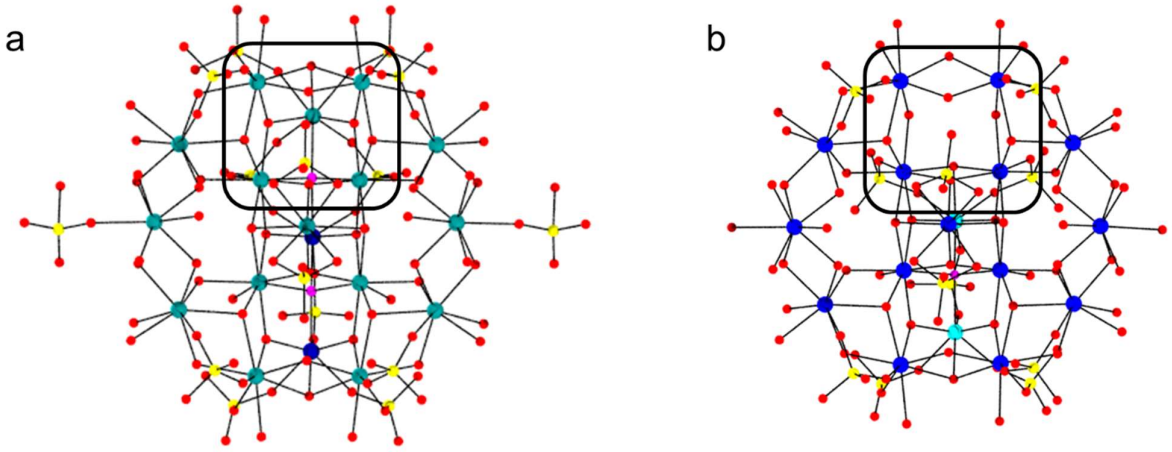

Figure 28. (a) Ball and stick representation of **Zr_{18}** and (b) **$[Hf_{17}O_8(OH)_{28}(SO_4)_{11}(H_2O)_{23}]^{2-}$**. Color code: eight-coordinated Zr (teal), seven-coordinated Zr (dark blue), eight-coordinated Hf (blue), seven-coordinated Hf (cyan), O (red), μ_4-O (pink), S (yellow). Hydrogen atoms omitted for clarity.

Hf_{18} cluster: The 18-mer **$[Hf_{18}O_{10}(OH)_{26}(SO_4)_{13}(H_2O)_{33}]$** (**$Hf_{18}$**) crystallizes in space group $P6_3/m$ from a mixture of $HfOCl_2 \cdot 8H_2O$ (0.3 M), $(NH_4)_2SO_4$ (0.5 M) and H_2SO_4 (0.75 M) that was heated at temperatures 60−95 °C for 5 days (Figure 29b). Contrary to **Zr_{18}** clusters formed at room temperature, formation of **Hf_{18}** needs higher temperatures. [120] The **Hf_{18}** is isostructural to **Zr_{18}**; however, the coordination of two Hf atoms (marked with red circles in (Figure 29) has been proposed to be either eight or seven, due to the uncertainty of one water ligand coordination. [2, 112]

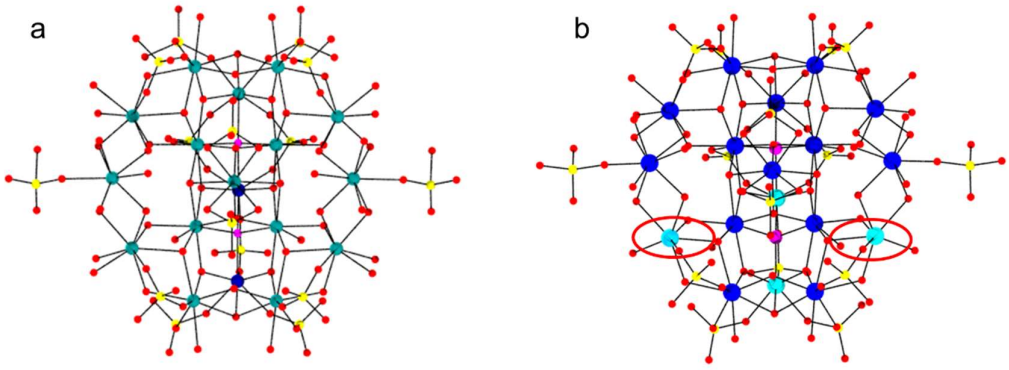

Figure 29. (a) Ball and stick representation of **Zr_{18}** and (b) **$Hf_{18}O_{10}(OH)_{26}(SO_4)_{13}(H_2O)_{33}]$** (**$Hf_{18}$**). Color code: eight-coordinated Zr (teal), seven-coordinated Zr (dark blue), eight-coordinated Hf (blue), seven-coordinated Hf (cyan), O (red), μ_4-O (pink), S (yellow). Hydrogen atoms omitted for clarity.

3.1 Summary of HfOC formation

Similar to the chemistry observed with Zr, the well-characterized **$[Hf_4(OH)_8(H_2O)_{16}]^{8+}$** is ubiquitous in aqueous solutions, but the introduction of additional ligands triggers the formation of other HfOC. For example, **Hf_6-1** clusters were obtained when peroxides were added, and the addition of sulfuric acid afforded **Hf_{17}** cluster. Further, using the

$HfOCl_2•8H_2O/(NH_4)_2SO_4/H_2SO_4$ mixtures, clusters of different nuclearity have been synthesized through modification of the reaction conditions (Table 4). Careful analysis of the reaction conditions indicated that the formation of HfOC is affected by the acidity of the solution and the concentration of SO_4^{2-}. The largest cluster **Hf_{18}** forms at low sulfate concentration. At low acid concentration, further addition of sulfate leads to **Hf_{11}** and **Hf_9**, while increasing the acid concentration results in the formation of **Hf_6-2**. The sulfate ligands seem to exert a double role in these systems: in small quantities, they promote the oligomerization by mediating the condensation of Hf centers, while in large quantities they impede the growth of the clusters by blocking the cluster surface to the approach additional metal centers.

Table 4. Different HfOC synthesized using the $HfOCl_2•8H_2O/(NH_4)_2SO_4/H_2SO_4$ systems at temperatures 60−95 °C.

Cluster	$HfOCl_2•8H_2O$ (M)	H_2SO_4 (M)	$(NH_4)_2SO_4$ (M)	Crystallization time (days)
Hf_{18}	0.3	0.75	0.5	5
Hf_{11}	0.3	0.25	4	3
Hf_9	0.2	0.5	3	10
Hf_6-2	0.3	1.25	1.5	3

4. Structure and properties of Titanium oxo clusters (TiOC)

The chemistry of titanium oxo clusters (TiOC) has been more extensively explored than that of Zr and Hf clusters, and many excellent reviews addressing different aspects of TiOCs have been published in the last decade.[40, 59, 121, 122] In comparison to the relatively well-behaved chemistry leading to Zr/Hf-oxo clusters, the design and synthesis of Ti coordination compounds is harder to achieve or predict due to the extremely favorable hydrolysis of Ti^{4+} in the presence of water. Consequently, no general rationale for the conditions required to form a particular cluster is currently available, even though the steric hindrance of alkoxy capping ligand has been proposed to play a key role in determining the condensation degree in the final compounds.[121] For example, the compact **$[Ti_7O_4(OEt)_{20}]$** structure exhibiting

six-coordinated Ti^{4+} centers has been obtained by hydrolysis of titanium tetraethoxide.[123, 124] However, hydrolysis of Ti^{4+} with bulkier ligands often results in titanium oxo clusters with an open structure which reduces the steric repulsion between the ligands.

Compared to Zr and Hf clusters, a much larger number of TiOC structures has been described, with cluster nuclearity ranging from as low as 2 to up 52 titanium centers. These clusters have a combination of alkoxides and carboxylates as the most commonly present capping ligands, albeit phosphorous and nitrogen moieties have also been reported. The synthesis of these compounds is also experimentally more complex compared to Zr- and HfOCs, as they require strict inert conditions to control the hydrolysis of titanium alkoxides precursors. Similar to Zr/Hf clusters, functional groups on the cluster surface of TiOCs can be introduced directly by mixing metal alkoxides with carboxylate ligands during the synthesis or post-synthetic ligand modification, which can proceed with or without rearrangement of the inorganic core. Finally, although lower or higher coordination numbers have been observed, Ti^{4+} generally adopts a six-coordinated octahedral environment in which TiO_6 units are connected to each other by μ_2-oxo or μ_3-oxo bridges, in contrast to the 7/8-coordination sphere for Zr and Hf compounds.

In this context, this section focus on representative Ti-oxo clusters, including two building units of Ti-MOFs. Specifically, **$[Ti_6O_6(OR)_6(OOCR')_6]$** (**Ti_6**) clusters, which are starting materials for the formation of MOFs like PCN-22, and have a similar structure to **Zr_6** clusters used as secondary building units in Zr-based MOFs are presented here. Likewise, **$[Ti_8O_8(OOCR)_{16}]$** (**Ti_8**) clusters are highlighted. **Ti_8** clusters are key precursors for MIL-125 MOFs, a key achievements in porous Ti-based materials.[40] Moreover, inspired by a recent report of **Hf_{18}** unique hydrolytic nanozyme reactivity,[125] we also highlight two octadecanuclear Ti-oxo clusters with distinct structures from the corresponding **Zr_{18}**/**Hf_{18}** clusters. Finally, the highly promising optical properties and the unique ligand exchange chemistry of Ti-oxo clusters, which proceed with either retention or reorganization of the metal oxo core, are also briefly discussed. [121, 126, 127] A list of the TiOC discussed here are presented in Table 5. For comprehensive tables of TiOC reported to date, previous reviews should be consulted.[40, 59, 121, 122]

4.1 Overview of selected TiOC structures

Ti_6 clusters: Among the hexanuclear titanium-oxo clusters disclosed, the **$[Ti_6O_6(O^iPr)_6(OOCH)_6]$** (**$Ti_6$-1**), which can be described as two staggered Ti-trimers connected through μ_3-oxo and μ_2-OOCH bridges (Figure 30a), is one on the most similar to the Zr_6 clusters discussed above. It has been isolated from reactions between titanium isopropoxide and formic acid in a molar ratio of 1:2.[128] In this **Ti_6-1** cluster, each titanium has a distorted octahedron geometry and is coordinated by three μ_3-oxo, two μ_2-OOCH and one terminal alkoxide ligands. The six carboxylate ligands connecting the two staggered Ti-trimers form an alternate up and down chain in **$[Ti_6O_6(O^iPr)_6(OOCH)_6]$** (Figure 30a), which is similar to the 'belt' region of **$[Zr_6(OH)_4O_4(OMc)_{12}]$** (Figure 30b). On the other hand, the Ti atoms in the **Ti_6** cluster are capped by alkoxide ligands, while in the **$[Zr_6(OH)_4O_4(OMc)_{12}]$** cluster the triangular units are capped by bidentate bridging and chelating carboxylate ligands. Moreover, considering the metal oxo core alone, there are two extra μ_3-oxo ligands in the Zr_6 cluster which connect the three zirconium atoms of each triangular unit. These differences probably arise because of the higher coordination number of Zr^{4+} in comparison to Ti^{4+}.

A Ti analogue of the stacked hexazirconium cluster **$[Zr_6(\mu_3\text{-}O)_2(\mu\text{-}O)_3(\mu\text{-}Hdihybo)_6(OH_2)_6]$** (Figure 12) has also been obtained under similar conditions. However, in structural terms K_2**$[Ti_6(\mu_3\text{-}O)_2(\mu\text{-}O)_3(OCH_3)_4(CH_3OH)_2(\mu\text{-}Hdihybo)_6]$**•$CH_3OH$ is more similar to the decked Ti_{18} cluster discussed below, due to the oxygen bridge between layers than to the staggered Ti_6 structure highlighted here (Figure 30).[93] Notably, a similar stacked **Ti_6** cluster has been reported, which interestingly, also contains tridentate ligands like H_2dihybo.[129]

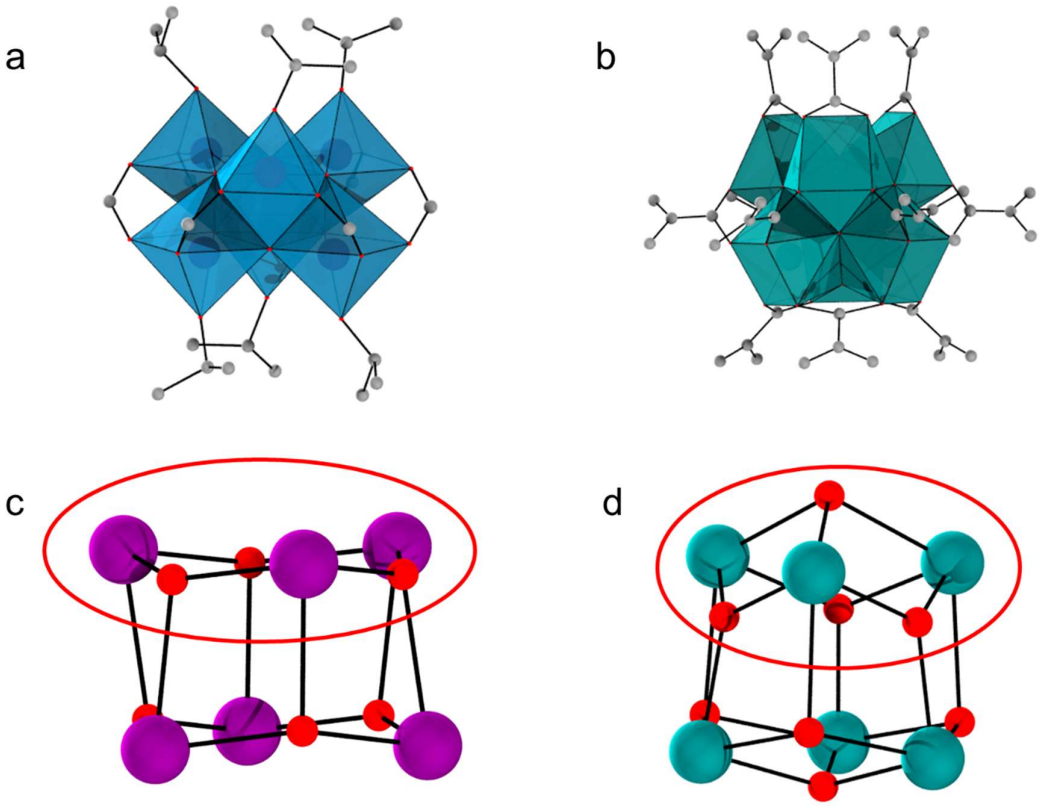

Figure 30. (a) Polyhedron representation of **$[Ti_6O_6(OR)_6(OOCH)_6]$** (**Ti_6** cluster). (b) Polyhedron representation of **$[Zr_6(OH)_4O_4(OMc)_{12}]$**. (c) The **$[Ti_6O_6]$** core of **$[Ti_6O_6(OR)_6(OOCH)_6]$**. (d) The **$[Zr_6(OH)_4O_4]$** core of **$[Zr_6(OH)_4O_4(OMc)_{12}]$**. Color code: {$TiO_6$} steel blue, Ti (violet), oxygen(red), carbon (grey). Triangular units are highlighted by red circles. Hydrogen atoms omitted for clarity.

Ti_8 cluster: Octameric oxo clusters of formula **$[Ti_8O_8(OOCR)_{16}]$** [R = C_6H_5, $C(CH_3)_3$, CH_3] have been obtained by reacting a titanium alkoxide with 10-fold of benzoic, pivalic and acetic acid respectively in acetonitrile at 100 ºC. X-ray diffraction of the **Ti_8** compounds revealed a ring of eight [TiO_6] moieties connected via corner-sharing, arranged in a wheel-shape geometry. ^{13}C and ^{1}H NMR spectroscopic measurements helped to distinguish the two crystallographically different carboxylate ligands, with eight carboxylates pointing up or down from the equatorial plane defined by the ring, and the remaining eight carboxylates coordinated in equatorial positions (Figure 31). These nanoclusters can be modified after synthesis by reaction with other organic acids, but such exchange often triggers a rearrangement of the metal oxo core. The exact mechanism of this reorganization is not yet fully understood.[130]

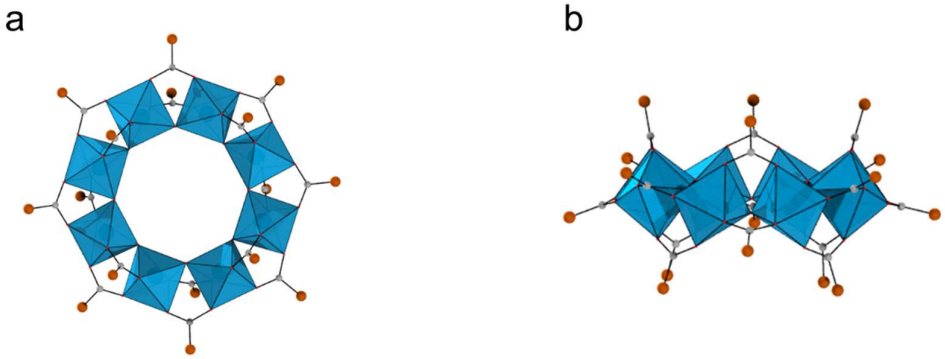

Figure 31. (a) Top and (b) side view of polyhedron representation of **$[Ti_8O_8(OOCR)_{16}]$** clusters. The color code is {TiO_6} steel blue, carbon (grey), R ligand (orange).

Ti_{18} clusters: $[Ti_{18}O_{28}H][O^tBu]_{17}$($Ti_{18}$-1 cluster) has been synthesized by reacting $Ti(O^tBu)_4$ with ca. 1 equivalent of water in *tert*-butyl alcohol for 5 days at 100 ºC. As revealed by single-crystal X-ray crystallography, the **Ti_{18}** metal oxo framework consists of a Keggin unit capped by five TiO moieties, which lie above five of the six approximately square faces defined by the metals in the Keggin unit (violet polyhedrons in Figure 32). Each of the five capping titanium centers adopt a distorted trigonal-bipyramidal geometry with the coordination number of 5. All seventeen terminal oxygen atoms are capped by *tert*-butyl groups. Some of the *tert*-butoxide groups, which are coordinated to Ti^{4+}, could be replaced by 2-methylbutoxide groups upon reaction with an excess of 2-methylbutanol with the $Ti_{18}O_{28}$ oxide core retention based on O^{17} NMR. In addition, proton exchange can convert the cluster symmetry from C_s to C_{2v}.[131]

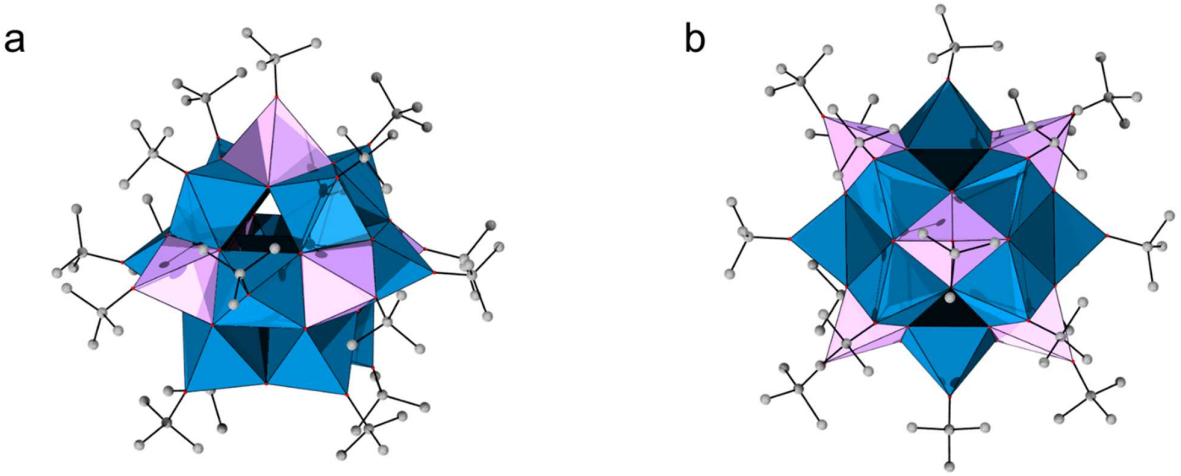

Figure 32. (a) Side and (b) top view of the polyhedron representation of **$[Ti_{18}O_{28}H][O^tBu]_{17}$** (**$Ti_{18}$-1** cluster). Color code: carbon (gray), oxygen (red), {TiO_6} and {TiO_4} (steel blue polyhedron), {TiO_5} (violate polyhedron).

Recently, another 18-mer TiOC structure, **$[Ti_{18}O_{27}(OH_2)_{30}(SO_4)_6]Cl_6$**•6TBAC•12$H_2O$ (**Ti_{18}-2** cluster) (TBAC = tetrabutylammonium chloride), has been isolated.[132] Similarly to observed for Zr- and HfOCs, introduction of sulfate anions in the reaction mixture led to isolation of a distinct structure. **Ti_{18}-2** cluster was synthesized at room temperature by slow evaporation of an aqueous mixture of $TiCl_4$, H_2SO_4 and TBAC with a ratio of 1:0.33:1. Later it was reported that simple dissolution of $TiOSO_4$ in water results in spontaneous self-assembly into {Ti_{18}}, in a similar way to the prompt formation of **$[Zr_4(OH)_8(OH_2)_{16}]^{8+}$** upon dissolution of $ZrOCl_2$ in water, although a low pH of solution inhibits the stacking or the formation of {Ti(Ti_5)} pentamers.[133] This cluster shows good solubility and stability in polar solvents like acidic water, alcohols and acetonitrile. The core of **Ti_{18}-2** cluster can be regarded as a decked trimer of three planar pentagonal {Ti(Ti_5)} building units connected by μ_2-O ligand (Figure 33), with the 3.6 Å distance between the layers. Within the pentagonal {Ti(Ti_5)} building unit, the central Ti adopts coordination number of seven, while the five Ti at the vertices are six coordinated and connected through μ_3-O atoms. Six sulfates cap the core through bridging bidentate coordination. This compound can be used for the surface modification of graphene oxide and as active titanium oxide photocatalysts.[132]

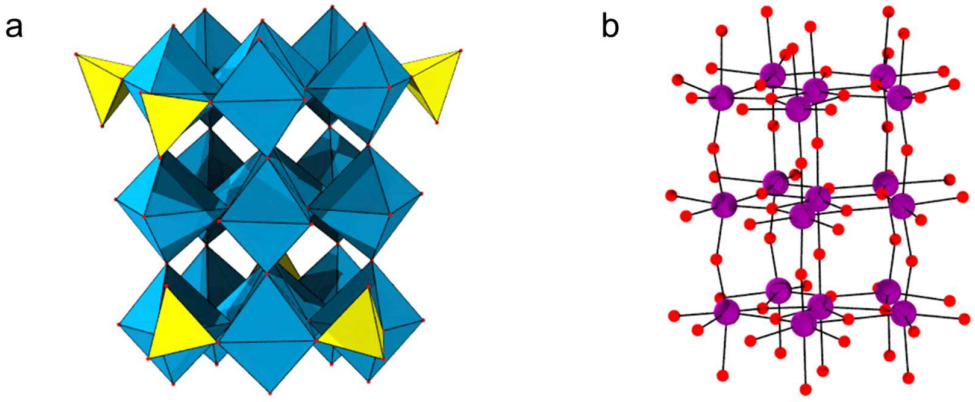

Figure 33. (a) Polyhedron representation of **$[Ti_{18}O_{27}(OH_2)_{30}(SO_4)_6]Cl_6$** (**$Ti_{18}$-2** cluster).(b) The metal oxo core of the **$[Ti_{18}O_{27}(OH_2)_{30}]^{18+}$**. Color code: Ti (violate), carbon (gray), oxygen (red), { SO_4} (yellow polyhedron), {TiO_6}, { TiO_7} (steel blue polyhedron).

Ti_{42} clusters: A fullerene-like shell structure of H_6**[Ti_{42}(μ_3-O)$_{60}$(O^iPr)$_{42}$(OH)$_{12}$]** has been successfully synthesized through mixing of Ti(O^iPr)$_4$ with formic acid.[134] This spheric structure consists of a series of pentagonal-bipyramidal {TiO_7} units connected to five tetragonal-pyramidal {TiO_5} moieties through sharing edges, which in turn share corners with four adjacent {TiO_5} groups (Figure 34). The 12 Ti atoms at the center of {TiO_7} units are seven-coordinated, while others are only pentacoordinated. The external surface features 42 isopropoxide molecules as terminal ligands. The highly symmetrical nature of this structure is evident from the Platonic {Ti_{12}} icosahedral arrangement of {TiO_7} units, and the Archimedean {Ti_{30}} icosidodecahedron formed by the {TiO_5} moieties. The shell structure has an internal diameter of ~1.05 nm and outside sphere of 1.53 nm, not including the isopropoxide ligands.

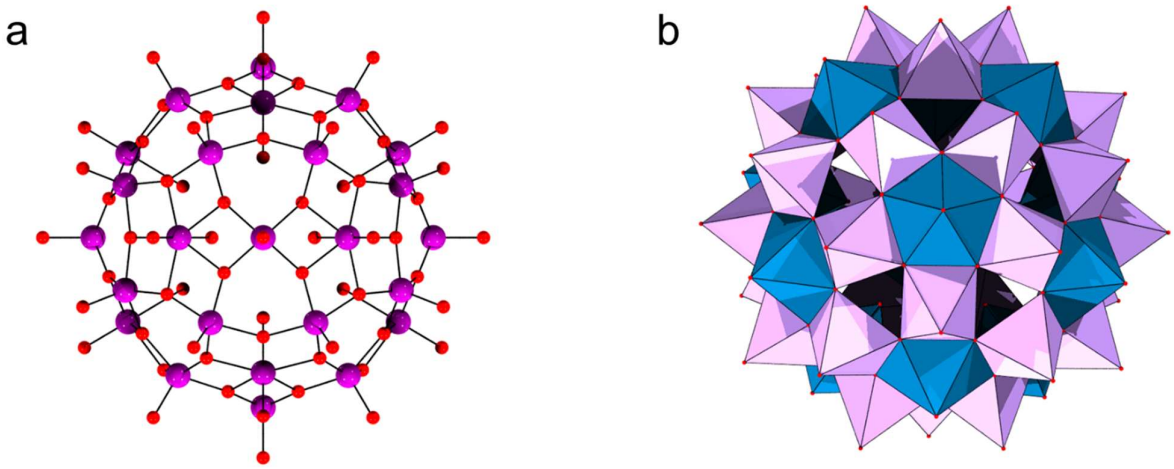

Figure 34. (a) Ball and stick representation and (b) polyhedron representation of the **{$Ti_{42}O_{60}$}** core of cluster H_6**[Ti_{42}(μ_3-O)$_{60}$(O^iPr)$_{42}$(OH)$_{12}$]**. Color code: Ti (violate), oxygen (red), {TiO_7} (steel blue polyhedron), {TiO_5} (lavender polyhedron).

4.2 Overview of TiOC properties and reactivity

4.2.1 Ligand exchange in TiOC

The unique ligand exchange chemistry of Ti oxo clusters can be used to modify their surface connectivity, and to tailor the properties of the resulting compounds, which allows for the elaboration of diverse nanostructures with potential applications in catalysis, thin-films, magnetism, or gas storage.[121, 135] However, the metal oxo core can either remain intact or rearrange during the ligand exchange process, depending on the ligands being exchanged.

Ligand exchange with retention of metal oxo core structure. Metal oxo clusters are usually stable when the leaving and entering ligands have the same charge and coordination denticity and geometry. Ligand exchange with retention of metal oxo core structure has been demonstrated by trans-alcoholysis reaction with **$[Ti_{11}O_{13}(O^iPr)_{18}]$**, **$[Ti_{12}O_{16}(O^iPr)_{16}]$** and **$[Ti_{16}O_{16}(OEt)_{32}]$**. Among these clusters, **$[Ti_{11}O_{13}(O^iPr)_{18}]$**, and **$[Ti_{12}O_{16}(O^iPr)_{16}]$** are potentially interesting building blocks for hybrid materials due to their ability for selective alkoxide exchange on the hexanuclear crown of pentacoordinate titanium atoms (violet polyhedron in Figure 35a, **$[Ti_{11}O_{13}(O^iPr)_{18}]$** has one less $\{TiO_5\}$ in this crown).[136] Similarly, **$[Ti_{16}O_{16}(OEt)_{32}]$** can undergo trans-alcoholysis in a controlled fashion. For example, with the linear aliphatic alcohols like n-propanol, only 8 terminal ethoxy groups on more electrophilic titanium atoms are replaced (Figure 35b). A sterically hindered alcohol will decrease the effectiveness of ligand exchange, while using an alcohol with increased acidity, such as phenol, leads to substitution of all terminal ligands. This can be explained by mechanism of the trans-alcoholysis reaction, which is a nucleophilic substitution involving a nucleophilic addition of the entering group. This substitution is followed by proton transfer from the entering group to the leaving group, and hence the increase of the acidity favors the ligand substitution.[137]

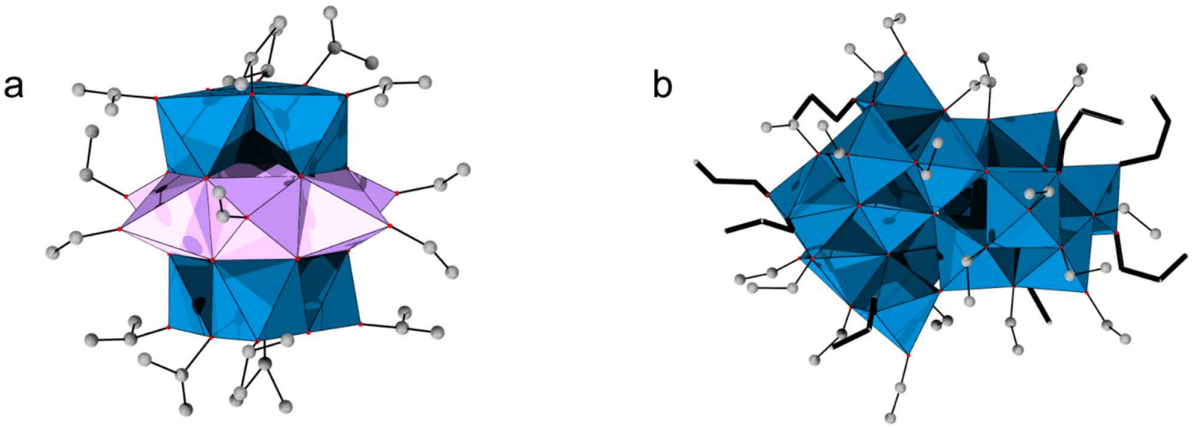

Figure 35. Ball-stick and polyhedron representation of (a) **[$Ti_{12}O_{16}(O^iPr)_{10}(OEt)_6$]** and (b) **[$Ti_{16}O_{16}(OEt)_{24}(O^nPr)_8$]**. Color code: {$TiO_5$} (violet polyhedron), {$TiO_6$} (steel blue polyhedron), carbon (gray ball). n-propanol (black wires). Hydrogen atoms omitted for clarity.

Ligand exchange with rearrangement of metal oxo core. As highlighted above, the probability of rearrangement or degradation of the metal-oxo core decreases if the leaving and entering groups have the same charge and coordination ability. However, even when these criteria are satisfied, a rearrangement of the metal oxo core can still take place. For example, when **[$Ti_{16}O_{16}(OEt)_{32}$]** reacted with an excess amount of acetylacetone (acac) in C_6D_6-toluene, the bridging OEt groups were replaced by acac groups, leading to cleavage of **[$Ti_{16}O_{16}(OEt)_{32}$]** and the formation of $Ti(OEt)_2(acac)_2$.[138] Similarly, the reaction between **[$Ti_7O_4(OEt)_{20}$]** and benzoic acid results in the formation of **[$Ti_6O_4(OEt)_{14}(OOCPh)_2$]** with a major rearrangement of the cluster core despite the presence of μ_2-OR groups in the starting cluster (Figure 36).[127] This exchange imparts different orientation of the two M-O vectors due to the different bite angle of μ_2-OR and μ_2-OOCR ligands, which may have a strong influence on the overall structure.

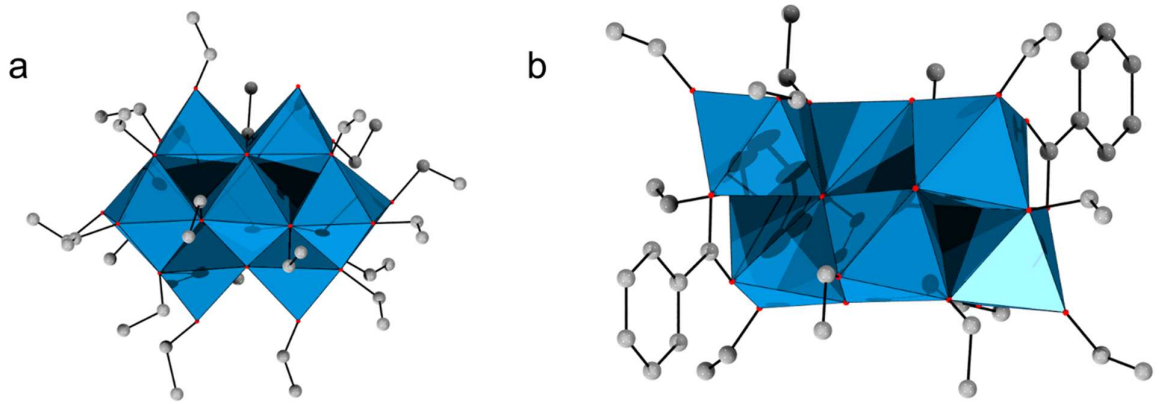

Figure 36. Ball and stick and polyhedron representation of (a) **[$Ti_7O_4(OEt)_{20}$]** and (b) **[$Ti_6O_4(OEt)_{14}(OOCPh)_2$]**. Color code: {$TiO_6$} (steel blue polyhedron), carbon (gray ball). Hydrogen atoms omitted for clarity.

Besides the alkoxy-carboxylate exchange mentioned above, a carboxylate-carboxylate exchange in carboxylate-based clusters can also trigger a structural rearrangement. For example, the highly porous MOF MIL-125 **[$Ti_8O_8(OH)_4(O_2CC_6H_4CO_2)_6$]** is prepared through

the reaction of **[$Ti_8O_8(OOCR)_{16}$]** (R = C_6H_5, $C(CH_3)_3$, CH_3) and terephthalic acid in a DMF–methanol mixture at 150ºC (Scheme 5). In this case, terephthalate triggers the complete rearrangement of **[$Ti_8O_8(OOCR)_{16}$]** starting unit, and a new cluster is present in the hybrid material. Specifically, the eight {TiO_6} units are connected via corner-sharing in **[$Ti_8O_8(OOCR)_{16}$]**, while in the **[$Ti_8O_8(OH)_4(O_2CC_6H_4CO_2)_6$]** the {$TiO_6$} are connected through both edge- and corner-sharing. This rearrangement changes the overall connectivity from 16 in **[$Ti_8O_8(OOCR)_{16}$]** to 12 in **[$Ti_8O_8(OH)_4$-$(O_2CC_6H_4CO_2)_6$]**. The reasons for this structural transformation are still unclear.[121]

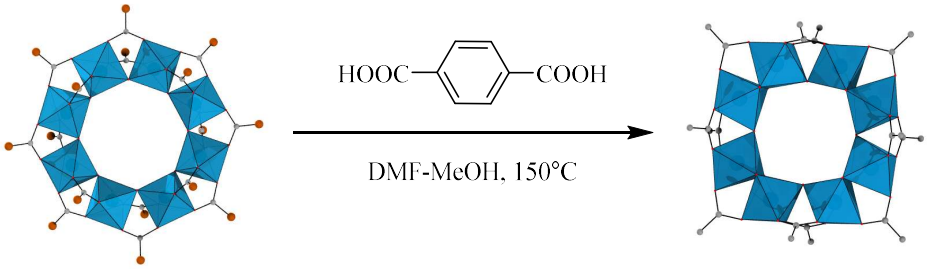

Scheme 5. Structural rearrangement of **[$Ti_8O_8(OOCR)_{16}$]** in the synthesis of **[$Ti_8O_8(OH)_4(O_2CC_6H_4CO_2)_6$]** (MIL-125). Color code: {TiO_6} steel blue polyhedron, R ligands (brown), carbon (gray), oxygen (red). Aromatic rings omitted for clarity.

4.3 Optical properties

In contrast to Zr and Hf oxo-clusters, discrete Ti oxo clusters are commonly photoactive in the UV and visible region. The band gap, which can be determined by diffuse reflectance spectroscopy, results from the interaction between the metal oxo core and its organic ligands. Thus, the presence of organic ligands not only stabilizes the metal oxo core but also provides unique way to modulate the band gap by introduction of different organic moieties. For example, the absorption threshold of **[$Ti_3O(O^iPr)_8(O_2CR')_2$]** (R' = C_6H_4Cl, C_4H_7) is localized in the UV region. However, when R' = $C_{13}H_9$, and $C_6H_4NO_2$, the absorption shifts to the visible region of the spectra. Likewise, a series of {Ti_6} hybrid clusters have been synthesized using different O-donor ligands such as carboxylate, phosphonate, and sulfonates, through ligand exchange of the **[$Ti_6O_4(O^iPr)_{10}(O_3PPhen)_2(OAc)_2$]** cluster in order to investigate the effect of

these ligands on the bandgap. In this case, electron-withdrawing organic ligands, such as aromatic carboxylates, reduce the bandgap of the correspondent Ti oxo compound.[139, 140]

These observations make the rational design of photocatalytic materials based on Ti oxo clusters very attractive. For example, MOFs built from Ti-oxo clusters demonstrated prominent photoactivity. The high porosity of MIL-125 allows for alcohol adsorption, which results in a reversible photochromic behavior upon UV-visible light irradiation. The high photonic sensitivity is promoted by the formation of a Ti(III)–Ti(IV) mixed-valence state under irradiation.[141] Moreover, hybrid organic-inorganic material based on TiO_2 and poly(hydroxyethyl methacrylate) network shows that the photonic sensitivity depends on their microstructure, which can potentially be used for producing new materials for photonic devices.[142]

5. Conclusion

In summary, discrete group IV metal oxo clusters are a diverse and versatile class of compounds, and a variety of structures has already been reported. The strong Lewis acidity of group IV metals favors their hydrolysis in the presence of water, and leads to the formation of M-O-M polymeric chains. However, such highly unpredictable reactivity is ‘tamed’ by the presence of alkoxides and/or chelating ligands like carboxylates, sulfates and phosphates, which leads to the formation of well-defined discrete cluster structures. The final cluster structure is clearly determined by the nature of the metal used. Due to the resemblance of Zr^{4+} and Hf^{4+}, several Zr and HfOCs are structurally similar, even though small adjustments in the reaction conditions for their synthesis are sometimes needed. On the other hand, smaller size and strong oxophilic character of titanium makes the control of its hydrolysis much more challenging than for Zr/Hf. Moreover, Ti usually adopts 6-coordination structure, which is distinct from the 8-coordination environment typically observed in Zr/Hf chemistry, thus probably contributing to structural differences between Ti and Zr/Hf clusters. Furthermore, the nature and the ratio of ligands present in the reaction mixture also influences the structure of cluster formed, as showcased by the different structures observed for Zr/Hf clusters in the presence or absence of sulfate ligands. Finally, the chemical properties of

ligands such as steric hindrance and acidity also play a role in the final cluster structure, with a classic example being the formation of carboxylate-based ZrOCs.

While synthesis and structure of these clusters have been extensively studied, their applications have been mostly focused on the synthesis of novel nanocomposites and metal-organic framework (MOF) materials for a variety of purposes. Such emphasis on new materials is closely related to the reasonable control achieved so far in the post-synthetic ligand exchange chemistry of carboxylate-based clusters for all three metals. A clear example of the success of this approach are the Zr-/HfOC-based MOFs that have gained prominence in catalysis and in gas/water adsorption over the last decade, due to their superior stability compared to other MOFs.[41, 143] Likewise, TiOCs have proved useful in the synthesis of photoactive Ti-based MOF and other nanomaterials, since the straightforward tuning of the optical gap can be achieved by changing the organic ligands that stabilize the cluster. The rather wide portfolio of materials obtained so far implicates understanding of the surface chemistry of MOCs as one of the fundamental challenges in order to enable the development of novel materials.

So far, the catalytic activity of group IV MOCs has been less explored compared to their use in the synthesis of new materials. Most of the relevant catalytic applications are those in which the MOCs are embedded in MOFs, such as the highly promising activity of Zr(IV) or Hf(IV) MOFs towards decomposition of nervous agents,[144] and in hydrolysis of amide bonds in peptides and proteins.[145-147] On the other hand, the catalytic activity of discrete MOCs remains virtually unexplored.[148] One of the few examples being disclosed recently, in which the hydrolytic potential of the discrete **Hf_{18}** cluster towards protein was evaluated using horse-heart myoglobin.[125] In this case, **Hf_{18}** cluster has been proposed as an efficient heterogeneous nanozyme for the hydrolysis of proteins, showcasing that MOCs in itself have quite attractive and unique catalytic features. In this sense, MOCs promising catalytic activity can be developed in two directions, either as discrete clusters or as part of more complex hybrid materials.

The chemistry of group IV MOCs presented here has been also supporting further developments in the structural and applied chemistry of mixed-metal clusters [97, 109, 149]

and tetravalent lanthanides like Ce(IV),[150, 151] and actinides (Th(IV), U(IV), Np(IV) and Pu(IV)).[152]

Table 5: Discrete of Ti, Zr and Hf oxo clusters presented in this review

Nuclearity	Oxo cluster	Main ligands	Ref.
Zr_3	**$[(L_{OEt})_3Zr_3(\mu_3\text{-}O)(\mu\text{-}OH)_3(\mu_3\text{-}PO_4)]$**$[NO_3]$	$[CpCo\{P(O)(OEt)_2\}_3]^-$	[65]
Zr_3	**$[Zr_3(\mu_3\text{-}O)(DMPD)_4(DMPDH)_2]$**	2,4-Dimethylpentane-2,4-diol	[74]
Zr_3	**$[(Cp_2Zr)_3(\mu_2\text{-}OH)_3(\mu_3\text{-}O)]$**$(BPh_4)$	Cp	[75]
Zr_3	**$[(CpZr)_3(\mu_2\text{-}OH)_3(\mu_3\text{-}O)(OOCH)_3]$**Cl	Cp, formate	[76]
Zr_3	**$[Zr_3(\mu_3\text{-}O)(\mu\text{-}OOCMe)_3(OOCMe)_2(\mu\text{-}O^iPr)_2(O^iPr)_3]$**	Acetate, propoxide	[153]
Zr_3	**$[Zr_3(\mu_3\text{-}O)(\mu_3\text{-}ONep)(\mu\text{-}ONep)_3(ONep)_6]$**	2,2-Dimethyl-1-propoxide	[153]
Zr_3	**$[Zr_3(\mu_3\text{-}O)(\mu\text{-}OOCMe)_3(\mu\text{-}ONep)_2(ONep)_5]$**	Acetate, 2,2-Dimethyl-1-propoxide	[153]
Zr_4	**$[Zr_4(OH)_8(OH_2)_{16}]Cl_8$**•$12H_2O$		[61]
Zr_4	**$[(L_{OEt})_4Zr_4(\mu_3\text{-}O)_2(\mu\text{-}OH)_4(H_2O)_2]$**$[NO_3]_4$	$[CpCo\{P(O)(OEt)_2\}_3]^-$ (Kläui Ligand)	[65]
Zr_4	**$[(L_{OEt})_4Zr_4(\mu_3\text{-}PO_3)_4]$**	$[CpCo\{P(O)(OEt)_2\}_3]^-$	[65]
Zr_4	**$[Zr_4(OH)_4(\mu\text{-}O_2)_2(\mu_4\text{-}O)(H_2O)_{12}](ClO_4)_6$**•$4H_2O$	Peroxide, H_2O	[66]
Zr_4	**$[Zr_4O_2(OMc)_{12}]$**	Methacrylate	[57] [81]
Zr_4	**$[Zr_4(O^nPr)_{16}]$**	Propoxide	[80]
Zr_4	**$[Zr_4O_2(OMc)_6(OPiv)_6]$**	Pivalate	[107]
Zr_4	**$[Zr_4(\mu_4\text{-}O)(\mu\text{-}O)(\mu\text{-}OOCH)_2(\mu\text{-}O^iPr)4(O^iPr)_6]$**	Propoxide, Formate	[153]
Zr_4	**$[Zr_2(\mu\text{-}iso\text{-butanoate})_2(\mu\text{-}O^iPr)_2(O^iPr)_4]_2$**	Isobutanoate, Propoxide	[153]

Zr_5	**$[Zr_5(\mu\text{-}O)_3(\mu\text{-}iso\text{-butanoate})_6(\mu\text{-}ONep)_2(ONep)_6]$**	Isobutanoate, 2,2-Dimethyl-1-propoxide	[153]
Zr_5	**$[Zr_5O_4((CH_3)_2BrCCO_2)_{10}(O^nPr)_2(^nPrOH)_4]$**	2-Bromo-isobutanoate, Propoxide	[55]
Zr_5	**$[Zr_5(\mu\text{-}O)_3(\mu\text{-}ONc)_6(\mu\text{-}ONep)_2(ONep)_6]\bullet(H\text{-}ONep)\bullet 1/2(C_7H_8)$**	3,3-Dimethylbutanoate, 2,2-Dimethyl-1-propoxide	[153]
Zr_6	**$[Zr_6(OH)_4O_4(OMc)_{12}]$**	Methacrylate	[57, 72]
Zr_6	**$[Zr_6(OH)_4O_4(OMc)_{12}(^nPrOH)]\bullet$**3McOH	Methacrylate	[85]
Zr_6	**$[Zr_6O_4(OH)_4(iso\text{-butanoate})_{12}(H_2O)]$**	Isobutanoate	[56]
Zr_6	**$[Zr_6(OH)_4O_4(OOCPh)_{12}(BzOH)]\bullet$**4BzOH	Benzoate	[85]
Zr_6	**$[Zr_6O_4(OH)_4(OH_2)_8(HCOO)_4(SO_4)_4]$**	Formate, SO_4^{2-}	[70]
Zr_6	**$[Zr_6(\mu_3\text{-}OH)_8(OH)_8(\kappa_2\text{-}bdmpza)_8]$**	bis(3,5-Dimethylpyrazol-1-yl)acetate	[154]
Zr_6	**$[Zr_6O_4(OH)_4(OPiv)_{12}]$**	Pivalate	[90]
Zr_6	**$[Zr_6O_4(OH)_4(OOCC(CH_3)_2Et)_{12}]$**	2,2-Dimethylbutanoate	[90]
Zr_6	**$[Zr_6O_4(OH)_4(OOC\text{–}Norb)_{12}]$**	*endo*-5-Norbornene-2-carboxylic acid	[86]
Zr_6	**$[Zr_6(OH)_8(H_2O)_8(HGly)_4(Gly)_4]\bullet(SO_4)_6\bullet 14H_2O$**	Glycine	[87]
Zr_6	**$[Zr_6O_2(OBu)_{10}(OMc)_{10}]$**	Methacrylate, Butoxide	[91]
Zr_6	**$[Zr_6O_2(OMe)_4(OBu)_2(OMc)_{14}]$**	Methacrylate, Methoxide, Butoxide	[91]
Zr_6	**$[Zr_6O_2(OPr)_{16}(O_2C(O)C_{10}H_6)_2(PrOH)_2]$**.	1-Hydroxy-2-Naphthoate	[92]
Zr_6	**$[Zr_6(\mu_3\text{-}O)_2(\mu\text{-}O)_3(\mu\text{-}Hdihybo)_6(OH_2)_6]$** $\bullet 2Bu_4NCl\cdot 2CH_3OH$	2,3-Dihydroxy benzaldehyde oxime	[93]
Zr_6	**$[Zr_6(\mu_3\text{-}O)_2(\mu_2\text{-}OBu)_{12}(O_3PPh)_4]$**	Phenylphosphonate	[94]
Zr_6	**$[Zr_6(\mu_3\text{-}O)_4(\mu_3\text{-}OH)_4(OOCCH_2{}^tBu)_9]$**	3,3-Dimethylbutanoate	[100]

Zr_6	**$[Zr_6O_4(OH)_4(OMc)_8(iso\text{-}butanoate)_4(BuOH)]$**	Methacrylate, Isobutanoate	[56]
Zr_6	**$[Zr_6(\mu_3\text{-}O)_2(4\text{-}aPhaa)_4(O^nPr)_{12}]$**	4-Aminophenylarsonate	[155]
Zr_6	**$[Zr_6(\mu_3\text{-}O)_2(tbpa)_4(O^nPr)_{12}]$**	*tert*-Butylphosphonate	[155]
Zr_6	H_2**$[Zr_6(\mu_3\text{-}O)(\mu_2\text{-}O)(tbpa)_5(O^nPr)_{12}]$**	*tert*-Butylphosphonate	[155]
Zr_7	**$[Zr_7O_2(\mu_2\text{-}O^iPr)_6(O^iPr)_6(O_3PCH_2CH_2CH_2Br)_6]$**	(3-Bromopropyl) phosphonate	[94]
Zr_8	**$[Zr_8O_6(carboxylate)_{12}]^{8+}$** (**$[M_8O_6(M'\text{–}TCPP)_3]$** M'= Fe, Co, Cu, no metal)	5,10,15,20-tetrakis(4-Methoxycarbonylphenyl) porphyrin (TCCP)	[95]
Zr_8	**$[Zr_8(OH)_{20}(H_2O)_{24}Cl_{12}]$**		[64]
Zr_9	**$[Zr_9(\mu_3\text{–}O)_8(\mu_3\text{–}OH)_6(carboxylate)_6]$**	4-Picolinate	[96]
Zr_9	**$[Zr_9(\mu_3\text{–}O)_8(\mu_3\text{-}OH)_6(carboxylate)_{12}]$**	4-Picolinate	[96]
Zr_9	**$[Zr_9O_6(OBu)_{18}(OOCC{\equiv}CEt)_6]$**	2-Pentynoate	[97]
Zr_{10}	**$[Zr_{10}O_6(OH)_4(OOC\text{–}C_6H_4OH)_8(OOC\text{–}C_6H_4O)_8]$** •6PrOH	Salicylate	[92]
Zr_{10}	**$[Zr_{10}O_8(OBu)_{16}(OOC\text{–}C_6H_4\text{–}CH_2Cl)_8]$**	4-(Chloromethyl) benzoate	[97]
Zr_{10}	H_4**$[Zr_{10}(\mu_4\text{-}O)_4(\mu_3\text{-}O)_4(ppa)_4(O^nPr)_{20}]$**	Phenylphosphonate	[155]
Zr_{12}	**$[Zr_6(OH)_4O_4(OAcr)_{12}]_2$**	Acrylate	[85]
Zr_{12}	**$[Zr_6O_4(OH)_4(OOCMe)_{12}]_2$**•6MeCOOH	Acetate	[98]
Zr_{12}	**$[Zr_6O_4(OH)_4(OOCCH_2Me)_{12}]_2$**•6Me$CH_2$COOH	Propanoate	[98]
Zr_{12}	**$[Zr_6O_4(OH)_4(OOCCH_2CH{=}CH_2)_{12}]_2$**•6$CH_2$=CH CH_2COOH	Vinylacetate	[98]
Zr_{12}	**$[Zr_6O_4(OH)_4(OOCCH{=}CMe_2)_{12}]_2$**•4$Me_2$C=CHCO OH	3,3'-Dimethylacrylate	[98]
Zr_{12}	**$[Zr_{12}(\mu_3\text{-}O)_8(\mu_3\text{-}OH)_8(MP)_{24}]$**•4(MPA)	3-Marcaptopropionoate	[99]
Zr_{12}	**$[Zr_6O_4(OH)_4(OOCEt)_{11}(acac)]_2$**	Propanoate, Acetylacetonate	[109]

Zr_{12}	**$[Zr_6O_4(OH)_4(OOCCH_2CH{=}CH_2)_{11}(acac)]_2$**	Vinylacetate, Acetylacetonate	[109]
Zr_{12}	**$[Zr_6O_4(OH)_4(OOCEt)_3(OMc)_9]_2$** •McOH•5Me$CH_2COOH$	Propanoate, Methacrylate	[98]
Zr_{12}	**$[Zr_6O_4(OH)_4(OOCMe)_8(OMc)_4]_2$**•6MeCOOH	Acetate, Methacrylate	[98]
Zr_{12}	**$[Zr_{12}(\mu_3\text{-}O)_{16}(OOCEt)_{12}(OOCMe)_8(\mu_2\text{-}OOCEt)_4]$**	Propanoate, Acetate	[107]
Zr_{13}	**$[Zr_{13}O_8(OCH_3)_{36}]$**	Methoxide	[101]
Zr_{17}	**$[Zr_{17}O_8(OH)_{24}(OH_2)_{12}(HCOO)_{12}(SO_4)_8]$** •6HCl·30$H_2O$	Formate, SO_4^{2-}	[70]
Zr_{18}	**$[Zr_{18}O_4(OH)_{38.8}(SO_4)_{12.6}]$•33$H_2O$**	SO_4^{2-}	[71]
Zr_{18}	**$[Zr_{18}O_{21}(OH)_2(OOCPh)_{28}]$**	Benzoate	[102]
Zr_{25}	**$[Zr_{25}O_{10}(OH)_{50}(O_2)_5(H_2O)_{40}](ClO_4)_{10}$**•x$H_2O$	Peroxide, Water	[66]
Zr_{26}	**$[Zr_{26}O_{18}(OH)_{30}(HCOO)_{38}]$**·5(HCOOH)·*k*$H_2O$	Formate	[103]
Zr_{70}	**$Zr_{70}(SO_4)_{58}(O/OH)_{146}.x(H_2O)$**	SO_4^{2-}	[68]
	Hafnium clusters		
Hf_4	**$[Hf_4(OH)_8(H_2O)_{16}]^{8+}$**		[113]
Hf_4	**$[Hf_4(OH)_8(H_2O)_{16}]Cl_8$**•($C_{36}H_{36}N_{24}O_{12}$)•16$H_2O$		[62]
Hf_4	**$[Hf_4(OH)_8(H_2O)_{16}]$**(p-toluenesulfonate)$_8$•4H_2O		[114]
Hf_4	**$[Hf_4(\mu\text{-}OH)_6(\mu\text{-}O_2)(H_2O)_{16}]$**•($ClO_4$)$_8$•15$H_2O$	O_2^{2-}	[115]
Hf_4	**$[Hf_4(\mu\text{-}OH)_4(\mu\text{-}O_2)_2(H_2O)_{16}]$**($ClO_4$)$_8$•5$H_2O$	O_2^{2-}	[115]
Hf_4	**$[Hf_4O_2(OMc)_{12}]$**	Methacrylate	[111]
Hf_4	**$[Hf_4(\mu_2\text{-}SAc)_6(\mu_2\text{-}BuO)_4(BuO)_2(\mu_3\text{-}O)_2]$**	Thioacetate	[116]
Hf_6	**$[Hf_6O_4(OH)_4(OMc)_{12}(BuOH)]$**	Methacrylate	[111]
Hf_6	**$[Me_3NH]_6[Hf_6(\mu\text{-}O_2)_6(\mu\text{-}OH)_6(OH)_{12}]$**•38$H_2O$	Peroxide	[117]
Hf_6	**$(NH_4)_5[Hf_6(O_4OH)(SO_4)_{10}(H_2O)_7]$**	SO_4^{2-}	[118]

Hf_9	**$(NH_4)_{14}[Hf_9O_8(OH)_6(SO_4)_{14}]$** •$nH_2O$	SO_4^{2-}	[58, 119]
Hf_{11}	**$(NH_4)_{11}[Hf_{11}O_7(OH)_{11}(SO_4)_{15}(H_2O)_6]$**•$nH_2O$	SO_4^{2-}	[58]
Hf_{12}	**$[Hf_{12}(\mu_3\text{-}O)_8(\mu_3\text{-}OH)_8(MP)_{24}$•5(MPA)**	3-Mercaptopropanoate	[99]
Hf_{12}	**$[Hf_6O_4(OH)_4(OOCMe)_{12}]_2$**•6MeCOOH•$6CH_2Cl_2$	Acetate	[98]
Hf_{12}	**$Hf_{12}O_8(OH)_{14}$(carboxylate)**	4,4′-biphenyl dicarboxylate	[156]
Hf_{17}	**$[Hf_{17}O_8(OH)_{24}(OH_2)_{12}(HCOO)_{12}(SO_4)_8]$**•6HCl•30 H_2O	Formate, SO_4^{2-}	[70]
Hf_{17}	**$[Hf_{17}O_8(OH)_{28}(SO_4)_{11}(H_2O)_{23}][SO_4]$**•$32.25H_2O$	SO_4^{2-}	[114]
Hf_{18}	**$[Hf_{18}O_{10}(OH)_{26}(SO_4)_{13}(H_2O)_{33}]$** (**$Hf_{18}$**)	SO_4^{2-}	[2, 112]
	Titanium clusters		
Ti_3	**$[Ti_3O(O^iPr)_8(OOCR')_2]$**	Carboxylate (**OOCR'**) R' = C_6H_4Cl, C_4H_7, $C_{13}H_9$, and $C_6H_4NO_2$	[140]
Ti_6	**$[Ti_6O_6(O^iPr)_6(OOCH)_6]$**	Isopropoxide, Formate	[128]
Ti_6	K_2**$[Ti_6(\mu_3\text{-}O)_2(\mu\text{-}O)_3(OCH_3)_4(CH_3OH)_2(\mu\text{-}Hdihybo)_6]$**•$CH_3OH$	2,3-Dihydroxy benzaldehyde oxime	[129]
Ti_6	**$[Ti_6O_4(OEt)_{14}(OOCPh)_2]$**	Ethoxide, Benzoate	[127]
Ti_6	**$[Ti_6O_4(O^iPr)_{10}(O_3PPhen)_2(OAc)_2]$**	Isopropoxide, Phenylphosphate	[138]
Ti_7	**$[Ti_7O_4(OEt)_{20}]$**	Ethoxide	[123], [124]
Ti_8	**$[Ti_8O_8(OOCR)_{16}]$**	Carboxylate (**OOCR**) R = C_6H_5, $C(CH_3)_3$, CH_3	[130]
Ti_8	**$[Ti_8O_8(OH)_4(O_2CC_6H_4CO_2)_6]$**	Terephthalate	[121]
Ti_{11}	**$[Ti_{11}O_{13}(O^iPr)_{18}]$**	Isopropoxide	[136]

Ti_{12}	**$[Ti_{12}O_{16}(O^{i}Pr)_{16}]$**	Isopropoxide	[136]
Ti_{16}	**$[Ti_{16}O_{16}(OEt)_{32}]$**	Ethoxide	[137]
Ti_{18}	**$[Ti_{18}O_{28}H][O^{t}Bu]_{17}$**	*tert*-Butoxide	[131]
Ti_{18}	**$[Ti_{18}O_{27}(OH_2)_{30}(SO_4)_6]Cl_6$**•6TBAC•$12H_2O$	SO_4^{2-}	[132] [133]
Ti_{42}	H_6**$[Ti_{42}(\mu_3\text{-}O)_{60}(O^{i}Pr)_{42}(OH)_{12}]$**	Isopropoxide	[134]

[a] Cp = cyclopentadienyl, BzO = benzoate, OOC–Norb = *endo*-5-Norbornene-2-carboxylate, TPPCOOMe = 5,10,15,20-Tetrakis(4-methoxycarbonylphenyl)porphyrin, HONep = 2,2-Dimethyl-1-propanol, HONc = 3,3-Dimethylbutanoate, tbpa = *tert*-Butylphosphonate, bdmpza = bis(3,5-Dimethylpyrazol-1-yl)acetate, 4-aPhaa = 4-Aminophenylarsonic acid

Declaration of Competing Interest

The authors declare that they have no known competing financial interests or personal relationships that could have appeared to influence the work reported in this paper

Author Contributions

Yujie Zhang: Writing - Original Draft (including figures). **Francisco de Azambuja:** Conceptualization, Writing - Review & Editing. **Tatjana N. Parac-Vogt:** Conceptualization, Writing - Review & Editing, Supervision.

Author Information

Web page: https://lbc.chem.kuleuven.be

ORCID

Tatjana N. Parac-Vogt – orcid.org/0000-0002-6188-3957

Francisco de Azambuja – orcid.org/0000-0002-5537-5411

Acknowledgements

We thank KU Leuven and Research Foundation Flanders (FWO) for generous financial support. YZ thanks Chinese Scholar Council (CSC) for doctoral fellowship (201804910511). F.d.A. thanks FWO for fellowship (195931/1281921N).

6. References

[1] Y.-J. Hu, K.E. Knope, S. Skanthakumar, M.G. Kanatzidis, J.F. Mitchell, L. Soderholm, J. Am. Chem. Soc., 135 (2013) 14240-14248.
[2] R.E. Ruther, B.M. Baker, J.-H. Son, W.H. Casey, M. Nyman, Inorg. Chem., 53 (2014) 4234-4242.
[3] G. Guillemot, E. Matricardi, L.-M. Chamoreau, R. Thouvenot, A. Proust, ACS Catal., 5 (2015) 7415-7423.
[4] T. Zhang, L. Mazaud, L.-M. Chamoreau, C. Paris, A. Proust, G. Guillemot, ACS Catal., 8 (2018) 2330-2342.
[5] T. Zhang, A. Solé-Daura, S. Hostachy, S. Blanchard, C. Paris, Y. Li, J.J. Carbó, J.M. Poblet, A. Proust, G. Guillemot, J. Am. Chem. Soc., 140 (2018) 14903-14914.
[6] A. Solé-Daura, T. Zhang, H. Fouilloux, C. Robert, C.M. Thomas, L.-M. Chamoreau, J.J. Carbó, A. Proust, G. Guillemot, J.M. Poblet, ACS Catal., 10 (2020) 4737-4750.
[7] M.T. Pope, Introduction to Polyoxometalate Chemistry, in: J.J. Borrás-Almenar, E. Coronado, A. Müller, M. Pope (Eds.) Polyoxometalate Molecular Science, Springer Netherlands, Dordrecht, 2003, pp. 3-31.
[8] P. Putaj, F. Lefebvre, Coord. Chem. Rev., 255 (2011) 1642-1685.
[9] X. López, J.J. Carbó, C. Bo, J.M. Poblet, Chem. Soc. Rev., 41 (2012) 7537-7571.
[10] H.N. Miras, J. Yan, D.-L. Long, L. Cronin, Chem. Soc. Rev., 41 (2012) 7403-7430.
[11] M. Arefian, M. Mirzaei, H. Eshtiagh-Hosseini, A. Frontera, Dalton Transactions, 46 (2017) 6812-6829.
[12] A. Misra, K. Kozma, C. Streb, M. Nyman, Angew. Chem. Int. Ed., 0 (2019).
[13] N.I. Gumerova, A. Rompel, Chem. Soc. Rev., (2020).
[14] S.-S. Wang, G.-Y. Yang, Chem. Rev., 115 (2015) 4893-4962.
[15] K. Kamata, K. Sugahara, Catalysts, 7 (2017).
[16] T.K.N. Luong, T.T. Mihaylov, G. Absillis, P. Shestakova, K. Pierloot, T.N. Parac-Vogt, Inorganic Chemistry, 55 (2016) 9898-9911.
[17] L.S. Van Rompuy, T.N. Parac-Vogt, Chemical Communications, 53 (2017) 10600-10603.
[18] T.K.N. Luong, I. Govaerts, J. Robben, P. Shestakova, T.N. Parac-Vogt, Chem. Commun., 53 (2017) 617-620.
[19] F. de Azambuja, T.N. Parac-Vogt, ACS Catal., 9 (2019) 10245-10252.
[20] F. de Azambuja, J. Lenie, T.N. Parac-Vogt, ACS Catal., 11 (2021) 271-277.
[21] F. de Azambuja, J. Moons, T.N. Parac-Vogt, Acc. Chem. Res., (2021) DOI: 10.1021/acs.accounts.1020c00666.

[22] Y. Cao, Q. Chen, C. Shen, L. He, Molecules, 24 (2019).
[23] D. Ravelli, M. Fagnoni, T. Fukuyama, T. Nishikawa, I. Ryu, ACS Catal., 8 (2018) 701-713.
[24] K. Suzuki, N. Mizuno, K. Yamaguchi, ACS Catal., 8 (2018) 10809-10825.
[25] C. Streb, K. Kastner, J. Tucher, Physical Sciences Reviews, 4 (2019) 20170177.
[26] Y.-Q. Lan, N. Li, J. Liu, B.-X. Dong, Angew. Chem. Int. Ed., n/a (2020).
[27] J.-W. Zhao, Y.-Z. Li, L.-J. Chen, G.-Y. Yang, Chemical Communications, 52 (2016) 4418-4445.
[28] K.P. Sullivan, Q. Yin, D.L. Collins-Wildman, M. Tao, Y.V. Geletii, D.G. Musaev, T. Lian, C.L. Hill, Frontiers in Chemistry, 6 (2018).
[29] A.V. Anyushin, A. Kondinski, T.N. Parac-Vogt, Chem. Soc. Rev., 49 (2020) 382-432.
[30] K. Zhou, G. Ding, C. Zhang, Z. Lv, S. Luo, Y. Zhou, L. Zhou, X. Chen, H. Li, S.-T. Han, J. Mater. Chem. C, 7 (2019) 843-852.
[31] L. Chen, W.-L. Chen, X.-L. Wang, Y.-G. Li, Z.-M. Su, E.-B. Wang, Chem. Soc. Rev., 48 (2019) 260-284.
[32] B. Huang, D.-H. Yang, B.-H. Han, Journal of Materials Chemistry A, 8 (2020) 4593-4628.
[33] M.H. Pablico-Lansigan, W.J. Hickling, E.A. Japp, O.C. Rodriguez, A. Ghosh, C. Albanese, M. Nishida, E. Van Keuren, S. Fricke, N. Dollahon, S.L. Stoll, ACS Nano, 7 (2013) 9040-9048.
[34] K. De Clercq, E. Persoons, T. Napso, C. Luyten, T.N. Parac-Vogt, A.N. Sferruzzi-Perri, G. Kerckhofs, J. Vriens, PNAS, 116 (2019) 13927-13936.
[35] S. de Bournonville, S. Vangrunderbeeck, H.G.T. Ly, C. Geeroms, W.M. De Borggraeve, T.N. Parac-Vogt, G. Kerckhofs, Acta Biomaterialia, 105 (2020) 253-262.
[36] U. Schubert, Chem. Soc. Rev., 40 (2011) 575-582.
[37] S. Gross, J. Mater. Chem., 21 (2011) 15853-15861.
[38] D.J. Tranchemontagne, J.L. Mendoza-Cortés, M. O'Keeffe, O.M. Yaghi, Chem. Soc. Rev., 38 (2009) 1257-1283.
[39] Y. Bai, Y. Dou, L.-H. Xie, W. Rutledge, J.-R. Li, H.-C. Zhou, Chem. Soc. Rev., 45 (2016) 2327-2367.
[40] H. Assi, G. Mouchaham, N. Steunou, T. Devic, C. Serre, Chem. Soc. Rev., 46 (2017) 3431-3452.
[41] L. Feng, J. Pang, P. She, J.-L. Li, J.-S. Qin, D.-Y. Du, H.-C. Zhou, Adv. Mater., 32 (2020) 2004414.
[42] U. Schubert, Macromolecular Symposia, 267 (2008) 1-8.
[43] M. Wen, G. Li, H. Liu, J. Chen, T. An, H. Yamashita, Environmental Science: Nano, 6 (2019) 1006-1025.
[44] X. Liu, X. Wang, F. Kapteijn, Chem. Rev., 120 (2020) 8303-8377.
[45] J. Li, P.M. Bhatt, J. Li, M. Eddaoudi, Y. Liu, Adv. Mater., 32 (2020) 2002563.
[46] A. Bavykina, N. Kolobov, I.S. Khan, J.A. Bau, A. Ramirez, J. Gascon, Chem. Rev., 120 (2020) 8468–8535.
[47] O. Sadeghi, L.N. Zakharov, M. Nyman, Science, 347 (2015) 1359-1362.
[48] O. Sadeghi, C. Falaise, P.I. Molina, R. Hufschmid, C.F. Campana, B.C. Noll, N.D. Browning, M. Nyman, Inorg. Chem., 55 (2016) 11078-11088.
[49] P. Yang, U. Kortz, Acc. Chem. Res., 51 (2018) 1599-1608.
[50] X.-Y. Zheng, J. Xie, X.-J. Kong, L.-S. Long, L.-S. Zheng, Coord. Chem. Rev., 378 (2019) 222-236.
[51] R.M. Bullock, J.G. Chen, L. Gagliardi, P.J. Chirik, O.K. Farha, C.H. Hendon, C.W. Jones, J.A. Keith, J. Klosin, S.D. Minteer, R.H. Morris, A.T. Radosevich, T.B. Rauchfuss, N.A. Strotman, A. Vojvodic, T.R. Ward, J.Y. Yang, Y. Surendranath, Science, 369 (2020) eabc3183.
[52] M. Dayah, in, ptable.com, 1997.
[53] W.M. Haynes, D.R. Lide, T.J. Bruno, CRC Handbook of Chemistry and Physics, CRC Press, Boca Raton, Florida, 2017.

[54] C.F.M. Baes, R. E., Titanium, Zirconium, Hafnium and Thorium, the Hydrolysis ofCations, Wiley-Inter-Science, New York, 1976.
[55] G. Kickelbick, D. Holzinger, C. Brick, G. Trimmel, E. Moons, Chem. Mater., 14 (2002) 4382-4389.
[56] F.R. Kogler, M. Jupa, M. Puchberger, U. Schubert, J. Mater. Chem., 14 (2004) 3133-3138.
[57] G. Kickelbick, U. Schubert, Chem. Ber., 130 (1997) 473-478.
[58] A. Kalaji, L. Soderholm, Inorg. Chem., 53 (2014) 11252-11260.
[59] W.-H. Fang, L. Zhang, J. Zhang, Chem. Soc. Rev., 47 (2018) 404-421.
[60] C. Liu, Y. Wang, Chem. Eur. J., n/a (2020).
[61] A. Clearfield, P.A. Vaughan, Acta Cryst., 9 (1956) 555-558.
[62] T.V. Mit''kina, O.A. Gerasko, M.N. Sokolov, D.Y. Naumov, V.P. Fedin, Russian Chemical Bulletin, 53 (2004) 80-85.
[63] A. Clearfield, J. Mater. Res., 5 (1990) 161-162.
[64] A. Singhal, L.M. Toth, J.S. Lin, K. Affholter, J. Am. Chem. Soc., 118 (1996) 11529-11534.
[65] Q.-F. Zhang, T.C.H. Lam, E.Y.Y. Chan, S.M.F. Lo, I.D. Williams, W.-H. Leung, Angew. Chem. Int. Ed., 43 (2004) 1715-1718.
[66] J.A. Sommers, D.C. Hutchison, N.P. Martin, K. Kozma, D.A. Keszler, M. Nyman, J. Am. Chem. Soc., 141 (2019) 16894-16902.
[67] L.A. Chiavacci, S.H. Pulcinelli, C.V. Santilli, V. Briois, Chemistry of Materials, 10 (1998) 986-993.
[68] S. Øien-Ødegaard, C. Bazioti, E.A. Redekop, Ø. Prytz, K.P. Lillerud, U. Olsbye, Angew. Chem. Int. Ed., 59 (2020) 21397-21402.
[69] L.A. Chiavacci, C.V. Santilli, S.H. Pulcinelli, C. Bourgaux, V. Briois, Chemistry of Materials, 16 (2004) 3995-4004.
[70] Q. Sun, C. Liu, G. Zhang, J. Zhang, C.-H. Tung, Y. Wang, Chem. Eur. J., 24 (2018) 14701-14706.
[71] P.J. Squattrito, P.R. Rudolf, A. Clearfield, Inorg. Chem., 26 (1987) 4240-4244.
[72] G. Kickelbick, M.P. Feth, H. Bertagnolli, M. Puchberger, D. Holzinger, S. Gross, J. Chem. Soc., Dalton Trans., (2002) 3892-3898.
[73] R. Deshmukh, M. Niederberger, Chem. Eur. J., 23 (2017) 8542-8570.
[74] M. A. Walters, K.-C. Lam, S. Damo, R. D. Sommer, A. L. Rheingold, Inorg. Chem. Commun., 3 (2000) 316-318.
[75] M. Niehues, G. Erker, O. Meyer, R. Fröhlich, Organometallics, 19 (2000) 2813-2815.
[76] F. Boutonnet, M. Zablocka, A. Igau, J. Jaud, J.-P. Majoral, J. Schamberger, G. Erker, S. Werner, C. Krüger, J. Chem. Soc., Chem. Commun., (1995) 823-824.
[77] G. Liu, Z. Ju, D. Yuan, M. Hong, Inorg. Chem., 52 (2013) 13815-13817.
[78] M. Maity, P. Howlader, P.S. Mukherjee, Crystal Growth & Design, 18 (2018) 6956-6964.
[79] W. Zhong, D. Alexeev, I. Harvey, M. Guo, D.J.B. Hunter, H. Zhu, D.J. Campopiano, P.J. Sadler, Angew. Chem. Int. Ed., 43 (2004) 5914-5918.
[80] V.W. Day, W.G. Klemperer, M.M. Pafford, Inorg. Chem., 40 (2001) 5738-5746.
[81] G. Trimmel, S. Gross, G. Kickelbick, U. Schubert*, Appl. Organomet. Chem., 15 (2001) 401-406.
[82] B. Moraru, G. Kickelbick, M. Battistella, U. Schubert, J. Organomet. Chem., 636 (2001) 172-174.
[83] Y. Chi, J.-W. Lan, W.-L. Ching, S.-M. Peng, G.-H. Lee, J. Chem. Soc., Dalton Trans., (2000) 2923-2927.
[84] S.O. Baumann, M. Puchberger, U. Schubert, Dalton Transactions, 40 (2011) 1401-1406.
[85] G. Kickelbick, P. Wiede, U. Schubert, Inorg. Chim. Acta, 284 (1999) 1-7.
[86] Y. Gao, F.R. Kogler, H. Peterlik, U. Schubert, J. Mater. Chem., 16 (2006) 3268-3276.
[87] L. Pan, R. Heddy, J. Li, C. Zheng, X.-Y. Huang, X. Tang, L. Kilpatrick, Inorg. Chem., 47 (2008) 5537-5539.

[88] I. Pappas, M. Fitzgerald, X.-Y. Huang, J. Li, L. Pan, Crystal Growth & Design, 9 (2009) 5213-5219.
[89] C. Hennig, S. Weiss, W. Kraus, J. Kretzschmar, A.C. Scheinost, Inorg. Chem., 56 (2017) 2473-2480.
[90] P. Piszczek, A. Radtke, A. Grodzicki, A. Wojtczak, J. Chojnacki, Polyhedron, 26 (2007) 679-685.
[91] B. Moraru, S. Gross, G. Kickelbick, G. Trimmel, U. Schubert, Monatshefte für Chemie / Chemical Monthly, 132 (2001) 993-999.
[92] G. Kickelbick, U. Schubert, J. Chem. Soc., Dalton Trans., (1999) 1301-1306.
[93] S.S. Passadis, M.G. Papanikolaou, A. Elliott, C.G. Tsiafoulis, A.C. Tsipis, A.D. Keramidas, H.N. Miras, T.A. Kabanos, Inorg. Chem., 59 (2020) 18345-18357.
[94] M. Czakler, U. Schubert, Monatshefte für Chemie - Chemical Monthly, 146 (2015) 1371-1374.
[95] D. Feng, H.-L. Jiang, Y.-P. Chen, Z.-Y. Gu, Z. Wei, H.-C. Zhou, Inorg. Chem., 52 (2013) 12661-12667.
[96] W. Gong, H. Arman, Z. Chen, Y. Xie, F.A. Son, H. Cui, X. Chen, Y. Shi, Y. Liu, B. Chen, O.K. Farha, Y. Cui, J. Am. Chem. Soc., 143 (2021) 657-663.
[97] C. Artner, M. Czakler, U. Schubert, Inorg. Chim. Acta, 432 (2015) 208-212.
[98] M. Puchberger, F.R. Kogler, M. Jupa, S. Gross, H. Fric, G. Kickelbick, U. Schubert, European Journal of Inorganic Chemistry, 2006 (2006) 3283-3293.
[99] F. Faccini, H. Fric, U. Schubert, E. Wendel, O. Tsetsgee, K. Müller, H. Bertagnolli, A. Venzo, S. Gross, J. Mater. Chem., 17 (2007) 3297-3307.
[100] P. Piszczek, A. Radtke, A. Wojtczak, T. Muzioł, J. Chojnacki, Polyhedron, 28 (2009) 279-285.
[101] B. Morosin, Acta Crystallogr. Sect. B, 33 (1977) 303-305.
[102] T. Xu, X. Hou, Y. Wang, J. Zhang, J. Zhang, B. Liu, Dalton Transactions, 46 (2017) 10185-10188.
[103] B. Nateghi, I. Boldog, K.V. Domasevitch, C. Janiak, CrystEngComm, 20 (2018) 5132-5136.
[104] U. Schubert, Coord. Chem. Rev., 350 (2017) 61-67.
[105] B. Buchegger, J. Kreutzer, B. Plochberger, R. Wollhofen, D. Sivun, J. Jacak, G.J. Schütz, U. Schubert, T.A. Klar, ACS Nano, 10 (2016) 1954-1959.
[106] V. Guillerm, S. Gross, C. Serre, T. Devic, M. Bauer, G. Férey, Chem. Commun., 46 (2010) 767-769.
[107] S. Petit, S. Morlens, Z. Yu, D. Luneau, G. Pilet, J.-L. Soubeyroux, P. Odier, Solid State Sciences, 13 (2011) 665-670.
[108] J. Kreutzer, M. Puchberger, C. Artner, U. Schubert, Eur. J. Inorg. Chem., 2015 (2015) 2145-2151.
[109] J. Kreutzer, M. Czakler, M. Puchberger, E. Pittenauer, U. Schubert, European Journal of Inorganic Chemistry, 2015 (2015) 2889-2894.
[110] P. Walther, M. Puchberger, F.R. Kogler, K. Schwarz, U. Schubert, Phys. Chem. Chem. Phys., 11 (2009) 3640-3647.
[111] S. Gross, G. Kickelbick, M. Puchberger, U. Schubert, Monatshefte für Chemie / Chemical Monthly, 134 (2003) 1053-1063.
[112] W. Mark, M. Hansson, Acta Crystallogr. Sect. B Structural Crystallography and Crystal Chemistry, 31 (1975) 1101-1108.
[113] G.M. Muha, P.A. Vaughan, The Journal of Chemical Physics, 33 (1960) 194-199.
[114] S.J. Dalgarno, J.L. Atwood, C.L. Raston, Inorg. Chim. Acta, 360 (2007) 1344-1348.
[115] J.A. Sommers, D.C. Hutchison, N.P. Martin, L. Palys, J.M. Amador, D.A. Keszler, M. Nyman, Inorganic Chemistry, (2021).
[116] F. Maratini, L. Pandolfo, S. Rizzato, A. Albinati, A. Venzo, E. Tondello, S. Gross, European Journal of Inorganic Chemistry, 2011 (2011) 3281-3283.

[117] S. Goberna-Ferrón, D.-H. Park, J.M. Amador, D.A. Keszler, M. Nyman, Angew. Chem. Int. Ed., 55 (2016) 6221-6224.
[118] V.Y. Kuznetsov, L.M. Dikareva, D.L. Rogachev, M.A. Porai-Koshits, J. Struct. Chem., 26 (1985) 923-929.
[119] A. Kalaji, L. Soderholm, Chem. Commun., 50 (2014) 997-999.
[120] A. Kalaji, S. Skanthakumar, M.G. Kanatzidis, J.F. Mitchell, L. Soderholm, Inorg. Chem., 53 (2014) 6321-6328.
[121] L. Rozes, C. Sanchez, Chem. Soc. Rev., 40 (2011) 1006-1030.
[122] P. Coppens, Y. Chen, E. Trzop, Chem. Rev., 114 (2014) 9645-9661.
[123] K. Watenpaugh, C.N. Caughlan, Chem. Commun., (1967) 76-77.
[124] V.W. Day, T.A. Eberspacher, W.G. Klemperer, C.W. Park, F.S. Rosenberg, J. Am. Chem. Soc., 113 (1991) 8190-8192.
[125] J. Moons, F. de Azambuja, J. Mihailovic, K. Kozma, K. Smiljanic, M. Amiri, T. Cirkovic Velickovic, M. Nyman, T.N. Parac-Vogt, Angew. Chem. Int. Ed., 59 (2020) 9094-9101.
[126] S. Yuan, T.-F. Liu, D. Feng, J. Tian, K. Wang, J. Qin, Q. Zhang, Y.-P. Chen, M. Bosch, L. Zou, S.J. Teat, S.J. Dalgarno, H.-C. Zhou, Chem. Sci., 6 (2015) 3926-3930.
[127] I. Mijatovic, G. Kickelbick, U. Schubert, European Journal of Inorganic Chemistry, 2001 (2001) 1933-1935.
[128] T.J. Boyle, T.M. Alam, C.J. Tafoya, B.L. Scott, Inorg. Chem., 37 (1998) 5588-5594.
[129] S.S. Passadis, S. Hadjithoma, A.G. Kalampounias, A.C. Tsipis, S. Sproules, H.N. Miras, A.D. Keramidas, T.A. Kabanos, Dalton Transactions, 48 (2019) 5551-5559.
[130] T. Frot, S. Cochet, G. Laurent, C. Sassoye, M. Popall, C. Sanchez, L. Rozes, European Journal of Inorganic Chemistry, 2010 (2010) 5650-5659.
[131] C.F. Campana, Y. Chen, V.W. Day, W.G. Klemperer, R.A. Sparks, J. Chem. Soc., Dalton Trans., (1996) 691-702.
[132] G. Zhang, C. Liu, D.-L. Long, L. Cronin, C.-H. Tung, Y. Wang, J. Am. Chem. Soc., 138 (2016) 11097-11100.
[133] K. Kozma, M. Wang, P.I. Molina, N.P. Martin, Z. Feng, M. Nyman, Dalton Transactions, 48 (2019) 11086-11093.
[134] M.-Y. Gao, F. Wang, Z.-G. Gu, D.-X. Zhang, L. Zhang, J. Zhang, Journal of the American Chemical Society, 138 (2016) 2556-2559.
[135] J.L.C. Rowsell, O.M. Yaghi, Angew. Chem. Int. Ed., 44 (2005) 4670-4679.
[136] V.W. Day, T.A. Eberspacher, W.G. Klemperer, C.W. Park, J. Am. Chem. Soc., 115 (1993) 8469-8470.
[137] G. Fornasieri, L. Rozes, S. Le Calvé, B. Alonso, D. Massiot, M.N. Rager, M. Evain, K. Boubekeur, C. Sanchez, J. Am. Chem. Soc., 127 (2005) 4869-4878.
[138] G.J.d.A.A. Soler-Illia, E. Scolan, A. Louis, P.-A. Albouy, C. Sanchez, New Journal of Chemistry, 25 (2001) 156-165.
[139] J.-X. Liu, M.-Y. Gao, W.-H. Fang, L. Zhang, J. Zhang, Angew. Chem. Int. Ed., 55 (2016) 5160-5165.
[140] M. Janek, T.M. Muzioł, P. Piszczek, Materials (Basel), 12 (2019) 3195.
[141] M. Dan-Hardi, C. Serre, T. Frot, L. Rozes, G. Maurin, C. Sanchez, G. Férey, J. Am. Chem. Soc., 131 (2009) 10857-10859.
[142] A.I. Kuznetsov, O. Kameneva, N. Bityurin, L. Rozes, C. Sanchez, A. Kanaev, Phys. Chem. Chem. Phys., 11 (2009) 1248-1257.
[143] M. Rimoldi, A.J. Howarth, M.R. DeStefano, L. Lin, S. Goswami, P. Li, J.T. Hupp, O.K. Farha, ACS Catal., 7 (2017) 997-1014.
[144] J.E. Mondloch, M.J. Katz, W.C. Isley Iii, P. Ghosh, P. Liao, W. Bury, G.W. Wagner, M.G. Hall, J.B. DeCoste, G.W. Peterson, R.Q. Snurr, C.J. Cramer, J.T. Hupp, O.K. Farha, Nature Materials, 14 (2015) 512-516.

[145] H.G.T. Ly, G. Fu, A. Kondinski, B. Bueken, D. De Vos, T.N. Parac-Vogt, J. Am. Chem. Soc., 140 (2018) 6325-6335.
[146] A. Loosen, F. de Azambuja, S. Smolders, J. Moons, C. Simms, D. De Vos, T.N. Parac-Vogt, Chem. Sci., 11 (2020) 6662-6669.
[147] H.G.T. Ly, G. Fu, F. de Azambuja, D. De Vos, T.N. Parac-Vogt, ACS Appl. Nano Mater., 3 (2020) 8931-8938.
[148] F. Faccioli, M. Bauer, D. Pedron, A. Sorarù, M. Carraro, S. Gross, Eur. J. Inorg. Chem., 2015 (2015) 210-225.
[149] Y.-J. Liu, W.-H. Fang, L. Zhang, J. Zhang, Coord. Chem. Rev., 404 (2020) 213099.
[150] M.C. Wasson, X. Zhang, K.-i. Otake, A.S. Rosen, S. Alayoglu, M.D. Krzyaniak, Z. Chen, L.R. Redfern, L. Robison, F.A. Son, Y. Chen, T. Islamoglu, J.M. Notestein, R.Q. Snurr, M.R. Wasielewski, O.K. Farha, Chem. Mater., 32 (2020) 8522-8529.
[151] I. Colliard, M. Nyman, Angew. Chem. Int. Ed., n/a (2021).
[152] K.E. Knope, L. Soderholm, Chem. Rev., 113 (2013) 944-994.
[153] T.J. Boyle, L.A.M. Ottley, M.A. Rodriguez, Polyhedron, 24 (2005) 1727-1738.
[154] A. Otero, J. Fernández-Baeza, A. Antiñolo, J. Tejeda, A. Lara-Sánchez, L. Sánchez-Barba, M. Fernández-López, I. López-Solera, Inorg. Chem., 43 (2004) 1350-1358.
[155] G.-H. Chen, Y.-P. He, S.-H. Zhang, L. Zhang, Inorg. Chem. Commun., 97 (2018) 125-128.
[156] M.J. Cliffe, E. Castillo-Martínez, Y. Wu, J. Lee, A.C. Forse, F.C.N. Firth, P.Z. Moghadam, D. Fairen-Jimenez, M.W. Gaultois, J.A. Hill, O.V. Magdysyuk, B. Slater, A.L. Goodwin, C.P. Grey, J. Am. Chem. Soc., 139 (2017) 5397-5404.